Universidad de Concepción

Facultad de Ingeniería

NEW TECHNOLOGY FOR NON-INVASIVE ELECTRICAL STIMULATION OF PERIPHERAL NERVES

Thesis submitted to the Faculty of Engineering of the Universidad de Concepción for the academic degree of Doctor of Engineering Sciences with a major in Electrical Engineering

AUTHOR: RODRIGO ANDRÉS OSORIO LÉPEZ
Supervisors: Pablo Esteban Aqueveque Navarro
Brian J. Andrews

June 2025
Concepción, Chile

ACKNOWLEDGMENTS

This thesis is a testament to the unwavering support and love I've received from my family and friends throughout this challenging journey. Their belief in me has been a guiding light during difficult times, and I am deeply grateful for their encouragement and sacrifices. I dedicate this work to them.

To my Wife, Valentina, whose unconditional support has been key to facing this challenge, you have always trusted me from the beginning; I love you endlessly. To my parents, Pamela and Rodrigo, who nurtured my curiosity and supported my educational endeavours from the very beginning. To my sister, Marcela, your admiration has motivated me to work harder and be the best example for you. To my baby kitty girls, Pimienta and Jengibre, you made my days with your craziness and your sincere love. To my advisors, Pablo and Brian, thanks for giving me the opportunity to start this journey as an investigator. Thank you for your advice, for trusting me, and for being such good academic role models (each in their own style).

I would like to thank CONICYT for its support through the scholarship CONICYT-PFCHA/Doctorado Nacional/2020—21202217, and ANID through the project FOVI220205 "ADVANCED SURFACE ELECTRODES: DEVELOPMENT AND

FABRICATION" for the realisation of this thesis.

Resumen

Las lesiones en la médula espinal (SCI por sus siglas en inglés) suelen provocar alteraciones motoras significativas, afectando gravemente la calidad de vida y los costos asociados al cuidado. Aunque la recuperación funcional tras una lesión medular es generalmente limitada, las técnicas de estimulación eléctrica ofrecen vías prometedoras para la restauración parcial del movimiento. Los diseños tradicionales de electrodos y las formas de onda utilizadas en la estimulación han permanecido prácticamente sin cambios desde la década de 1890, lo que ha derivado en una baja selectividad espacial y escasa penetración en los tejidos, limitando su aplicación a nervios superficiales.

Este estudio investiga la estimulación por corrientes interferenciales (ICS por sus siglas en inglés) en combinación con nuevas geometrías de electrodos y técnicas de posicionamiento anatómico, utilizando modelado avanzado por elementos finitos y simulación de nervios. Los hallazgos revelan nuevas posibilidades de activación del músculo cuádriceps, esencial para actividades como ponerse de pie y caminar. Se evaluaron distintas formas de electrodos, incluyendo cuadradas, circulares y anillos concéntricos, para determinar su impacto en la eficiencia de activación muscular.

Los resultados indicaron que la estimulación interferencial activa eficazmente el cuádriceps, siendo la configuración de electrodos cuadrados la que generó

respuestas musculares comparables a las de la estimulación eléctrica funcional estándar (FES por sus siglas en inglés), aunque requirió mayores amplitudes de corriente. Otras configuraciones mostraron una eficacia variable en la generación de contracciones musculares consistentes. Por primera vez, esta investigación demuestra la posibilidad de "redirigir" electrónicamente la región de activación en tres dimensiones, adaptándose a desplazamientos en los puntos motores.

El estudio también examina las percepciones de dolor e incomodidad asociadas a los distintos diseños de electrodos, encontrando que, si bien algunas configuraciones de estimulación interferencial disminuyen la incomodidad, pueden requerir intensidades de corriente superiores a las de la estimulación tradicional para lograr respuestas musculares óptimas. En conjunto, la investigación destaca el potencial de esta técnica, junto con diseños de electrodos optimizados, para mejorar las terapias de rehabilitación en personas con trastornos neuromusculares. Se proyectan futuros estudios orientados al perfeccionamiento de estos diseños y a la evaluación de los efectos a largo plazo sobre la función muscular.

Abstract

Spinal cord injuries (SCIs) often lead to significant motor impairments, severely affecting quality of life and care costs. Although functional recovery post-SCI is generally limited, Electrical Stimulation (ES) techniques present promising avenues for partial restoration of movement. Traditional electrode designs and stimulation waveforms have remained largely unchanged since the 1890s, resulting in inadequate spatial selectivity and tissue penetration, which constrain applications to superficial nerves.

This study investigates Interferential Current Stimulation (ICS) in conjunction with novel electrode geometries and anatomical positioning, utilising advanced Finite Element (FE) and nerve modelling. The findings reveal new activation possibilities for the quadriceps muscle, which is critical for activities such as standing and walking. Various electrode shapes, including square, circular, and concentric ring designs, were evaluated for their impact on muscle activation efficiency.

Results indicated that ICS effectively activates the quadriceps, with the ICS-Square configuration yielding muscle responses comparable to those of standard FES, albeit requiring higher current amplitudes. Other configurations showed varying effectiveness in generating consistent muscle contractions. For the first

time, this research demonstrates the potential for electronically "steering" the activation region in 3D, adapting to shifts in motor points.

The study also examines the perceptions of pain and discomfort associated with various electrode designs, finding that while some ICS configurations alleviate discomfort, they may require higher current than traditional FES to achieve optimal muscle responses. Overall, the research highlights ICS's potential, in conjunction with optimised electrode designs, to enhance rehabilitation therapies for neuromuscular disorders. Future studies are planned to refine these designs and investigate the long-term effects on muscle function.

Contents

List of Tables

List of Figures

List of Abbreviations

- AF ——— Activating Function
- CNS ——— Central Nervous System
- CRE ——— Concentric Ring Electrode
- DBS ——— Deep Brain Stimulation
- EMG ——— Electromyography
- ES ——— Electrical Stimulation
- FEM ——— Finite Element Model
- FES ——— Functional Electrical Stimulation
- F-H ——— Frankenhaeuser-Huxley
- H-H ——— Hodgkin-Huxley
- ICS ——— Interferential Currents Simulation
- MP ——— Motor Point
- NMES ——— Neuro Muscular Electrical Stimulation
- OAB ——— Overactive Bladder
- PDE ——— Partial Derivative Equation
- PES ——— Peripheral Electrical Stimulation
- PNS ——— Peripheral Nervous System

- SCI ——————— Spinal Cord Injury
- TENS ——————— Transcutaneous Electrical Nerve Stimulation
- TI ——————— Temporal Interference
- VAS ——————— Visual Analogue Scale

Chapter 1

Introduction

The author was introduced to non-invasive functional electrical stimulation (FES) and the recent application of FES Rowing for paraplegics, an emerging application offering increased cardiovascular and bone health therapy in spinal cord injury and other neurological disorders [1; 2]. FES rowing has also been introduced as a new form of adaptive rowing and is now featured in major competitive events such as the World Indoor Rowing Championships, CRASH-Bs [3]. I was also invited to explore characteristics of electrical stimulation, particularly the electrode and its interface with the skin, that could potentially surpass current implementations and potentially improve the therapeutic benefits and rowing performance.

After delving into the techniques of FES and FES Rowing, the methods described did not appear to enable some target nerves that are either more deeply located or where their main motor point undergoes large displacement during motion, for example, the femoral nerve and its branches. The described techniques did not indicate how these deeper nerves could be stimulated without skin damage by

exceeding safe levels of current density. In addition, present electrodes are not well localised to avoid undesirable collateral activation of nearby nerves. Finally, many individuals have incomplete spinal cord injury, particularly after the introduction of car seat belts. Addressing any of these challenges could pave the way for innovations that enhance performance and therapy, improve the overall experience for both athletic and recreational use of FES Rowing techniques:

1. Difficulty in generating high quadriceps force contraction, particularly during the “catch” to early “drive” phase of rowing.
2. Limitation due to pain and discomfort by activating skin afferent axons when applying FES.
3. Difficulty in reaching deep femoral nerve branches throughout the rowing cycle.

These addressed limitations are not exclusive to FES Rowing, but to all FES-based rehabilitation methods. Then, the initial focus is on setting the following research questions:

1. Is it possible to achieve functional stimulation and a comfortable patient experience by applying the same electrical stimulation technique?
2. How can deeper neuron fibres be reached and produce stronger muscle activation?

Thus, my primary motivation was to propose modifications to existing techniques and/or evaluate new approaches to electrical stimulation methods that address the

research questions presented. Specifically, evaluating high-frequency modulation techniques, namely Interferential Current Stimulation in this case, in relation to electrode geometries and positioning modifications to optimise the effect of electrical stimulation and elicit functional muscle contractions.

In the remainder of this chapter, I will present relevant background, identify gaps, and articulate my thesis hypotheses, research questions, and aims.

1.1 Spinal Cord Injury

Spinal Cord Injury (SCI) is a condition attributed to a complete or partial disruption in the corticospinal tract. These injuries can principally be caused by trauma or an abnormal pressure on the spinal cord [4; 5; 6]. SCI patients present an interruption in the spinal nerve pathways, affecting the communication between motor or sensory nerves with the Central Nervous System (CNS). The latter leads to complete or partial paralysis due to the reduction of motor control. The paralysis is produced below the location of the injury, affecting different segments of the body [4].

Spinal cord injury (SCI) significantly contributes to health loss through premature mortality and long-term disabilities [7]. According to the World Health Organisation (WHO), over 15 million people live with SCI, with a higher prevalence in males. Life expectancy for individuals with SCI is closely linked to neurological impairment and preventable secondary conditions. In low and middle-income countries, the hospitalised mortality rate for people with SCI is nearly three times

higher than in high-income countries, due in part to poor access to quality health services. Misconceptions and mobility barriers hinder full societal participation. Children with SCI are less likely to start or progress in school, while adults face unemployment rates over 60%. The social and economic consequences for individuals with SCI, their caregivers, and families are significant, with indirect costs, such as lost earnings, often exceeding direct costs, particularly in the first year following the injury [8].

Although the incidence of SCI is relatively small compared to conditions like stroke, SCI typically occurs at a much younger age, which results in a near-normal life expectancy for many individuals. However, this extended lifespan comes at a significantly higher cost of care. Individuals with SCI often require long-term rehabilitation, assistive devices, and specialized medical treatments, all of which contribute to substantial lifetime healthcare expenses. Studies estimate that the lifetime cost of care for a person with SCI can range from 1.5 million to 5 million, depending on the severity of the injury and the level of care required [9; 10].

Electrical Stimulation (ES), particularly low-cost non-invasive techniques, have been incorporated into treatment plans to enhance functions during the rehabilitation of patients with SCI. The potential of electrical stimulation following SCI is promising, demonstrating encouraging initial outcomes in clinical trials [11]. The systematic use of ES in individuals with SCI creates a means to optimise neural activity below the injury site, while simultaneously minimising secondary complications and enhancing overall health [12]. One specific treatment method

is FES Rowing, an indoor rowing activity that utilises electrical stimulation to induce muscle contractions in the limbs of patients with partial or total SCI. FES Rowing offers a compelling option for promoting physical activity among individuals with spinal cord injury. Recent research indicates that FES Rowing contributes positively to cardiovascular and bone health [1; 2; 13]. Gibbons et al. [1] found that FES Rowing resulted in a higher metabolic cost compared to other ES-assisted or non-ES workouts, making it an excellent stimulus for cardiovascular health. Furthermore, it alleviates upper limb pain for wheelchair users with SCI [14].

1.2 Peripheral Electrical Stimulation

The Peripheral Nervous System (PNS) corresponds to an integrated mechanism composed of nerve branches from the CNS. This system communicates with the outside world and can sense external influences such as pressure, temperature, touch, and pain [15; 16]. In response to sensory excitement, most of the time, it induces excitation in muscles to move. So, when activation is due to a sensory stimulus, the afferent sensory nerves produce an electrochemical reaction that propagates an electrical impulse to communicate the external sensation to the CNS. The PNS uses the exact mechanism to generate movement: The efferent nerves carry the electrical stimulus to specific muscles and induce contraction or relaxation that moves the musculoskeletal system [15; 16; 17]. The fig. 1.2.1, from Lynch et al. [18], shows the neural connection mechanism of the CNS and motor

muscles (Quadriceps and Hamstrings). This Scheme illustrates the propagation of the contraction order in the muscle to generate the knee flexion movement.

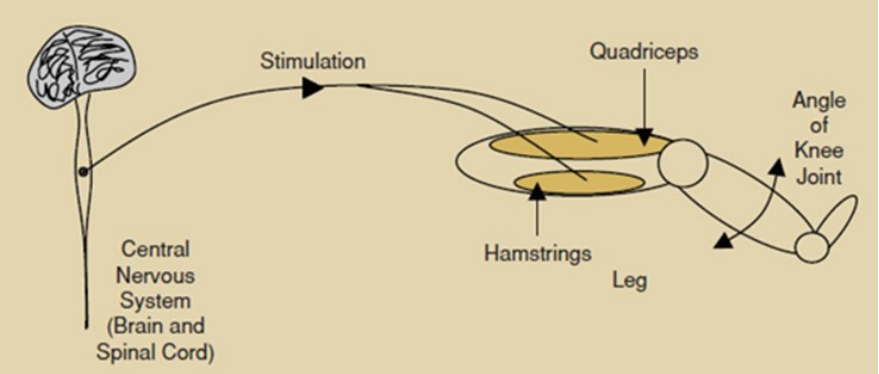

Figure 1.2.1: Scheme of neural connection from the Central Nervous System and motor muscles of the upper leg.

Peripheral nerve Electrical Stimulation (PES) is a technique that produces sensory or motor activation in the PNS using external electric stimulation. We can artificially emulate the PNS electrical functions using this external electrical stimulation. Specifically, Neuro Muscular Electrical Stimulation (NMES) is one type of PNS that focuses on stimulating sensory and motor fibres [18; 19; 20].

The most common uses of NMES are related to:

- Pain Relief: Transcutaneous Electrical Nerve Stimulation (TENS) is a technique that consists of applying low-intensity ($<10\ mA$) alternating currents ($50\sim200\ Hz$) superficially to induce analgesia. The analgesic effect is produced by stimulating high-diameter nerve fibres ($A\beta$) that block narrow-diameter nerves (fibres $A\delta$ and C) pain neuroreceptors [15; 19; 21].

- Motor Control: Functional Electrical Stimulation (FES) compensates for the musculoskeletal system's lack of control. An external device can produce

excitation on specific motor points and generate muscle contractions through this method. FES stimulation requires a stimulus frequency between 20∼50 Hz. The current intensity will depend on the desired movement and the location. It is widely used to rehabilitate and train patients with paralysis or who have suffered strokes [18; 22].

A typical NMES procedure is presented in 1.2.2. Initially, the skin in the area to be stimulated is cleaned, typically with an alcohol-based solution. Next, surface electrodes are placed over the targeted muscle, and the electrical parameters of the stimulator are then configured.

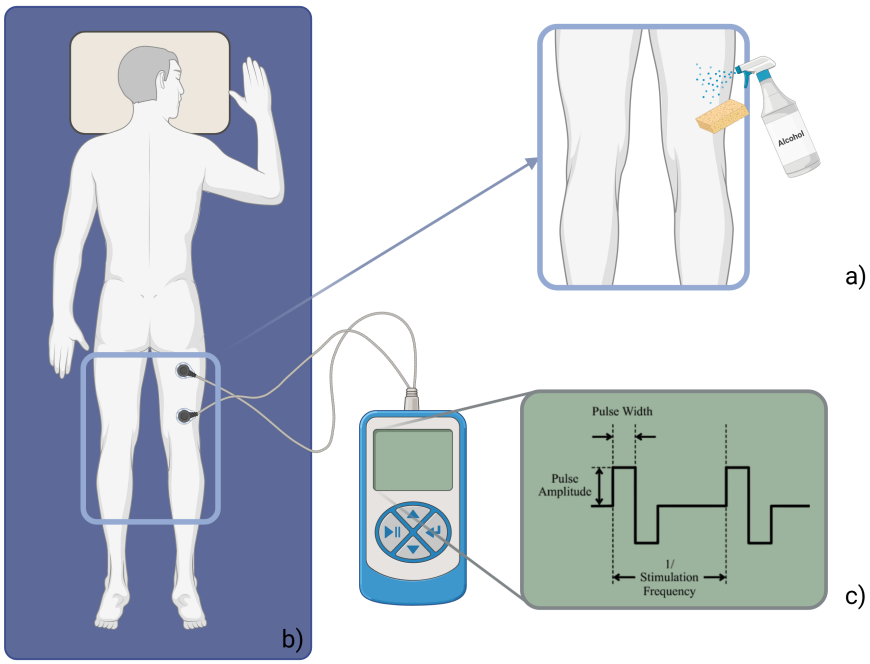

Figure 1.2.2: Representation of a typical NMES procedure. a) Cleaning the stimulation area skin with an alcohol-based solution. b) Placing the electrodes over the target muscle. c) Configuring the electrical parameters according to the therapy.

1.3 NMES parameters

There are many parameters to consider when applying NMES: current intensity, frequency, stimulus waveform, pulse width, electrode shape, size, and location [16; 18]. The experiments presented in this thesis focus on the effect of stimulus frequencies and electrode shapes on producing different neural activation conditions.

Some studies claim that higher frequencies ($> 2{\sim}10\ kHz$) create a more comfortable stimulation [19; 20; 21]. Former studies have shown that, at high frequencies, we can observe a reduction of the skin-electrode impedance [22; 23]. Also, high frequencies can deeply penetrate skin and muscle tissue as they meet lower impedance. The inconvenience of using high frequencies is that the stimulus is faster than the neurons' time response, not producing functional excitations in most cases [17; 23]. High frequencies are suitable for pain relief treatments, stimulating high diameter nerve fibres (Aβ) that block narrow diameter nerves (fibres Aδ and C) pain neuroreceptors [15; 19; 21]. High-frequency stimuli are unsuitable for generating muscle contractions as they do not activate slow motor fibres. Producing deep muscle contractions becomes a significant challenge in stimulus penetration, fibre selectivity, and skin sensation. On the other hand, low frequencies (20∼80 Hz) stimulations generate functional contractions on superficial muscles. Still, they encounter high skin impedance, making reaching deep fibres and motor neurons difficult, but an easy activation of superficial skin sensory receptors [16]. The outer layer of the skin, known as the Stratum Corneum, serves

as a barrier to the movement of hydrophilic and ionised species, making it the most resistive part of the skin-electrode interface impedance [24]. An increased skin-electrode interface impedance requires higher current amplitudes to penetrate the tissues above the nerve or muscle motor unit, in most cases eliciting skin afferents that produce pain or discomfort.

Electrode shape and size determine the zones where neural excitation can be produced. Alon et al. [25] conclude that large electrodes produce less discomfort due to a bigger area to distribute current. The inconvenience with those electrodes is the lack of nerve selectivity, and more extensive activation areas can stimulate unwanted nerves near the target nerve. Forrester et al. [26] compared round, square, and square with serrated edge electrodes of different sizes and placements. Among the tested electrodes, the results showed no meaningful relationship to tolerance of electrical stimulation. Other studies have demonstrated that Concentric Ring Electrodes (CREs) have greater sensitivity and selectivity [27; 28; 29]. Von Oosterom et al. [27] confirmed the latter by comparing CRE with disc electrodes. Also, CREs reduce the edge effect and generate uniform current density distributions, according to Besio et al. [28].

1.4 Chapter Discussion

The primary hypothesis to be evaluated in this research is that Interferential Current Stimulation (ICS) over the femoral nerve, utilising multipolar concentric ring electrodes, produces stronger muscle activation with less sensory discomfort

compared to conventional single-channel side-to-side electrodes. This was evaluated by examining the effects of electric fields on the nerve using finite element anatomical models. The proposed electrical stimulation techniques were then tested in vivo, measuring motor responses by assessing thigh deformations and utilising a McGill questionnaire to evaluate the subjective experience of discomfort.

Based on the main hypothesis and identifying gaps in studies that explore the effects on neural activation using ICS for muscle contraction control, and the motor and sensory responses elicited by the application of ICS therapies, a series of research questions emerged during the investigation and application of the proposed electrical stimulation techniques based on ICS and optimised electrode positioning. Answering these questions will help to characterise the effects of ICS on electrically excitable tissues compared to classic techniques such as FES:

1. How do different electrode geometries impact the intensity of induced muscle contractions and the sensation of discomfort during Functional Electrical Stimulation and Interferential Current Stimulation?

2. How does the electrode positioning influence the elicited muscle contractions while applying FES and ICS?

3. Can comparable muscle contraction intensities be achieved with ICS compared to FES, while simultaneously reducing pain sensation?

4. Can the region of ICS nerve activation be extended to accommodate the displacement of motor points?

5. Can the region of ICS nerve activation be electronically "steered" to enable automatic adjustment without requiring the electrodes to be removed and reapplied manually?

During the execution of this thesis, the hypothesis and research questions were rigorously tested by assessing the impacts of varying electric fields on axonal activation within in silico finite element method (FEM) models. This approach facilitated the identification of differences in the activation regions associated with electrical stimulation techniques by manipulating electrode geometry, positioning, and stimulation frequency. Furthermore, the validity of these findings was reinforced by implementing the proposed electrical stimulation techniques in in vivo experiments involving both lower and upper limb applications, allowing for a more comprehensive evaluation of the elicited motor and sensory effects.

Subsequent chapters will provide insights into how innovative functional electrical stimulation techniques, based on signal modulation and novel electrode geometries, may contribute to the development of more comfortable and effectively controlled muscle contractions. This document provides insights into the mathematical principles and biophysics of neural activation, presenting the methodology implemented to evaluate hypotheses based on finite element modelling and in vivo testing of electrical stimulation, which assesses the effects of new proposed techniques.

This thesis investigates the performance enhancements achieved through innovative electrical stimulation strategies, by taking the FES Rowing targeting the quadriceps

as a reference model to assess diverse experiments. Specifically, it focuses on techniques that utilise kilohertz-frequency modulation along with optimised electrode shape and placement. However, other cases of use, such as hand and finger motor control, are employed to explain the mechanisms that underlie these novel electrical stimulation techniques.

Chapter 2

Mathematical Methods for Evaluating Electrical Stimulation

The Activating Function and Cable Equation based axon models equations have advanced the field by allowing us to model the expected field of activation (Activating Function) and the axon's mechanism of action potential generation and its propagation (Cable Equation), respectively [30; 31; 32; 33; 34; 35].

2.1 Activating Function

Rattay [30] postulated one of the most accepted theories of the mechanism of neural stimulation. He introduced the concept of Activating Function (AF) as a function proportional to the second derivative of the extracellular potentials along the nerve axon, as presented in eq. (2.1.1):

$$AF = \lambda^2 \frac{\partial^2 V_e}{\partial x^2} \tag{2.1.1}$$

where λ corresponds to the fibre length constant, V_e is the extracellular potentials, and x is an axis parallel to the axon. The AF provides information on the neuron's exterior environment, indicating the likelihood of generating an action potential. AF values greater than zero indicate the likelihood of depolarisation of the neural membrane. Values lower than zero indicate a likely hyperpolarised zone. Therefore, the AF provides a useful tool to evaluate profiles of stimulation electrodes, i.e., quantify the depth or spread of the electric fields produced by the electrical stimulation. The scheme edited from [36] in fig. 2.1.1 illustrates the latter interpretation.

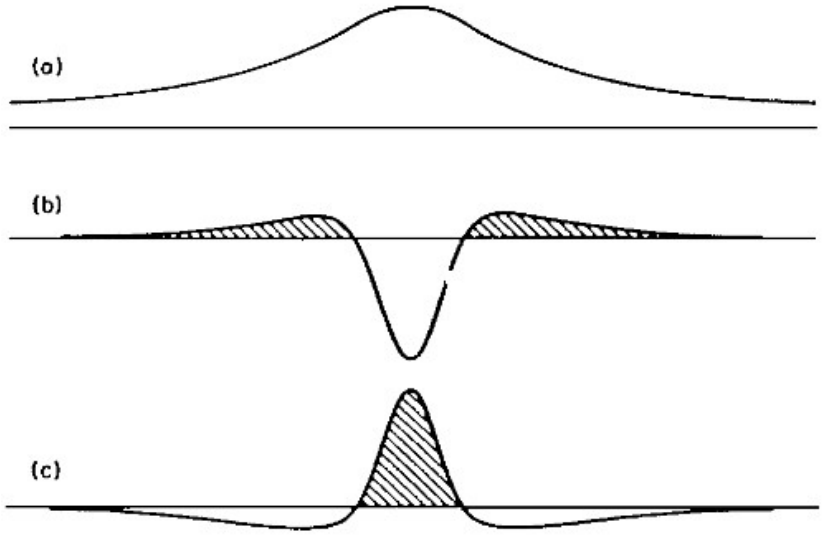

Figure 2.1.1: Activating Function along the nerve axis during a stimulation pulse, the dashed areas indicate zones likely to generate an action potential. The horizontal axis represents zero values. a)Extracellular potential. b)Activating Function for an anodal stimulation. b)Activating Function for a cathodal stimulation.

2.2 Hodgkin Huxley based axon models

The Hodgkin Huxley differential equations [37] can be used to develop axon models such as the MRG model [38] and the H-H axon model when used alongside cable theory. The cable theory is a mathematical-computational method that models the spatial and temporal propagation of action potentials on axon and dendrite membrane [39; 40]. The coupling to an H-H-based axon model is essential as this gives us more insight into the dynamics of an axon's signal propagation. The Hodgkin-Huxley differential equations introduce more detailed biophysics, such as the dynamics of the gated ion channels presented in a nerve.

In its general form, the Cable Theory Equation can be expressed as:

$$\lambda^2 \frac{\partial^2 V_m(x,t)}{\partial x^2} = \tau \frac{\partial V_m(x,t)}{\partial t} + V_m(x,t) \tag{2.2.1}$$

where V_m(x,t) is the membrane potential as solved for using FEM, and the x axis is parallel to the axon, and t corresponds to time. λ corresponds to a space constant and τ the time constant [40]. The H-H axon model, with cable theory at its core, calculates the static potential of the axon membranes. In determining the propagation of action potentials, we perform a time-dependent study. The H-H axon model calculates the potentials on each time step, using the potentials on the previous time step $(t-1)$ as input for the current timestep (t). Analysing the potentials across a time series allows us to see if an action potential is generated, indicated by the potential values crossing a threshold of $-55mV$ [41].

2.3 Chapter Discussion

These models serve as essential instruments for assessing the impact of electrical stimulation through analytical and multiphysics modelling. The activation function identifies the body regions influenced by the stimulation method, while the axon model assesses whether the stimulation technique has the requisite elements to trigger an action potential.

Chapter 3

Interferential Currents Stimulation

Interferential Current Stimulation (ICS) is an electrical stimulation technique based on delivering these fields at slightly different kHz frequencies, for example, 4000 Hz and 4050 Hz, with the intention that excitable tissue below the skin might be activated at the difference or beat frequency (50 Hz in this example) generated by the alternating voltage caused by successive constructive and destructive interference of the two waves [42]. The fig. 3.0.1, obtained from [43], illustrates the modulation process generated by the interaction of sinusoidal interferential currents.

The method has been used and described since the 1950s, but experienced physical therapy practitioners are still undecided on its application or superiority over any other method of transcutaneous stimulation. ICS is suggested for deep tissue stimulation due to reduced tissue impedance at higher frequencies, allowing for deeper penetration and predominant nerve stimulation via the beat effect [44; 45]. In the last 10 years, there has been a resurgence of this technique under the name

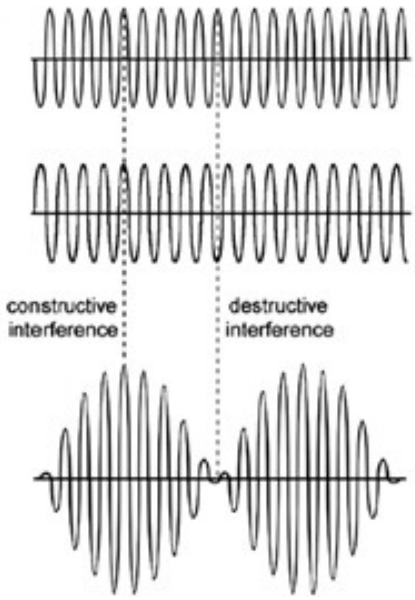

Figure 3.0.1: Amplitude modulated signal via ICS. The two sinusoidal signal interferences at the top generate the modulated signal at the bottom.

of Temporal Interference (TI). TI is mainly oriented to Deep Brain Stimulation combined with Kilohertz modulation techniques [46]. In this document, we will make reference to the original ICS naming, as the target structures are peripheral nerves and muscles.

Applying ICS requires two synchronised electrical stimulator sources and four electrodes (two anodes, two cathodes). The intersection of both stimulation currents generates the resultant modulated current. Its maximum amplitude is developed along the diagonal, extending at 45° between electrodes from different sources [42; 44]. The fig. 3.0.2 presented in [42] illustrates the location of the maximum effect in an ICS using a four-electrode configuration. The electrodes are paired with its front electrode, describing a 180° line. The intersection between the two lines represents a 90° angle. The resultant current at its maximum modulation happens in the middle between the 90° angles. These areas where the modulation

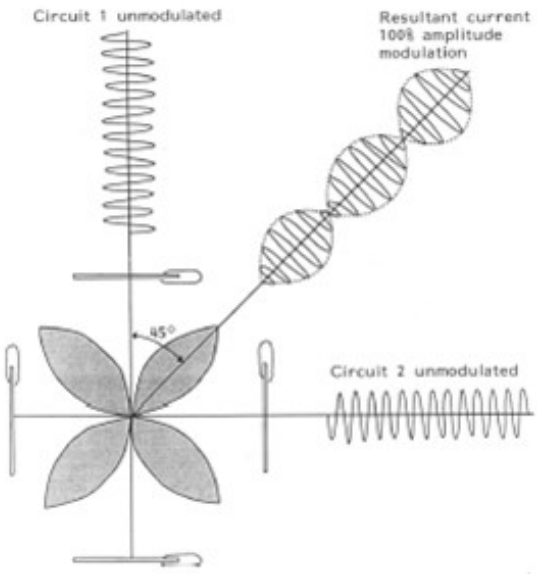

Figure 3.0.2: Pattern of interference current effect for a four-electrode configuration. The maximum effect is generated at 45°.

is near its maximum amplitude will be called modulated fields [42].

3.1 Mathematical principles behind Interferential Currents

We can recognise two frequencies in the resultant signal: a high frequency or carrier and a low frequency or beat. The mathematical models to determine carrier (eq. (3.1.1)) and beat (eq. (3.1.2)) frequencies are:

$$f_{\text{carrier}} = \frac{f_1 + f_2}{2} \tag{3.1.1}$$

$$f_{\text{beat}} = |f_1 - f_2| \tag{3.1.2}$$

where f_1, f_2 are the input frequencies for both high-frequency input currents. Both input frequencies must be high enough to penetrate tissue to produce deep muscular activation, and the modulated fields must be positioned near the target nerve.

According to [46], the total effect of the modulated currents can be modelled as:

$$V_{\text{total}} = V_1 \sin(2\pi f_1 t) + V_2 \sin(2\pi f_2 t) \tag{3.1.3}$$

where V_1 and V_2 are the amplitude of the potentials produced by both current inputs.

Since the inputs are sine waves, eq. (3.1.3) can be written in terms of Euler expressions:

$$V_{\text{total}} = V_1 e^{i2\pi f_1 t} + V_2 e^{i2\pi f_2 t} \tag{3.1.4}$$

Then, considering eq. (3.1.2):

$$V_{\text{total}} = e^{i2\pi t \frac{f_1+f_2}{2}} \left[V_1 e^{i2\pi t \frac{f_1-f_2}{2}} + V_2 e^{-i2\pi t \frac{f_1-f_2}{2}} \right] \tag{3.1.5}$$

Thus, V_{total} describes a potential that oscillates with the $f_{carrier}$, and its peaks oscillate with the f_{beat}. Then, the beat oscillation can be described by the V_{total} envelope. The envelope can be obtained by multiplying eq. (3.1.5) with its conjugated:

$$|\text{ENV}_{V_{\text{total}}}| = \sqrt{V_1^2 + V_2^2 + 2V_1 V_2 \cos(2\pi f_{\text{beat}} t)} \tag{3.1.6}$$

where $ENV_{V_{total}}$ is the module of the envelope of the modulated potential.

As the cosine term is bounded by ± 1, eq. (3.1.6) oscillates between $\sqrt{(V_1+V_2)^2}$ and $\sqrt{(V_1-V_2)^2}$. Then, the amplitude modulation can be rewritten as:

$$AM_V = ||V_1 + V_2| - |V_1 - V_2|| \tag{3.1.7}$$

where AM_V corresponds to the amplitude-modulated potential of the total effect of the ICS.

To define the modulated electrical field $E_{(X,Y,Z)}$ and the activation $AF_{(X,Y,Z)}$ the process is the same. Finally, the three-axis AF can be defined as:

$$AM_{AF} = \left|\left|\mathbf{AF}_{1_{(X,Y,Z)}} + \mathbf{AF}_{2_{(X,Y,Z)}}\right| - \left|\mathbf{AF}_{1_{(X,Y,Z)}} - \mathbf{AF}_{2_{(X,Y,Z)}}\right|\right| \tag{3.1.8}$$

Then, combining eq. (2.1.1) and eq. (3.1.8):

$$AM_{AF} = \left|\left|\frac{\partial^2 V_{e1}}{\partial(x,y,z)^2} + \frac{\partial^2 V_{e2}}{\partial(x,y,z)^2}\right| - \left|\frac{\partial^2 V_{e1}}{\partial(x,y,z)^2} - \frac{\partial^2 V_{e2}}{\partial(x,y,z)^2}\right|\right| \tag{3.1.9}$$

Equation eq. (3.1.9) allows for a tridimensional analysis of the electric fields and activation function envelope produced by interferential currents. This is an approach to the decodification that the neural membrane performs.

3.2 Biophysics of Interferential Current Stimulation

The section 3.1 described how two high-frequency sources stimulating tissue could produce an interfered current zone. So, How is the neural response in these interfered zones? What is the effect in the zones that are not interfered with? The quick answer to these questions is that neurons in the interfered zone will be excited, while those in the non-interfered zones will not be activated at the beat frequency [46; 47; 48]. These works explain these phenomena by simulating ICS in different nerve models.

Grossman et al. [47] presented that the neural membrane acts as a low-pass filter. This property allows the nerve to be activated just for specific stimulus frequencies. The latter could explain why low-frequency modulated currents can trigger a neural activation from the ICS point of view.

Mirzakhalili et al. [46] postulate that neurons' filtering properties are insufficient to interpret the interferential effect. So, they affirm that neurons can rectify and filter the modulated currents. The demodulation effect proposed by [46] is presented in fig. 3.2.1, showing a 20 Hz modulated stimulation of the neural membrane.

The figure shows that filtering the interferential stimulus does not generate the low-frequency effect (step A). In B, a demodulator rectifies the signal, obtaining the modulated frequency of 20 Hz. C shows that the passive axon model does not

respond to high-frequency oscillations. Finally, D shows the full effect of all the previous steps combined, where the modulated effect can be interpreted.

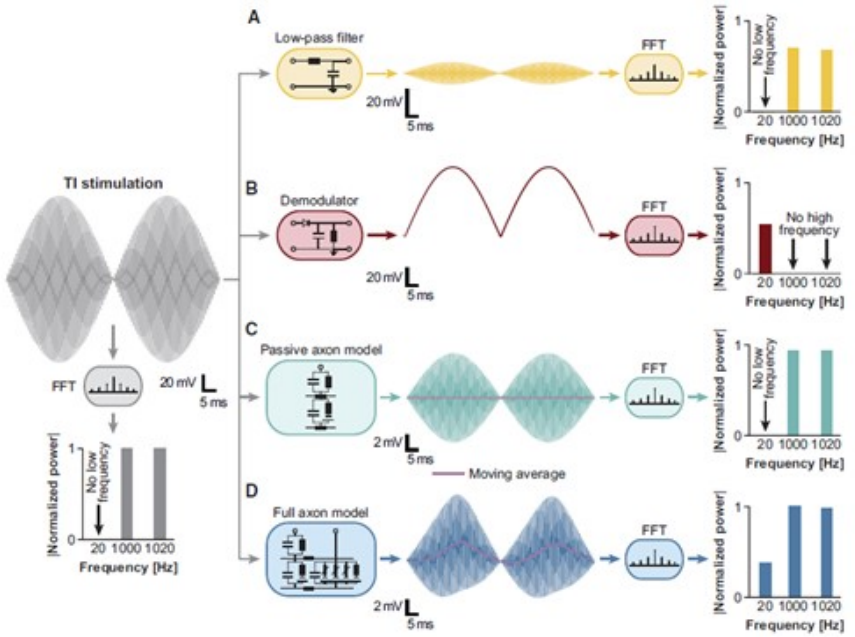

Figure 3.2.1: Demodulation effect of neural membrane proposed by Mirzakhalili et al. A) Result of low-pass filtering with no low-frequency component. B) Demodulator that rectifies and extracts low-frequency components. C) The passive axon model is not being affected by high-frequency stimulus. D) Full axon model with filter and rectification properties.

So, it can be said that neurons involved in the interfered zones can demodulate and interpret the low-frequency effect without being affected by high-frequency components of the stimulation. However, ICS generates activation when the interfered field's envelope is near its maximum [46]. The latter can be illustrated as in fig. 3.2.2, showing zones where the kilohertz input stimuli collide, producing an ICS modulation (interference zones) and areas where one of the stimuli is predominant near its electrodes (non-interference zones).

A neuron located outside the interference zone is a neuron that is being reached by one of the high-frequency currents. In these zones, the interferential effect is

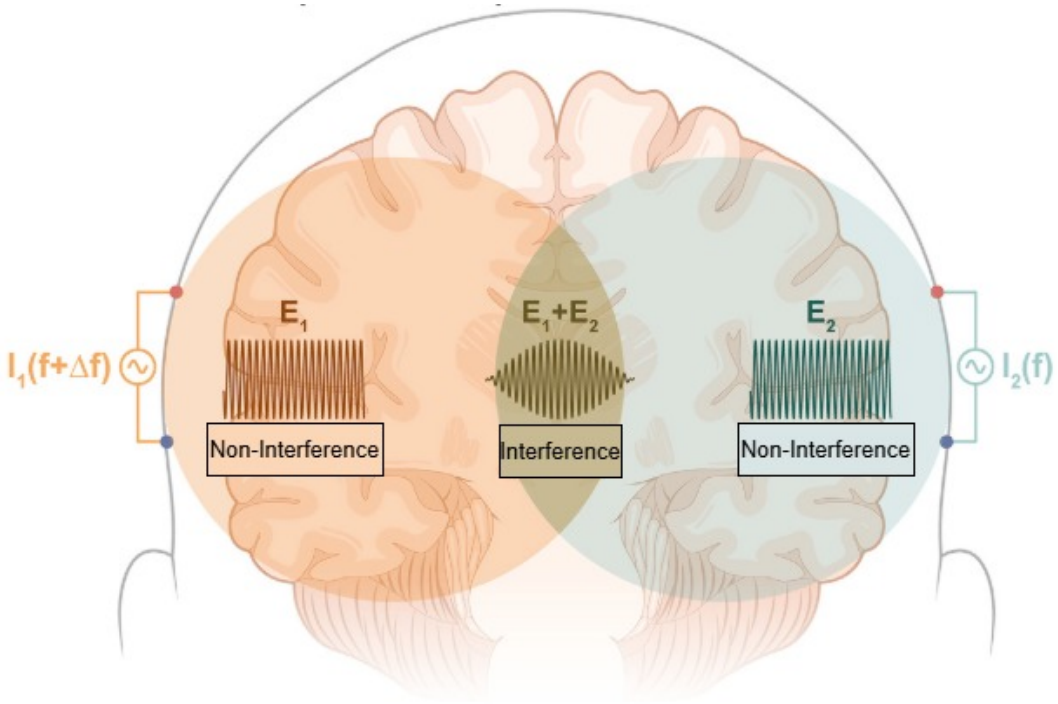

Figure 3.2.2: Diagram illustrating the intersection of the kilohertz stimulations and the generation of interference and non-interference zones.

not produced or strong enough to generate excitation. Mirzakhalili et al. [46] presented three challenging assumptions to understand what happens with the neurons in the non-interference zones:

- No effect: Neural membranes do not respond to high-frequency fields but are activated by slower-frequency components.
- Conduction Block: High-frequency stimulus inhibits the generation of action potentials due to time responses of the neural membrane.
- Other effects: A non-specified and randomised response of the neural membrane.

Conduction blocking is an inhibitory effect that affects the propagation of action

potentials along the nerve. This effect is produced by kilohertz stimulation between 20-40 kHz [49]. One of the principal characteristics of Nerve Blocking is that it is a reversible effect. The blocking ends as soon as the kilohertz stimulation has finished. However, a "carry-over" block effect can be produced so that the nerve can be blocked for a reduced period (<1 minute) without stimulation.

Zhao et al. [50] presented a simulation model based on the Frankenhaeuser-Huxley (F-H) axon model to determine the influence of applying local kilohertz electrical stimulation and its incidence in the propagation of action potentials. In fig. 3.2.3 is shown: a) the modelled axon, test and blocking stimulation experiment, and b) the resultant action potentials from the F-H axon model indicating the effective blocking produced by a 30 kHz, 10 mA stimulation.

The first assumption presented in [46] is incorrect. Several studies affirm that neurons respond to high-frequency stimuli [17; 49; 51; 52; 53]. Most of these studies validate the second assumption of conduction blocking, where the kilohertz stimuli are predominant, and no interference is produced.

3.3 FEM Simulation models of Interferential Currents

Simulation models bring another perspective on analysing electrical stimulation and ICS effects. One of its advantages is that we can easily modify parameters to evaluate variations in its behaviour. Simulation software allows us to implement

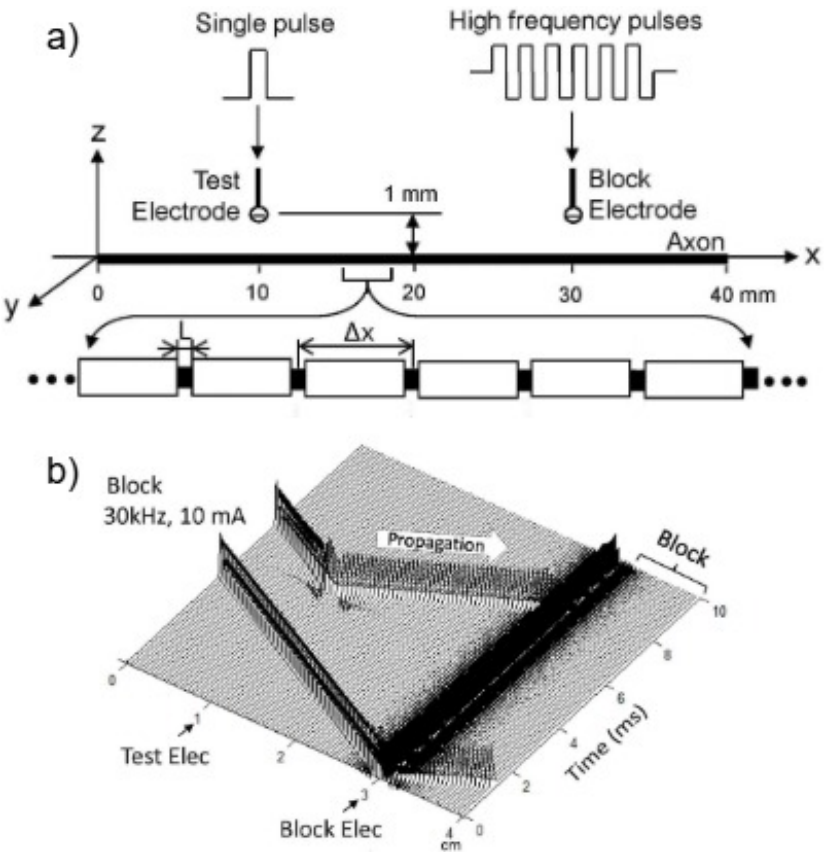

Figure 3.2.3: Simulation of the influence of the application of kilohertz electrical stimulation by Zhao et al. a) Scheme of the simulated experiment, using a 40 mm axon, applying a kilohertz stimulation of 30 kHz, 10 mA biphasic squared pulses and a single monophasic square pulse as a test stimulus. b) Membrane potentials calculated using the F-H axon model show the action potential generated by the test pulse and its propagation until it reaches the blocking zone.

biophysics models rapidly while considering tissue properties, such as conductivity and electrical permittivity.

Finite element modelling (FEM) is a numerical method for solving differential equations within boundary value problems [54]. The solutions are found by discretising space to construct a mesh of finite elements, which provides the numerical domain for the solution.

FEM provides a convenient method for setting up 3D models of structures, and

as such, the method can be extended to biophysical modelling of anatomical structures and physiological processes. The field of biophysical modelling is extensive and includes studies in organ dynamics [55], bone and prosthesis stress analysis [56; 57; 58; 59], stimulation electrode design [60; 61; 62], and stimulation of the neuromuscular and nervous systems [63; 64; 65; 66; 67; 68; 69; 70].

Recent studies have applied these methods to evaluate different scenarios of ICS application. Jabban et al. [48] present a simulated biophysical model of the upper limb to evaluate the effects of Somatotopic sensory feedback when applying interferential currents. They used Sim4life (Zurich MedTech AG) simulation software to model an upper-arm phantom, considering the Ulnar and Median nerves. Then, the electric fields are evaluated to determine the regions of neural activation. This group concludes that ICS can enable sensation stimulating the target nerves and reduce the skin sensation below the electrodes, although higher current intensities may be needed.

Cao et al. [71] modelled a single neuron model in a spherical head approximation. This study aimed to determine the neural response of a Hodgkin-Huxley neuron model using ICS to produce Deep Brain Stimulation (DBS). They observed that this simplified model does respond as expected for ICS. Although, they commented that nerves not only respond to the envelope of the interfered field. Finally, they conclude that a diode-based modulation may be a more accurate approach to the neural membrane response.

Manzouri et al. [72] modelled a conductive cylinder volume with different

neural fibres inside. They sought to demonstrate the mechanism of selectivity of activation in response to interferential current therapy. The simulation model was implemented in two stages: the volume conductor modelled in COMSOL and a McNeal neural model implemented in SIMULINK (MathWorks, Massachusetts, USA). They evidenced the presence of interfered zones and non-interfered zones inside the sphere. The fibres were exposed to only high-frequency stimuli in the zones where the interference was zero. Those nerves inside the non-interfered zone were unable to generate activation. This effect was especially evident under the electrodes; thus, this may explain how ICS can stimulate deep structures without activating cutaneous nerves.

3.4 Experimental Investigation on Interferential Currents

The ICS has been studied and applied since the 1950s, but lately, it has attracted more scientific community interest. It has many applications, such as analgesic treatments, specific muscle contractions, autonomic system control, and promoting bone and vascular healing [20; 42]. ICS is suggested for deep tissue stimulation due to reduced tissue impedance at higher frequencies, allowing for deeper penetration and predominant nerve stimulation via the beat effect [44; 45].

While various studies have explored ICS for Pain Relief [42] and Deep Brain Stimulation [73; 47], there is a lack of research on the neural activation mechanism triggered by ICS, particularly in the context of Functional Electrical Stimulation

(FES). Very few empirical studies have compared the transcutaneous current input with the excitatory output in terms of interstitial voltage, induced neural activation or muscle force. Animal experiments investigated the viability of Intracortical Stimulation (ICS) for motor control, as detailed in [74], which elicited activations on the sciatic nerves of mice, resulting in ankle dorsiflexion responses.

Adedoyin et al. [44] present the results of an experiment with osteoarthritic knee pain patients. The group was divided into interferential stimulation (standard ICS) and placebo groups (electrode positioning, detuned ICS). The results show that the interferential stimulation group had more effective knee pain reduction than the placebo group. Using ICS and TENS, Koca et al.[75] compared the effectiveness of reducing carpal tunnel syndrome pain. They concluded that ICS had better results than TENS in pain relief and highlighted its potential for ICS pain treatments. Although ICS is better than TENS, more studies with a more significant number of patients are needed to confirm that it is better.

Among the works focused on muscle contractions, Kozasa et al. [76] show NEMS's result over the soleus muscle using standard FES configuration and ICS. The results show that ICS produces higher plantar flexion torque and minor pain sensation than FES. They comment that these results may contribute to rehabilitation treatments for patients with central motor paralysis. Rogan et al. [77] studied the hamstring extensibility of football players. They found that the players can achieve an increased hamstring extension while ICS is applied rather than without stimulation. These results show the potential of ICS for motor rehabilitation

treatments. Bellew et al. [78] compared ICS with Russian waves, a known therapy for muscle strengthening. They propose that ICS serve as an effective waveform choice for stimulating muscle force. These results provide substantial new evidence that has important clinical implications for choosing waveform parameters when eliciting muscle force through NMES.

ICS muscle control treatments are not restricted to muscles responsible for limb movement. Zivkovic et al. [79] evaluated the effect of combining diaphragmatic breathing exercises with abdominal ICS in children with bladder and bowel dysfunction. They conclude that this treatment is beneficial in constipated dysfunctional voiders. Moore et al. [80] used ICS to induce gastrointestinal mobility in patients with motility disorders. They present this treatment as an alternative therapy to reduce constipation symptoms, a non-invasive and non-pharmacological intervention. Iizumi et al. [81] studied the effects of ICS on the superior laryngeal nerve. They suggest that this technique allows to induce swallowing and masticatory functions.

Interferential currents can also stimulate endocrine system glands. Hasegawa et al. [82] aimed to stimulate submandibular and sublingual glands by a noninvasive technique. The main objective was to increase the saliva production of patients with dry mouths. They found that ICS promotes saliva secretion by stimulating submandibular and sublingual glands, not producing pain or physical stress.

Interestingly, Ganne [83] reported that bone stimulation using ICS therapy might benefit bone healing for certain fractures. This method has the potential to be a

complement to the standard surgery treatments for bone fractures. Santos et al. [84] present an application based on ICS for attenuating blood pressure increase and vasoconstriction during exercise. The results show a promising use of this method for healthy subjects.

As reviewed, ICS has several applications and has demonstrated its beneficial impact on human health. However, all the previous works agree that more tests should be conducted to ensure the effectiveness of these treatments.

3.5 Influence of Electrode Positioning and Shape on the Application of Interferential Currents

Electrode positioning and shape seem to be highly important in specific motor muscle contractions. Botter et al. [85] mentioned that electrode positioning is critical for optimizing muscle tension and minimising discomfort. We must ensure that only the targeted muscle is excited in this case. The following section mentions possible positioning methods and electrode shapes controlling the position and depth of the interferential effect in ICS.

Most of the works mentioned in section 3.4 used a distribution of electrodes around the body segment located in the target structure, as shown in fig. 3.5.1 from [80]. As mentioned, the maximum interferential amplitude happens at a 45°intersection between the electrode projection. In those cases, the maximum amplitude can be found near the centre of the body segment. But what happens when our target

is not in the centre of the segment? How can we redirect the stimulation action lines to another position?

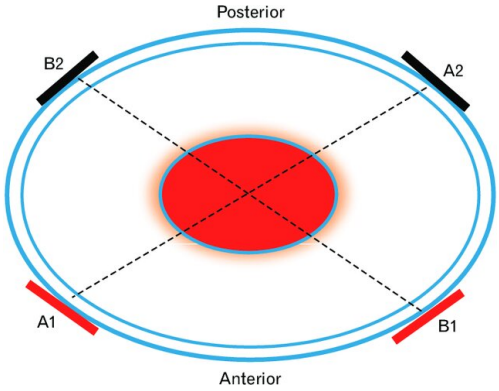

Figure 3.5.1: Scheme of a typical electrode placement configuration around the target. The intersection of the ICS can be found in the central region.

One solution is to reduce the inter-electrode distance from both stimulation sources, which will change the electrodes' projected action line angle. As the action lines change positions, the 45°intersection happens deeper (increasing distance) or superficially (decreasing distance). Another technique is to place the electrodes alongside the body segment instead of around it. In this configuration, we can concentrate the stimulation in a more specific zone.

Another aspect to consider is the area of action. Placing the electrodes with higher inter distances may increase the area where the stimulation is being applied. The latter may be beneficial if we target prominent structures like the diaphragm but not specific enough to target a single muscle or nerve branch. Having a more extensive area of action may be a problem for motor control stimulation since agonist and antagonist muscles are close to each other most of the Time. How can we reduce this area of stimulation?

The most common electrodes for superficial NMES are square-shaped layers with areas between 5∼20 cm^2 as shown in fig. 3.5.2. Different dimensioned electrodes have different selectivity and stimulation depths [86]. Considering that we are using four electrodes, the action area may not be narrow even if we get the electrode closer.

Figure 3.5.2: Square-shaped electrodes placed on a patient's arm during a pain relief ICS treatment.

Concentric ring electrodes appear to be an excellent solution for reducing the action area for stimulation. These electrodes consist of different ring-shaped electrodes with a central disc electrode. Multi-polar configurations can be mounted according to the number of ring electrodes. The main advantage of using concentric ring electrodes for a multi-polar setup is to reduce the electrical stimulation area [87; 88]. In fig. 3.5.3 is presented a scheme of a concentric electrode designed by Cassar et al. [89].

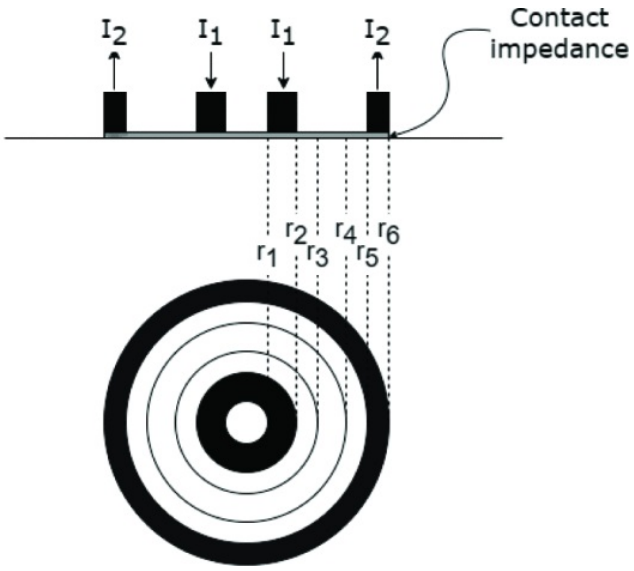

Figure 3.5.3: Concentric electrode design. Modelled by Cassar et al.

3.6 Chapter Discussion

Interferential current stimulation is a significant modality for promoting effective muscle contractions, reaching deeper neural structures, and alleviating the sensitivity of skin-afferent pain receptors. However, there is a notable absence of experimental evidence substantiating these benefits.

Given the multifaceted factors that influence the generation of modulated signals through interferential current stimulation, this technique is considerably complex in both understanding and application. The variation in electrical parameters and electrode configurations yields insights into its intricate nature, thus presenting numerous opportunities for its application.

There is a notable absence of experimental studies exploring the potential application of ICS in motor control therapies. This gap results in a limited

understanding of the mechanisms that underpin the motor and sensory responses influenced by modulated kilohertz currents. Consequently, there is also a deficiency in optimization techniques aimed at enhancing muscle contraction forces while mitigating the pain sensation associated with the activation of superficial afferent nerves. Our initial hypothesis posits that ICS can elicit these responses, particularly when electrode placement is optimized. In this context, we underscore the key motivations for investigating ICS as a viable alternative to FES in neurorehabilitation.

Chapter 4

Challenges in Non-Invasive Nerve Stimulation

Non-invasive electrical stimulation techniques, including Functional Electrical Stimulation, Russian wave stimulation, and non-invasive sacral root stimulation, have emerged as valuable tools in the field of neurorehabilitation. These methodologies confer therapeutic advantages without requiring surgical procedures and are applicable across various motor and autonomic functionalities, such as limb rehabilitation, postural control, and visceral modulation [18; 19; 20]. Their adaptability positions these techniques as promising interventions for enhancing recovery in individuals with various neurological disorders.

FES is extensively employed to facilitate rowing, gait and cycling exercises for individuals with spinal cord injuries; moreover, its application extends to upper limb rehabilitation in stroke patients, particularly in improving hand functionality. By engaging paralysed or weakened muscles through carefully timed stimulation, FES plays a crucial role in task-specific training [18; 22]. In this context, Russian

wave stimulation, known for its high-frequency burst patterns, has demonstrated efficacy in augmenting muscle strength and endurance [90].

Additionally, sacral root stimulation has gained clinical relevance in managing overactive bladder (OAB), a condition often associated with neurological impairments like spinal cord injury and multiple sclerosis. This approach modulates sacral afferent input, thereby regulating detrusor overactivity and enhancing patient quality of life [5].

Rowing is considered a case of use in this study because of its biomechanical and neuromuscular parallels to established FES applications, such as cycling and standing. Rowing facilitates rhythmic, reciprocal lower limb activation while simultaneously engaging the trunk and upper extremities, which is vital for effective postural transitions like sit-to-stand movements [91; 92; 93]. It also contributes to cardiovascular conditioning, full-body coordination, and bilateral effort, making it a valuable modality in neuromuscular recovery protocols that utilize electrical stimulation [93].

4.1 Rowing Exercise and FESRowing therapy

Rowing is a cyclical exercise that requires a coordinated and sequential movement of the lower and upper limbs [91]. This technique utilizes almost all the muscles, requires complex coordination between upper and lower limbs, and requires the athlete to move backwards, which is unnatural in other sports [92; 93]. This exercise demands high energy consumption, elevating cardiovascular and

pulmonary activity [93].

Rowing exercise execution can be divided into four phases [91; 92; 94] illustrated in fig. 4.1.1 by Held et al. [94]:

1. Catch: Defined as the beginning of the stroke. In the initial position, the legs flexed, the trunk inclined to the Front, and the arms fully extended (fig. 4.1.1.a).

2. Drive: To release the catch, the rower first extends the legs, maintaining extended upper limbs. And the trunk inclination (fig. 4.1.1.b).

3. Finish: The end of the stroke. The rower pulls the handle towards its ribs by flexing the upper limbs in this phase and inclining the trunk backwards (fig. 4.1.1.c).

4. Recovery: The rower returns from Finish to the catch position, following an inverse stroke sequence (fig. 4.1.1.d).

This research focuses on the impact of the lower limbs on rowing exercise. Thus, this document references the drive and catch phases of biomechanics.

FES Rowing is an exercise-oriented therapy that uses electrical stimulation to induce and control movement in the lower limbs to recreate rowing exercises. This technique combines voluntary movements (upper limbs) with electrically stimulated lower body exercise [95; 1; 96; 97]. These systems are in the experimental trial stage. Due to the instrumentation (stimulation and measurement devices), these experiments were carried out indoors using ergometers to simulate on-water rowing.

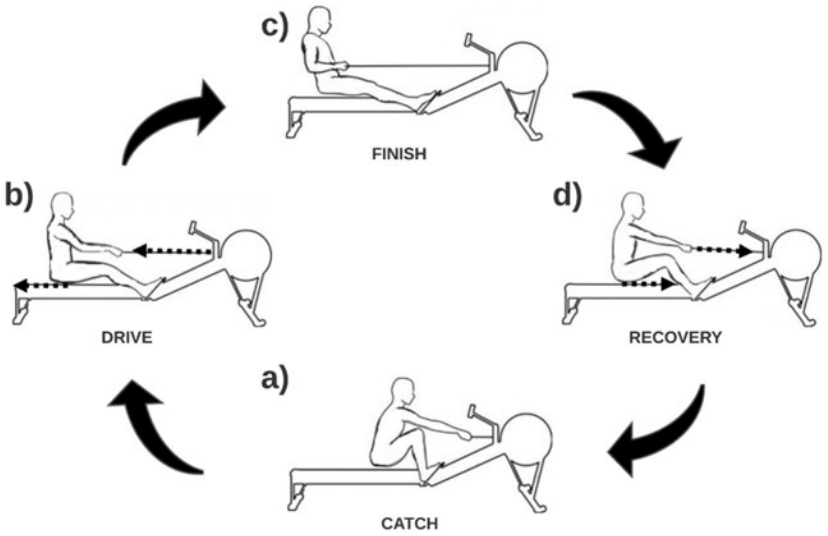

Figure 4.1.1: Rowing Cycle and its four stages: a) Catch, b) Drive, c) Finish, d) Recovery.

The fig. 4.1.2 shows the setup needed for FES Rowing training. Its principal aim is for individuals with spinal cord injury (SCI) who have reduced mobility, but it can also be applied to non-disabled or elite rowers' training.

People with SCI are among the most inactive population. Due to this, FES Rowing arises as an attractive alternative for increasing SCI patients' physical activity. Recent studies have shown that FES Rowing benefits cardiovascular and bone health [1; 2; 13]. Gibbons et al. [1] showed that FES Rowing produced an elevated metabolic cost compared with other FES-assisted or non-FES exercises, which is an excellent stimulus for cardiovascular health. It also reduces upper limb pain for people with SCI who use wheelchairs.

Chandran et al. [96] studied the effect of the tibiofemoral forces during FES Rowing. They affirm that mechanical bone stimulation by training is a non-pharmacologic mechanism for bone loss after SCI. FES Rowing produces weight-bearing activities

Figure 4.1.2: Training with an experimental FES Rowing system.

by applying forces on lower limb bones and junctions. Ye et al. [97] showed a systematic review of the clinical benefits of FES Rowing for individuals with SCI. They remark on the increase in oxygen consumption as an indicator of an effective high-intensity exercise and determine its efficacy.

4.2 Challenges in Non-Invasive Peripheral Nerve Stimulation

4.2.1 Motor Point Identification and Tracking

The motor point (MP) of a muscle is defined as the skin location closest to the terminal nerve branches; at this point, the muscle contraction is achieved with lower current intensities, i.e., where the activation thresholds are the lowest [98; 99; 100].

NMES procedures benefit from a priori mapping of MPs, guiding the positioning of stimulation electrodes. This optimises stimulation, maximising muscle contraction and reducing the discomfort due to the low activation thresholds. Thus, placing the electrodes over the MP is suggested [85; 98; 99; 100; 101; 102], and endorsed in different applications as botulinum neurotoxin administration [103; 104] and exoskeletons design and adjustments [105; 106].

Motor Point Maps have been presented to identify MP locations in the upper and lower limbs. Botter et al. [85] presented an atlas of motor points for the lower limbs, revealing a distribution of motor points within the quadriceps (vastus medialis, rectus femoris, and vastus lateralis), biceps femoris, and hamstring muscles for the 53 healthy subjects assessed. More specifically, they observed considerable inter-subject variability in the position of each motor point. Flodin et al. [107] presented a heatmap for guiding the location of the quadriceps muscle's motor point, finding a significant inter-individual variation in the locations of the motor point. Likewise, Moon et al. [103] reported a sex-dependent location of motor points more medially in male subjects.

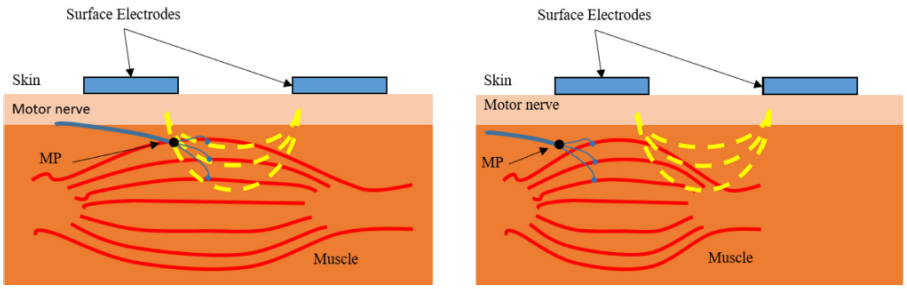

Figure 4.2.1: Diagram of the motor point shifting effect in response to a muscle contraction.

The muscles contract during movement, shifting muscle fibres and motor nerves.

However, the skin does not change its shape in the same proportion. As illustrated in fig. 4.2.1 by Ichikawa et al. [108], the motor point changes its position during a contraction, potentially moving outside the influence of the stimulation when applying FES.

In-vivo [109; 110; 111; 112] and ex-vivo [113; 114; 115] studies explored the relative location between muscle and skin. In particular, Fukui et al. [109] state that the skin slides over fascia layers, producing a change in the alignment of the skin and the underlying structures during movement. Wilke et al. [110] and Elsais et al. [111] studied these displacements using ultrasound measurements over the hamstrings and electromyography recording of the hip adductor, respectively. Both works considered isometric contractions for their studies and reported a relative muscle displacement of around 5 mm to the skin. Choi et al. [112] studied the movement of skin markers placed on different arm points. The subjects were asked to flex the elbow from fully extended to fully flexed. The results showed marker displacements up to 7.8 cm. They reported a differential displacement between muscle and the markers on the skin during contraction. Gonzalez et al. [116] demonstrated that the stimulation site significantly influences the elbow flexion angle at which contraction torque is maximal using an electrode array over the biceps brachii. These studies suggest that the motor point location likely changes during movement, possibly decreasing the electrically elicited muscle force for a fixed stimulation site.

Studies have explored how joint movements generate shifting of the motor points

and quantified their displacements. Ichikawa et al. presented a setup for tracking the motor point of the biceps brachii [117] and a motor point tracking study based on the elbow joint angle [108], registering a displacement of 1.2 *cm* in the transverse direction and 3 *cm* in the longitudinal direction in a range of elbow flexion of 90°. They stated that muscle contraction shifts the motor point and recedes the stimulus's current path. Hirai et al. [118] presented a similar approach, studying the triceps brachii motor point shift and finding a distal displacement of the located motor points. Matsubara et al. [119] studied the motor point shifting of the biceps brachii for different elbow flexions and palm orientations using electrode arrays and mechanomyography. These studies focus on tracking motor points in the upper limb, while lower limbs may present the same behaviour. The motor point shifting issue becomes critical when planning sports rehabilitation therapies, where it is necessary to precisely locate motor points of different muscle groups that will be cyclically contracted.

Another option is to directly target the nerve, avoiding tracking the MPs. This is particularly problematic as the principal branches of the motor nerves are deeper than the MPs. In the case of the femoral nerve, its principal branch starts from the lumbar plexus (roots L2, L3, and L4) and enters the femoral triangle, an area delimitated by the inguinal ligament, sartorius, and adductor longus muscles. This region in the upper anterior thigh leaves the femoral nerve exposed since there are no muscles in front of it, as illustrated in fig. 4.2.2 (obtained from [120]). Stimulating the femoral nerve region may activate its principal branch, generating a synergistic activation of the anterior thigh muscles.

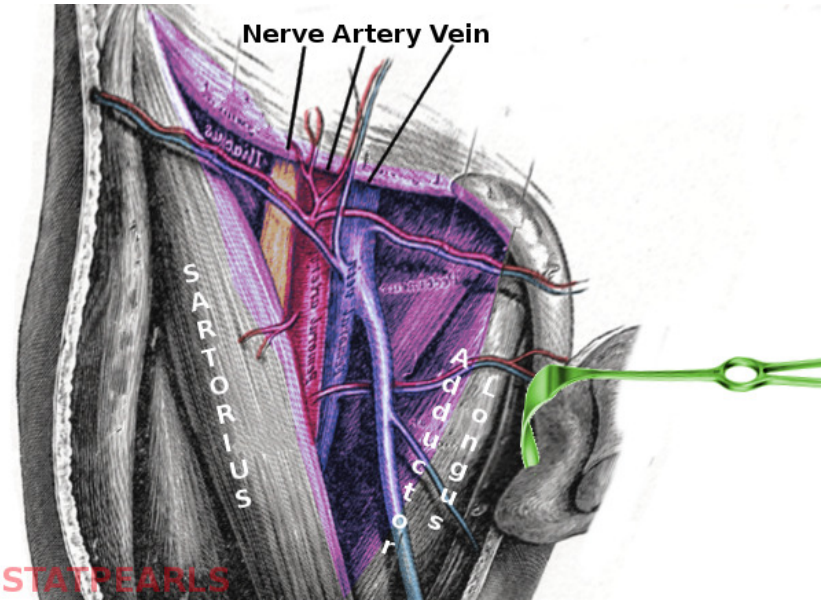

Figure 4.2.2: Illustration of the anatomy of the femoral triangle.

4.2.2 Control of Sequential Muscle Activation

As revised in section 4.1, the complete rowing cycle requires different movements that involve groups of lower limbs, upper limbs and core muscles. The complexity of the rowing technique demands an articulated sequence of muscle activation. Moreover, as a cycle, a coordinated activation of agonist and antagonist muscles enables restoration of the initial position and the start of the next cycle.

Studies have investigated muscle recruitment during the rowing cycle to better understand how forces are generated and transmitted [121; 95; 122; 123]. Wilson et al. [121] studied the recruitment patterns of gluteus maximus, rectus femoris, vastus lateralis, biceps femoris, gastrocnemius, and tibialis anterior muscles during the rowing stroke. They registered electromyography (EMG) and force of the mentioned muscles. The principal findings they reported were that during the drive phase, all monitored muscles were active, showing coactivation, even between

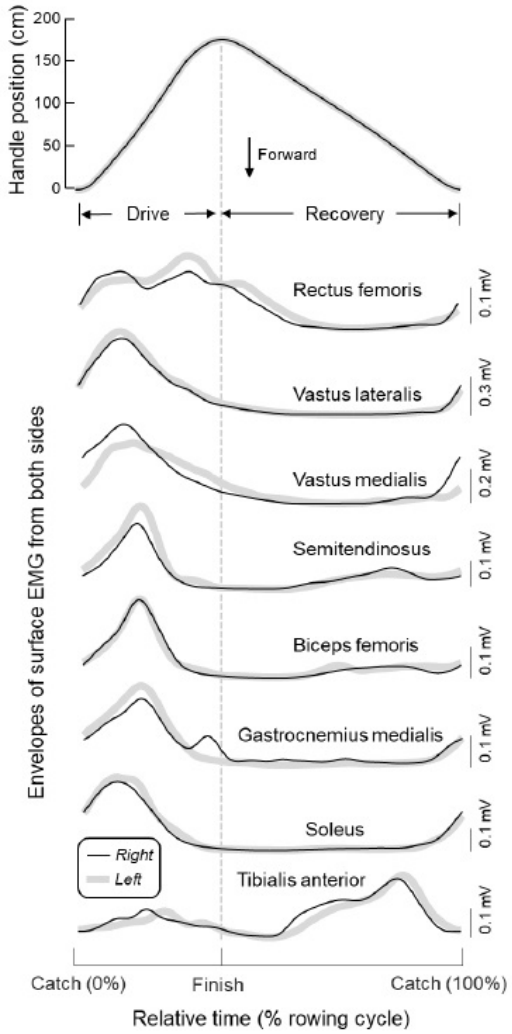

Figure 4.2.3: Electromyography measures of different thigh muscles during a complete cycle of rowing.

seemingly antagonistic muscles like the biceps femoris (knee flexor) and vastus lateralis (knee extensor). The gastrocnemius and biceps femoris played dual roles, including knee extension in late drive. Vieira et al. [95] studied the activation timing of the lower limb muscles involved in rowing. They measured EMG in eight muscles: the soleous, gastrocnemius medialis, tibialis anterior, rectus femoris, vastus lateralis, vastus medialis, semitendinosus, and biceps femoris, determining that vastus lateralis, vastus medialis, and soleus contribute the most to knee

extension, leaving the catch position and entering the drive phase. The timing of muscle activity was consistent, with no significant left-right differences. The sequence and pattern of activation registered by [95] is shown in fig. 4.2.3.

Knowing the muscles that contribute the most during a defined movement exercise allows us to determine better electrical stimulation strategies to recreate the movement. These muscles will be our targets and give us an indication of where the electrodes should be placed.

4.2.3 FES-Induced Discomfort and Pain

FES's main aim is to compensate for motor dysfunctions; however, its potential for physical therapy has been demonstrated. Although FES techniques present the disadvantage of generating mild discomfort or even pain due to the co-activation of sensory afferents near the target motor nerves [124; 125].

The latter is mainly produced by using surface hydrogel electrodes, which reduce the selectivity of neural structures. Also, as presented in section 1.3, the electrical parameter configurations can activate both sensory and motor nerves. The presence of discomfort by the patients may limit the effectiveness of the therapy, with an elevated risk of withdrawing the treatment [124].

Even so, surface hydrogel electrodes are preferred for sports rehabilitation assisted by FES because they are easy to place and dispose of. Optimisation of electrical parameters and electrode configurations is an alternative for reducing the evoked discomfort sensations [125].

Different studies have worked on finding the optimal procedure for reducing discomfort while using FES. Naaman et al. [126] compared different surface electrode sizes, types, and positioning, finding that size did not affect the discomfort reduction. Placing the electrode over the nerve rather than the motor point reduces discomfort. However, this technique may not be suitable for applications that need strong activations. Sakugawa et al. [127] studied the effect of pressure over the surface electrode over the reduction of discomfort. They found that applying pressure lowered the perceived discomfort while applying NMES on the femoral nerve. The latter seems to happen due to an approaching of the electrode to the targeted deep nerve. Chae et al. [128] compared percutaneous and surface electrodes in patients with chronic hemiplegia, where stimulation with percutaneous electrodes was significantly better tolerated. Nevertheless, in sports rehabilitation, percutaneous needle electrodes may not be suitable and potentially risky due to the constant movement.

For applications that require surface electrodes, there is a motivation to keep studying new strategies of electrode positioning, shapes, and electrical parameter configurations to optimise the selectivity and thus reduce the evoked surface discomfort inherent in FES techniques.

4.2.4 Chapter Discussion

As presented in section 4.2.1, section 4.2.2, and section 4.2.3, there are non-solved issues related to FES therapy effectiveness in the field of sports physical rehabilitation.

This thesis aims to propose and evaluate alternatives for FES therapy that potentially address these issues. It proposes combining modulated kilohertz stimuli (which perform local reduction of sensory afferent activations and higher penetration to reach deep nerves) with concentric electrodes (which improve selectivity), improving the techniques used for sports rehabilitation aided by NMES.

The present investigation uses the FES Rowing as a reference model to analyse the effects of innovative electrical stimulation strategies, particularly those employing kilohertz-frequency modulation. It further examines the optimisation of electrode design and positioning to enhance motor responses and patient comfort. While the techniques discussed are primarily validated within the context of FESRowing, their potential applications extend to other areas, such as upper limb rehabilitation in stroke patients and sacral stimulation for bladder control. These broader implications underscore the significance of this study in advancing non-invasive neuromodulation techniques across diverse clinical rehabilitation domains.

Finite element modelling and in-vivo testing were used to compare and evaluate the effectiveness of the proposed techniques. Different electrode positioning, shapes, and limb positions will be used to compare these techniques with conventional FES techniques. The points of comparison were muscle activation and reduction of discomfort. Along with these experiments, a novel technique for electrical steering of activation zones was proposed. The main advantage of this technique is that it does not require relocalisation of the electrodes.

Chapter 5

Thesis Hypotheses, Aims and Objectives

5.1 Hypothesis

Interferential current stimulation over the femoral nerve using multipolar concentric ring electrodes produces stronger muscle activation and less sensory discomfort than the standard single-channel FES using side-to-side electrodes.

5.2 General Objective

To propose new electrical stimulation strategies based on interferential currents using different electrode configurations on human limbs, validating them through computational models and in vivo trials.

5.3 Specific Objectives

1. To develop a finite element anatomical model of the upper thigh, square-shaped, concentric ring, and segmented electrodes.

2. To evaluate the effect of interferential current stimulation by simulating and analysing activation function distributions and nerve fibre activation predictions using the Hodgkin-Huxley axon model.

3. To define in-vivo trial protocols for FES and ICS for lower limb muscle stimulation and evaluate the response of healthy subjects' lower limbs by performing in-vivo tests, applying the proposed stimulation strategies, and comparing the motor effects on the lower limbs with the sensations reported by the subjects.

4. To evaluate a novel technique of electrical steering of the activation zones based on ICS unbalanced channel currents.

5.4 Scope and Limitations

This investigation aims to determine the feasibility of applying ICS using non-conventional electrode shapes and positioning. First, a step methodology of in silico and in vivo tests was prepared to probe the concepts of ICS functioning and test the applicability of the proposed new FES strategies. As an exploratory experiment, the number of volunteers is limited. This investigation is limited to applying in vivo tests on healthy volunteers.

Chapter 6

Methods

This investigation aims to evaluate new electrical stimulation strategies based on interferential currents. Two testing scenarios were chosen: thigh rectus femoris-induced contractions, which simulate the required contractions during the rowing drive phase, and finger flexor selective control, which is an ideal test bed for evaluating fine modifications to the stimulation strategies and configurations.

The strategies to be evaluated consider different electrode geometries (squares, rings, concentric and multiconcentric rings) and positioning (opposite, perpendicular, or collinear to the target nerve). They aim to stimulate motor points of the muscle of interest or reach the main branch of the nerve. Two stages of evaluation are presented: in-silico computational simulation and in-vivo experimentation.

6.1 Computational Modelling

Computational simulations help us understand the multiphysics behind the interaction of interferential currents. Moreover, when considering electrode configurations not currently used in clinical practice or tested by other researchers, these models provide insight into what to expect when applying ICS with the proposed electrode shapes and positioning by analysing the activating function and axon membrane potentials. Thus, they help design the testing protocols for human subjects.

6.1.1 Anatomical FEM-Design Considerations

An anatomical approximation model of the human thigh was modelled using the in-built Electric Current module in COMSOL Multiphysics v6.2. The anthropometric references were obtained from a cadaveric study of the femoral nerve [129], indicating that the mean thickness of the femoral nerve found was 0.72 cm, located at 3 cm depth.

A three-layered structure was used to model the most representative biological tissues: skin, fat, and muscle. The femur and the femoral nerve were included in the muscle volume. To reduce the complexity of the FEM model, a cylindrical approximation was implemented, considering measurements in table 6.1.1. An example of the cylindrical approximation of the human thigh is shown in fig. 6.1.1.

Gomez-Tamez et al. [130] showed the difference between geometric simplifications

Table 6.1.1: Dimensions of the different structures on the thigh FEM model.

Anatomical Structure	Measure *cm*
Thigh radius	8
Thigh length	10
Skin thickness	0.5
Fat thickness	0.5
Muscle radius	7
Femur radius	1.75
Femoral nerve radius	0.36

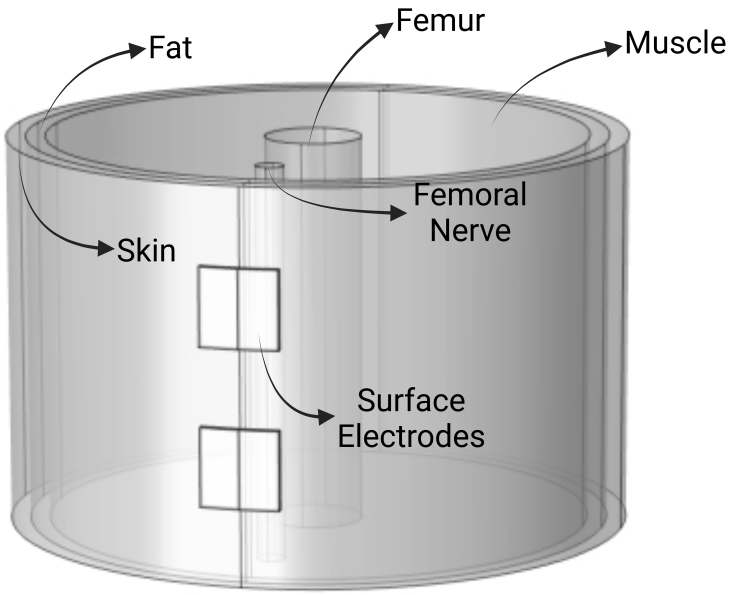

Figure 6.1.1: Example of a cylindrical approximate thigh FEM model.

and anatomical MRI-based models for FES. They compare a parallel rectangular layer model, a cylindrical layer model, and an anatomic thigh model. The models were implemented in COMSOL Multiphysics. The results showed that even with errors associated with interpreting activation thresholds, the cylindrical approach approximates better to the anatomical model than the parallel layer model. Also, these approximations followed the same variation tendency due to size and interelectrode distance changes. Thus, cylindrical approximations are suitable for these types of modelling tasks.

The dielectric tissue properties used on the models were obtained from the Tissue Properties database of the ITIS Foundation [131] and were selected for a working frequency of 4025 Hz, presented in table 6.1.2.

Table 6.1.2: Dielectric properties of biological tissues and electrode materials at a working frequency of 4025 Hz.

Material	Electrical Conductivity S/m	Relative Permittivity
Skin	2.01 x e^{-4}	1.13 x e^{3}
Fat	4.28 x e^{-2}	2.38 x e^{3}
Nerve	3.46 x e^{-2}	4.96 x e^{4}
Muscle	3.37 x e^{-1}	5.23 x e^{4}
Bone	1.02 x e^{-1}	1.34 x e^{3}
Electrode	8 x e^{6}	7
Hydrogel	38 x e^{-4}	1

Osorio et al. [132] presented a FEM study to evaluate the influence of mesh sizes and geometries on the calculation of electric potentials and activating function. For peripheral nerves using cylindrical simplifications, finer meshes are suitable for equilibrating a good performance on the electric variable calculations and reduced computational costs. Triangular and square mesh tessellations did not present notable differences. It also evaluates the effect of using Multiscale meshing techniques. Multiscale meshing allows us to control the number of elements, greatly reducing the computational cost. This technique defines different rules for mesh constructions according to their relative sizes. This means it is possible to define the volumes within the domain that require the smallest meshes and allow the rest of the domain to have relatively larger elements to help with the computational cost.

Thus, the finite element mesh of the tested models was created using triangular tessellations and a Multiscale approach. The femoral nerve and the electrodes

were set to have finer meshes (less distance between elements) rather than the skin, fat, muscle and bone structures. The table 6.1.3 shows the ranges of finite element mesh distances used for the FEM models. The fig. 6.1.2 shows the FEM mesh with the Multiscale technique. It shows a more dense concentration of elements in the nerve and electrode domains.

Table 6.1.3: Comparison of different mesh sizes ranges in a model of the human thigh

Standard Mesh type	Element size range *cm*
Normal	0.291 - 1.62
Finer	0.0647 - 0.89

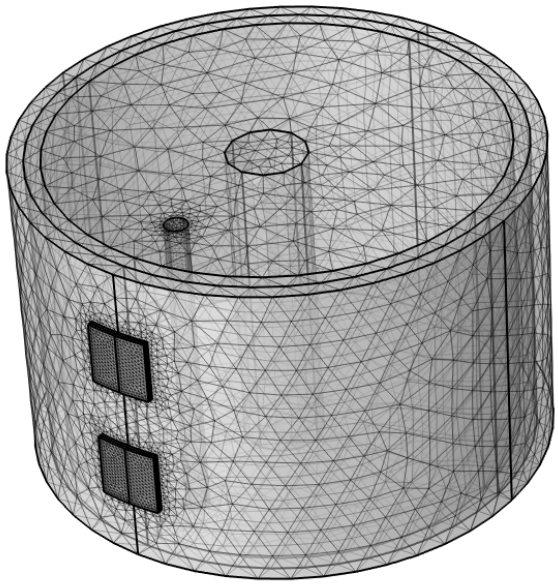

Figure 6.1.2: Thigh FEM mesh constructed using triangular tessellations and multiscale technique.

6.1.2 FEM Electrode Modelling

To specify the application of stimulating currents in the simulations, gel-based surface electrodes were modelled, having as a reference the off-the-shelf Valutrode

Axelgaard (Axelgaard Manufacturing Co., California, USA) electrodes. These electrodes consist of a conductive gel layer in contact with the skin layer and a conductive layer.

Three electrode shapes were modelled: Squared, Concentric, and Multiconcentric. The size specifications are shown in table 6.1.4.

Table 6.1.4: Modelled electrode dimensions

Electrode	Dimensions mm	Area mm^2
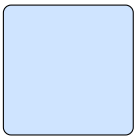	Side: 20	400
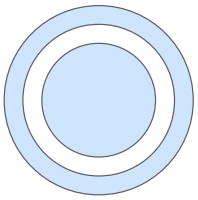	Central electrode radius: 7.5 mm Ring inner radius: 10 mm Ring outer radius: 12.5 mm	400 each
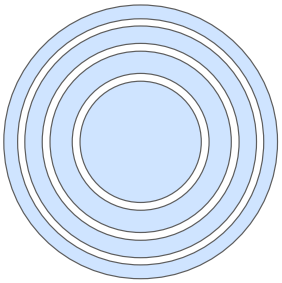	Central electrode radius: 8 mm First ring inner radius: 9 mm First ring outer radius: 12 mm Second ring inner radius: 13 mm Second ring outer radius: 15.25 mm Third ring inner radius: 16.25 mm Third ring outer radius: 18 mm	200 each

The configuration presented in fig. 6.1.1 was used for simulating the single-channel bipolar FES. Six different electrode configurations were modelled to test the ICS. These models are presented in fig. 6.1.3.

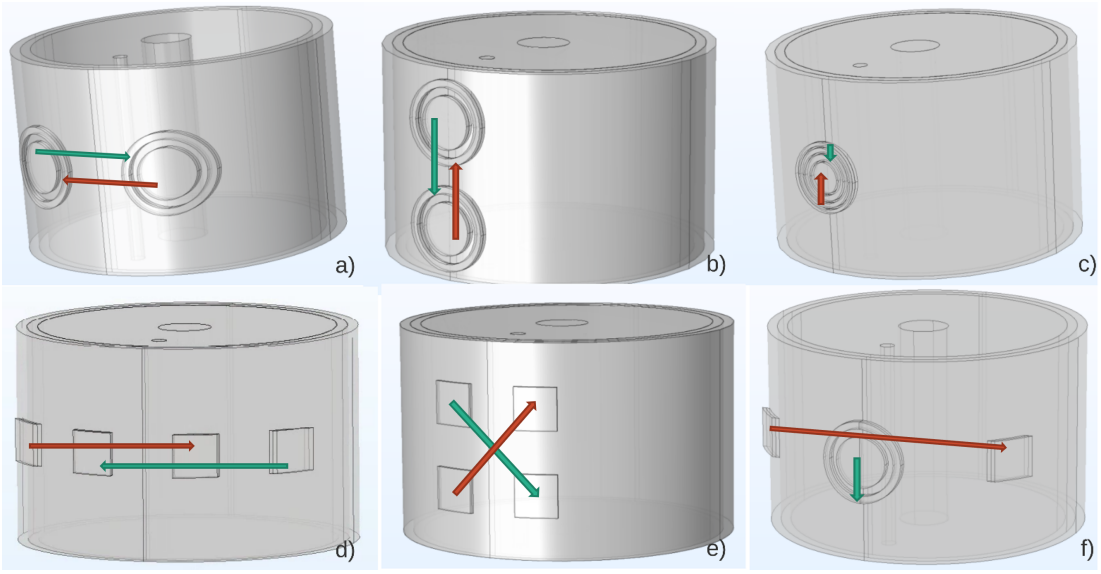

Figure 6.1.3: FEM models for ICS simulations. The green arrow indicates the pairing of channel 1, and the red arrow indicates the pairing of channel 2. a) Dual concentric ring – lateral, b) Dual concentric ring – collinear, c) Multiconcetric ring, d) Double pair side to side – front line, e) Double pair side to side – front double line, f) Hybrid (concentric and side to side).

6.1.3 Electric Parameters

The electric parameters used in the FEM simulations were configured as follows:

Single Channel FES:

- Frequency: 50 Hz.
- Waveform: Sinusoidal biphasic.
- Current Amplitude: 55 mA.

Interferential Currents:

- Frequency: 4000 Hz (Channel 1) and 4050 Hz (Channel 2). f_{beat} 50 Hz, $f_{carrier}$ 4025 Hz.

- Waveform: Sinusoidal biphasic each channel.
- Current Amplitude: 50 mA each channel.

6.1.4 Activating Function Calculation

Cut Lines were defined in the COMSOL models to calculate the unidirectional AF. The Cut Lines were positioned on the nerve axis (Z-axis) at the skin, skin to the nerve, and nerve level. The eq. (3.1.9) was implemented in its single-dimensional expression to calculate AM_{AF_z} on these levels.

For each configuration, three 1D activation function profiles are presented, calculated at the nerve, skin, and between nerve and skin levels. The 1D AF profiles are represented as mesh plots that show the unidirectional AF along the Cut Lines and how it changes over time, as shown in fig. 6.1.4. The left axis represents one period of the beat frequency (0 - 0.02 s), the right axis Cut Line length (0 - 10 cm), and the vertical axis activating function magnitude.

AF volumetric distributions were calculated using eq. (3.1.9) in its three-dimensional expression $AM_{AF_{(x,y,z)}}$. The AF was calculated for the entire volume and scaled by a logarithmic transformation. The fig. 6.1.5 shows an example of three views of the 3D AF distribution for the multiconcentric electrode configuration.

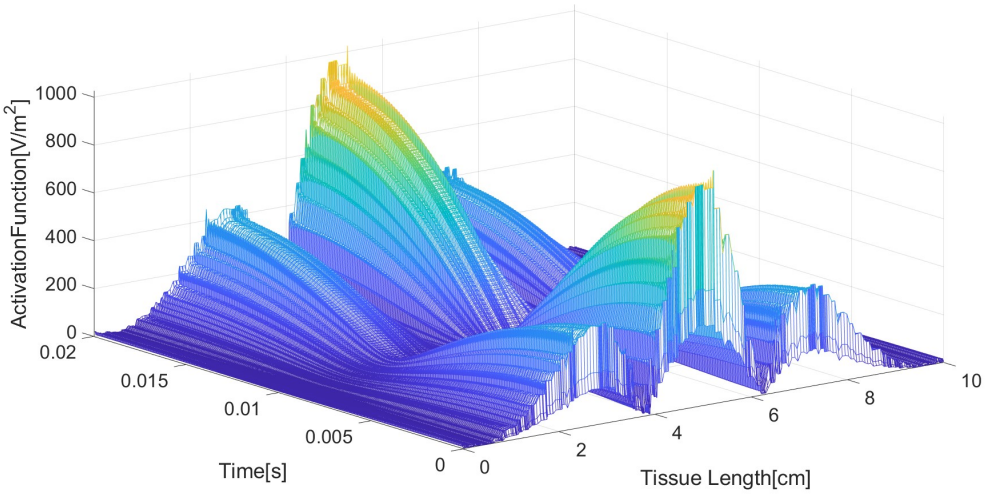

Figure 6.1.4: Example of 1D Activation Function profile at the nerve level simulating an ICS with a multiconcentric ring electrode configuration. Calculated using eq. (3.1.9).

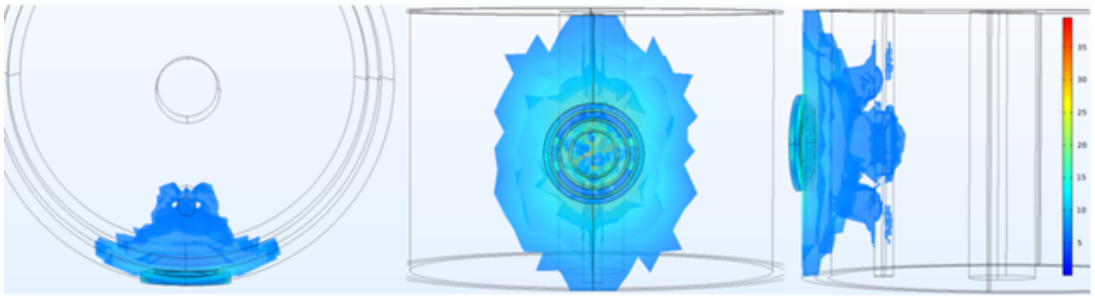

Figure 6.1.5: 3D Activation Function distribution for multiconcentric ring electrode configuration.

6.1.5 Hodgkin-Huxley Axon Model Coupling

As introduced in chapter 2, computational axon models are mathematical representations of nerve activation mechanisms. These models use extracellular potentials as input to determine the generation of action potentials and predict their propagation.

The previous FEM models were coupled with a Hodgkin-Huxley axon model. Dokos

presents this implementation in [133], which is modelled directly in COMSOL using the Partial Derivative Equation (PDE) in-built module. The input for the model was the femoral nerve extracellular potentials, calculated directly from COMSOL.

The H-H axon model is blind to the type of stimulation, and the potentials were not preprocessed nor calculated its envelope. The objective is to evaluate the generation of action potentials at the beat frequency, indicating that the nerve is activated at the configured modulated frequency. The model was configured for a 10 μm axon, resting membrane potential of 60 mV, and a simulation window of 50 ms.

The fig. 6.1.6 shows an example of the calculated membrane potentials for FES at 50 Hz with square electrode configuration. On the graphic, note that the central cathode is placed at a height of 5 cm, and the peaks show the generated action potentials. The APs are presented bidirectionally, with a separation of 20 ms between each AP corresponding to a 50 Hz activation.

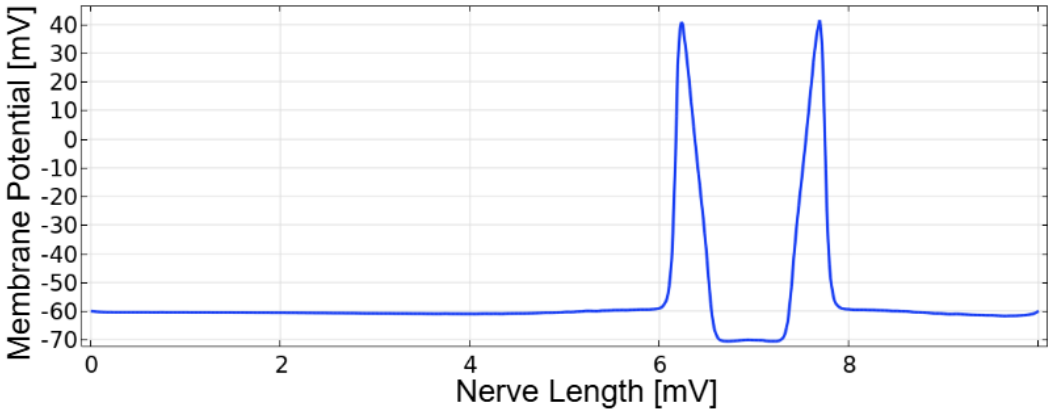

Figure 6.1.6: H-H activation prediction for FES at 50 Hz with square electrodes.

6.1.6 Unbalanced-Channels Electrical Steering

Grossman et al. [47] tested a technique to electrically move the activation zones towards different neural structures without replacing the surface electrodes. This technique uses interferential currents but configures the current amplitude output at a ratio between the two channels. They tested with implantable electrodes on rats to selectively move their whiskers, varying the ratio of the output channels of the stimulator.

Based on that technique, which we advocate naming "Unbalanced-Channels Electrical Steering," it is proposed to use the electrical movement of the activation zones, combined with surface electrodes, to target different peripheral neural structures. This technique can potentially control muscle groups sequentially, reducing the number of electrodes or stimulator output channels or tracking moving structures such as motor points.

Using the thigh FEM models, an in-silico validation of the phenomena was conducted in COMSOL. Squared and concentric electrodes were tested to evaluate the movement of the activation zones based on the calculation of the 3D modulated activating function $AM_{AF_{(x,y,z)}}$ using eq. (3.1.9). The tested output ratios were 1:1, 7:3, 4:1, 9:1, and 49:1, with a combined 50 mA output. The fig. 6.1.7 illustrates the thigh models used to test the Unbalanced-Channels Electrical Steering technique; the channels were paired separately, with channel 1 on the right and channel 2 on the left of the thigh. The dielectric properties and electric variables remain consistent with those previously presented.

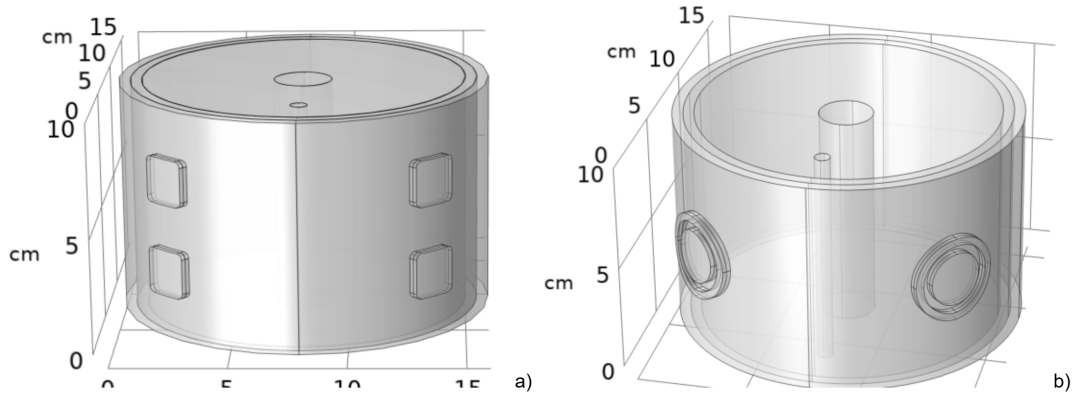

Figure 6.1.7: Thigh FEM models for evaluating the Unbalanced-Channels Electrical Steering technique. a) Square Electrodes, b) Concentric Electrodes.

6.1.7 High-Order ICS Modulation

Harmonic signals are commonly employed in radio electronics and electrical systems to measure alternating low-frequency electrical signals. In radio engineering systems, a sinusoidal form is also utilised for transmitting high-frequency signals [134]. Complex signals can be expressed as a sum of harmonic signals through trigonometric functions [134; 135].

High-order ICS Modulation is a proposed technique based on conventional harmonic signal construction to create stimulation waveforms compared to squared pulses, but it takes advantage of the modulated signal effect described for interferential currents. Two pre-modulated signals are considered as input for generating an ICS. For example:

Channel 1:

$$i_1(t) = \frac{\cos(7\omega t) + \cos(8\omega t) + \cos(9\omega t) + \cos(10\omega t) + \cos(11\omega t)}{10} \tag{6.1.1}$$

Channel 2:

$$i_2(t) = \frac{0.97\cos(12\omega t) + \cos(13\omega t) + 0.57\cos(14\omega t) + 0.24\cos(15\omega t) + 0.08\cos(16\omega t)}{5.72} \tag{6.1.2}$$

where ω is the angular frequency, with an arbitrary frequency f. The channel 1 input considers the 7^{th} to 11^{th} harmonics of the chosen frequency, while the channel 2 input considers the 12^{th} to 16^{th} harmonics. Using $f = 50Hz$, each channel generates the signals shown in fig. 6.1.8 and fig. 6.1.9, respectively.

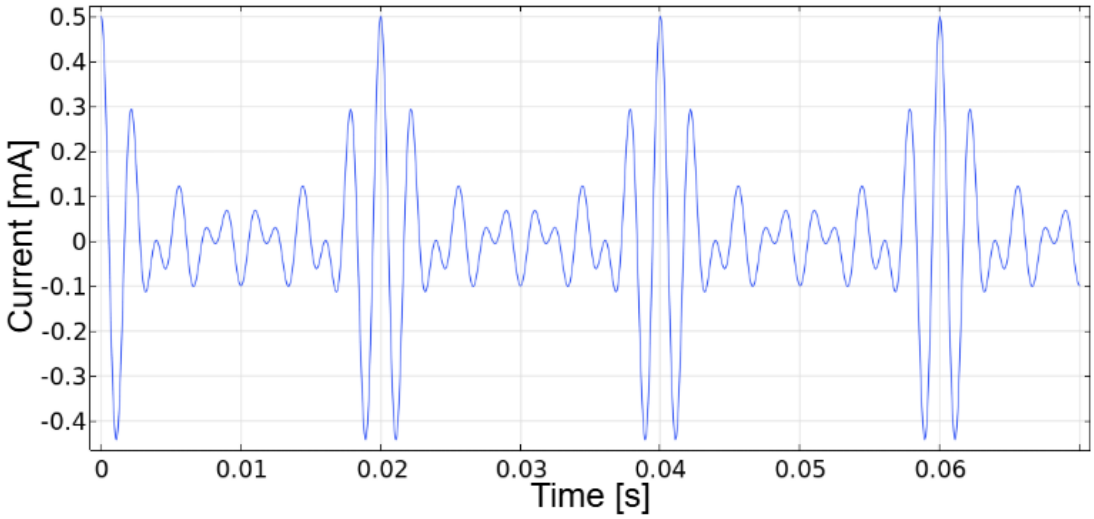

Figure 6.1.8: Output of the signal generated by eq. (6.1.1).

Using the basis of ICS, the resultant current will be produced by the collision of these outputs. Thus, the resultant synthesised signal will be:

$$i_{ICS(t)} = i_1(t) + i_2(t) \tag{6.1.3}$$

Generating the modulated signal shown in fig. 6.1.10, where it can be seen a periodicity of 0.02 s between each peak.

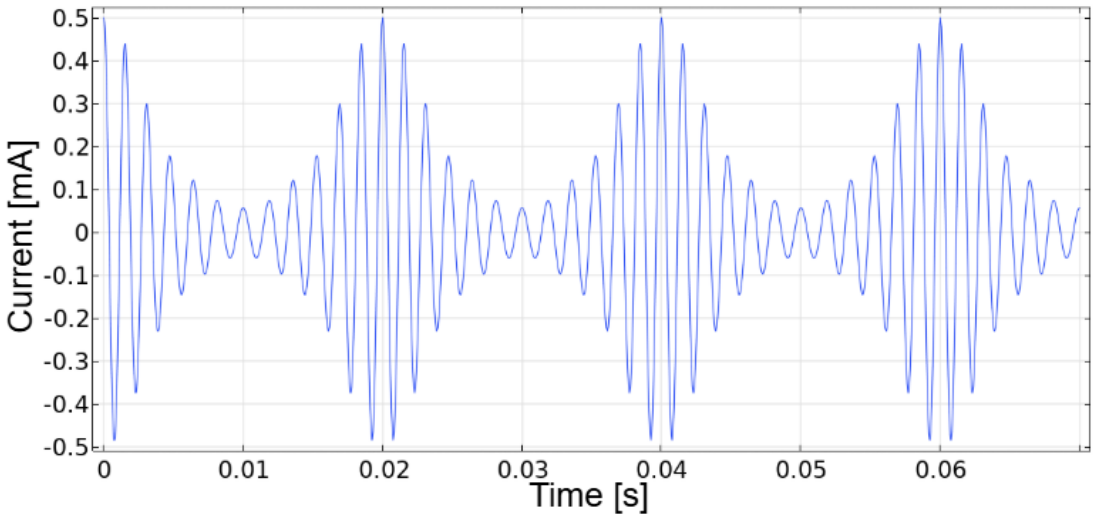

Figure 6.1.9: Output of the signal generated by eq. (6.1.2).

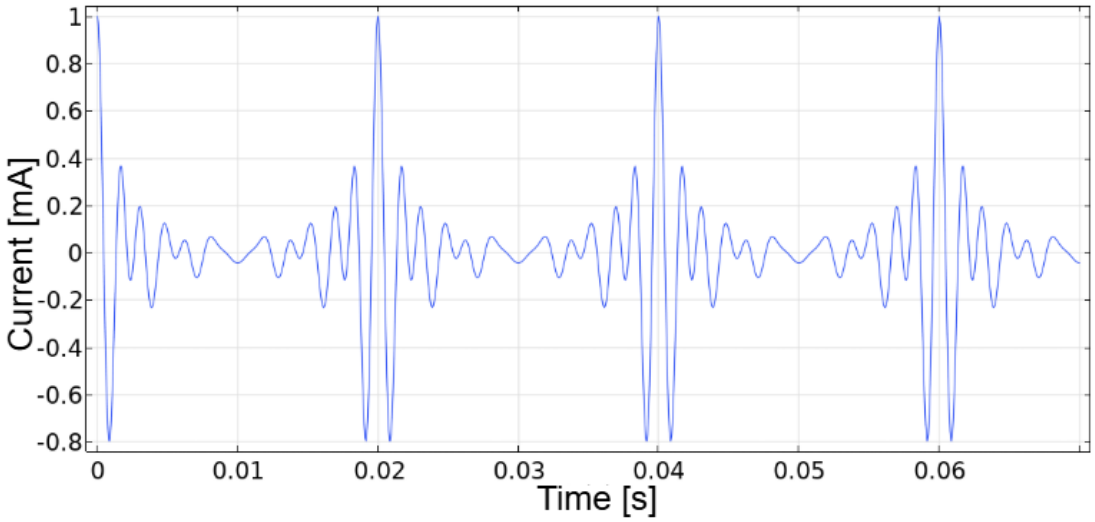

Figure 6.1.10: Output of the signal generated by eq. (6.1.3).

A basic cylindrical arm model was developed in COMSOL v6.2 to evaluate the High-Order ICS modulation. The model features a cylindrical representation of the arm, considering isotropic muscle tissue with an embedded nerve. Three distinct surface electrode configurations were modelled: Crosses Square, Collinear Nested Concentric, and Opposite Nested Concentric illustrated in fig. 6.1.11. An implementation of the Hodgkin-Huxley axon model from [133] was utilised to assess the generation of action potentials in the modelled nerve.

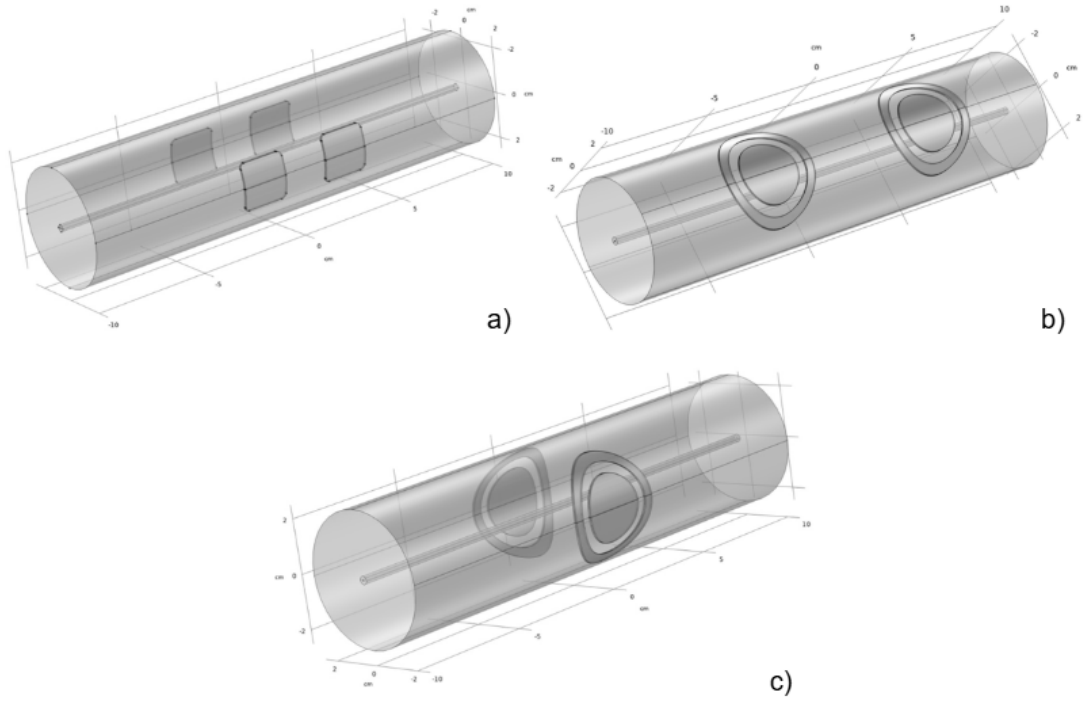

Figure 6.1.11: Cylindrical arm models for testing the high-order modulation technique. a) Cross square, b) Collinear Nested Concentric, c) Opposite Nested Concentric.

6.2 In-Vivo Experiments

In-vivo experiments contribute to evaluating the feasibility and practicality of applying ICS to human subjects using the proposed electrode configurations. These tests assess the motor and sensory response of applying the developed stimulation techniques.

6.2.1 Ethics

The study was conducted with the participation of healthy volunteers. Eligible participants included adults who did not possess any diagnosed respiratory or cardiac conditions that might impede physical activity, as well as individuals

without mobility restrictions in their lower limbs. Furthermore, participants were excluded if they had a history of cardiac issues, had implanted devices such as pacemakers, or were allergic to any materials used in the study. All subjects attended an introductory session in which the study's procedures and objectives were thoroughly elucidated, and they provided written informed consent prior to the commencement of the experiment. This study was conducted in accordance with the Declaration of Helsinki guidelines and received approval from the Vice-Rectorate for Research and Development at the Universidad de Concepción, Chile (CEBB 1605-2024).

6.2.2 Electrode Design and Manufacturing

The electrodes used in this study were laser-cut from commercially available 5x5 cm Valutrode Axelgaard (Axelgaard Manufacturing Co., California, USA) electrodes. The designs adhered to the dimensions outlined in table 6.1.4, incorporating a flange to prevent cutting the connector to the stimulator cables. The models were developed using Autodesk Inventor Professional (Autodesk, California, USA) and exported via cable to a CNC CO_2, 100W Laser Cutting Machine. The electrode dimensions are presented in table 6.2.1.

Table 6.2.1: Modelled electrode dimensions

Electrode	Dimensions mm	Area mm^2
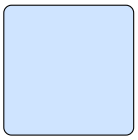	Side: 40	1600
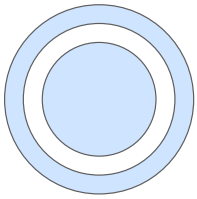	Central electrode radius: 11.3 mm Ring inner radius: 16.3 mm Ring outer radius: 19.8 mm	400 each
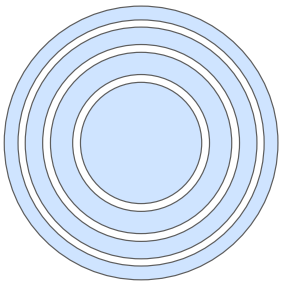	Central electrode radius: 15.8 mm First ring inner radius: 18.8 mm First ring outer radius: 24.8 mm Second ring inner radius: 27.8 mm Second ring outer radius: 32.2 mm Third ring inner radius: 35.4 mm Third ring outer radius: 38.8 mm	200 each

The laser intensity was configured not to burn the electrodes' hydrogel and conductive layer, preventing the edges from carbonising. This carbonisation may generate current density peaks, which can cause discomfort and tissue damage.

The process of cutting one electrode requires approximately one minute. Given the arrangement of the Axelgaard electrodes in conjunction with the laser cutting method, an entire batch of electrodes can be cut within less than one hour.

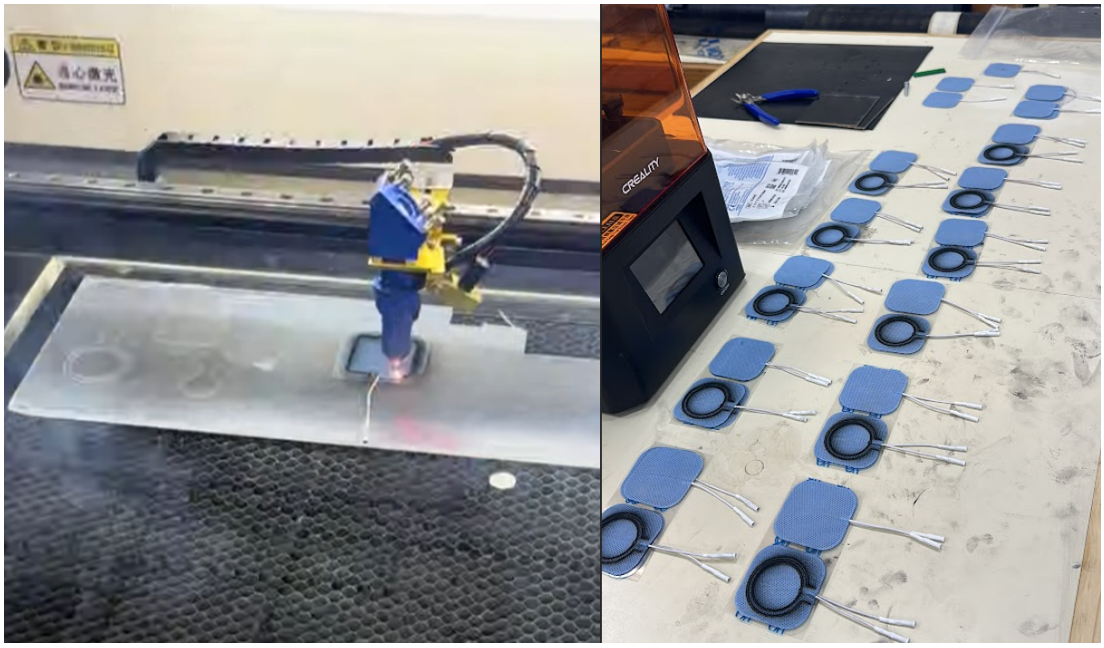

Figure 6.2.1: Laser cut process for making custom electrode geometries. 4x4 squared electrodes (left) and ring electrodes (right).

A demonstrative video of the electrode manufacturing process can be found in gitHub repository - Electrode Manufacturing.

6.2.3 Rectus Femoris Stimulation

As stated in section 4.1, the lower limbs play a critical role during the rowing exercise. Moreover, the quadriceps provide the greatest amount of force for the execution of the drive phase. These experiments aim to evaluate the effects of applying different NMES techniques over the Rectus Femoris portion of the quadriceps. The tests are separated into three stages:

- Motor Point Tracking: To evaluate the displacement of the MPs during simulated knee position emulating the drive phase.

- 50 Hz Functional Electrical Stimulation: The control test, the standard technique for functional muscle contractions.

- Interferential Currents Stimulation and New Electrode Configurations: The primary objective of this proposal is to develop a stimulation technique that alleviates discomfort sensations while enhancing the strength of muscle contractions.

To compare the forces produced by each stimulation technique, an assessment of the deformation of the thigh elicited by the contraction of the quadriceps was measured. A BIOPAC MP35 (BIOPAC Systems, Inc., California, USA) data acquisition unit was used to detect quadriceps contractions. The Measure unit was connected to a resistive rubber band and placed around the volunteer's thigh belly to transduce the thigh deformation into a measurable electric potential. The fig. 6.2.2 illustrates the positioning of the rubber band to measure the quadriceps contractions.

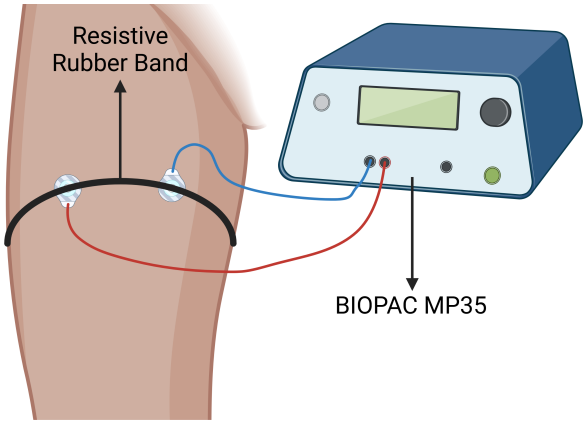

Figure 6.2.2: Rectus femoris contraction detector using a BIOPAC MP35 measurement unit and a resistive rubber band placed around the thigh. The deformations of the thigh are reflected in the rubber band by its stretching.

The McGill Pain Questionnaire was administered following each stimulation session to evaluate the subject's perception of discomfort. This questionnaire is organized into three categories of word descriptors: sensory, affective, and evaluative. These descriptors help subjects articulate their individual pain experiences. It also features an intensity scale and additional items that assess various pain characteristics. The questionnaire design aims to yield quantitative clinical pain measures suitable for statistical analysis [136]. A Spanish translation of the McGill questionnaire was used during the study, presented in fig. 6.2.3. The translation was made because all the subjects were native Spanish speakers.

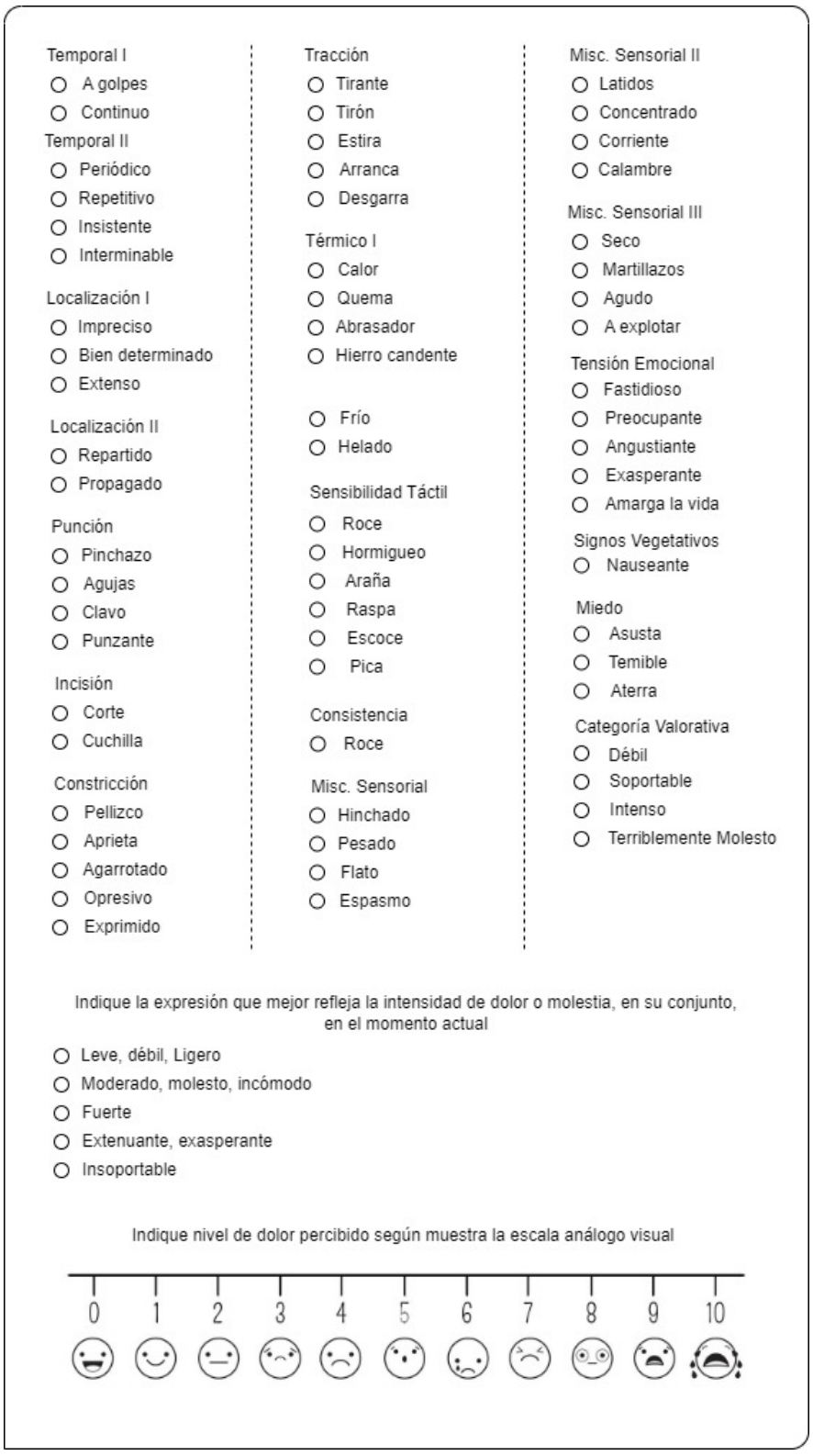

Figure 6.2.3: Modified McGill pain questionnaire, translated to Spanish.

6.2.3.1 Motor Point Tracking

An Ultima Neo Pro electrical stimulator (Pain Management Technologies, Ohio, USA) was utilized in this study. The stimulus was configured with a pulse width of 250 μs and a frequency of 20 Hz, and a monophasic squared wave. The current intensity was gradually increased from 1 mA to 30 mA, if necessary, to identify the motor point location and activation threshold. A monopolar setup was employed to map motor point locations with a 5x10 cm^2 patch electrode alongside a 1 cm^2 pen electrode. The patch anode was placed on the frontal thigh surface, positioned two-thirds down the thigh length, with the iliac crest as a reference point. The pen cathode was manoeuvred over the skin while scanning for the motor point. The motor point atlas by Botter et al. [85] was referenced to minimize the search area for the rectus femoris proximal motor point. To enhance skin-electrode contact, ultrasound gel was used to cover the pen electrode.

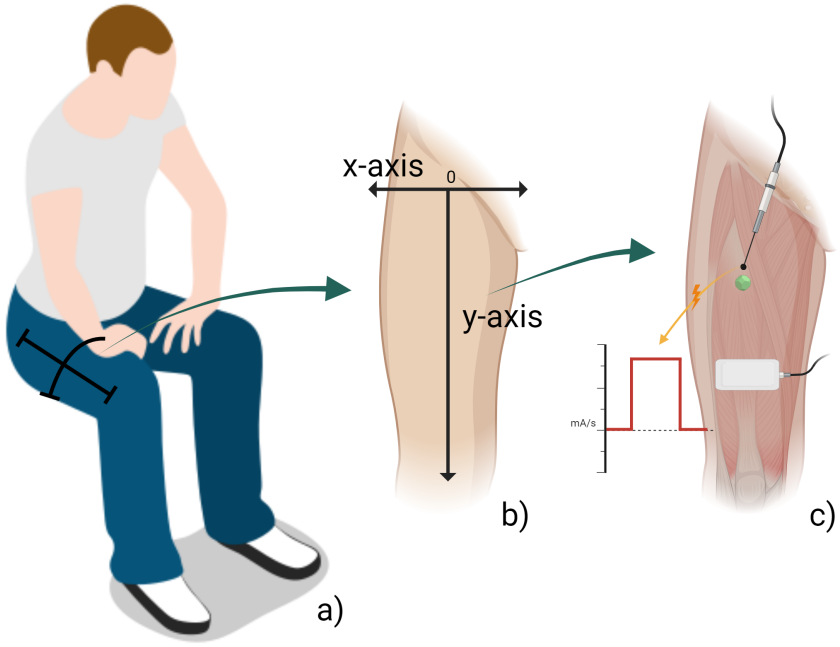

Figure 6.2.4: Thigh measurement references and motor point identification. a) Thigh length was measured from the iliac crest to the anterior part of the patella, and thigh thickness was measured around the belly of the quadriceps. b) Cartesian plane (x, y) to locate the motor points positions. c) An electrical stimulus is applied to find the rectus femoris motor point.

Participants were instructed to wear loose shorts and sit comfortably, ensuring both feet were flat on the floor with a 90° knee bend. The length of the dominant leg's thigh was assessed using the iliac crest and the anterior aspect of the patella as reference points. Thigh thickness was measured at the midpoint of the quadriceps, about one-third down the thigh from the iliac crest, as shown in fig. 6.2.4. Scanning occurred at three knee extension angles: 90°, 120° (partially extended), and 180° (fully extended). Participants positioned their feet on a chair in front of them to facilitate these different extensions.

The motor point was identified for each position at the skin location where the lowest current intensity causes a visible and palpable muscle contraction [85].

These motor points were marked with a plastic adhesive jewellery diamond. We defined their spatial location using the intersection of the thigh mid-line and the coronal projection of the iliac crest as a reference, based on the Cartesian plane illustrated in fig. 6.2.4. The coordinates of the motor points (x, y) were recorded as absolute values for every subject.

6.2.3.2 50 Hz Functional Electrical Stimulation

Standard single-channel stimulation was implemented after identifying the best electrode position through motor point tracking. Participants were comfortably seated in chairs with their feet flat on the floor. A second chair was placed in front of the subject to adjust to various knee flexion levels and act as a footrest. The overall test scheme is illustrated in fig. 6.2.5.

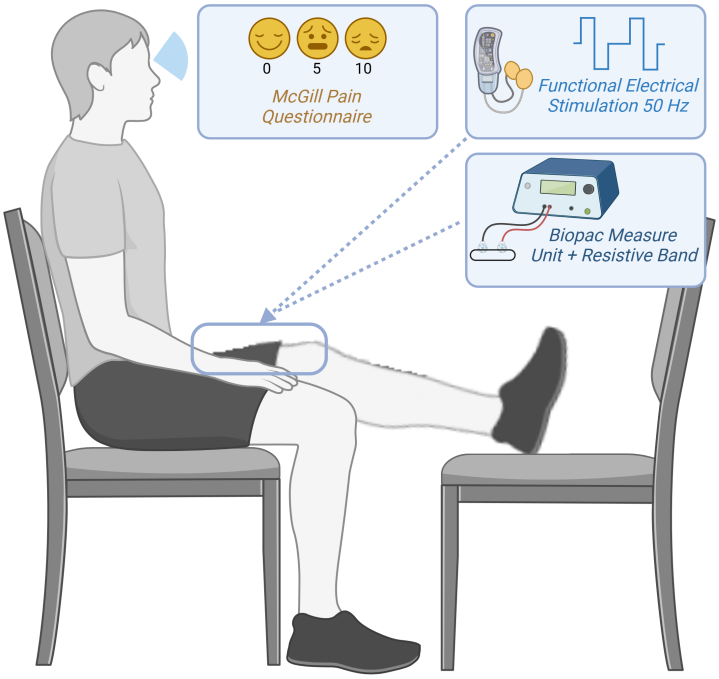

Figure 6.2.5: Diagram of the 50 Hz FES experiment setup.

The BIOPAC MP35 data acquisition unit was used to detect quadriceps contractions. The Measure unit was connected to a resistive rubber band and placed around the volunteer's thigh belly to transduce the thigh deformation into a measurable electric potential. Two 4x4 cm squared electrodes were placed at the 90° (cathode) and 180° (anode) MP locations, as illustrated in fig. 6.2.6.

The stimulator was set up to provide symmetrical biphasic rectangular pulses at 50 Hz for 5 seconds. The current amplitude was gradually raised in 1 mA increments until a visible contraction occurred, and the current required was noted as the threshold activation value.

After stimulation, the McGill Pain Questionnaire was used to evaluate participants' comfort levels. These metrics acted as control measures for comparison against interferential stimulation. The stimulation procedure was repeated for knee flexion angles of 120° and 180°.

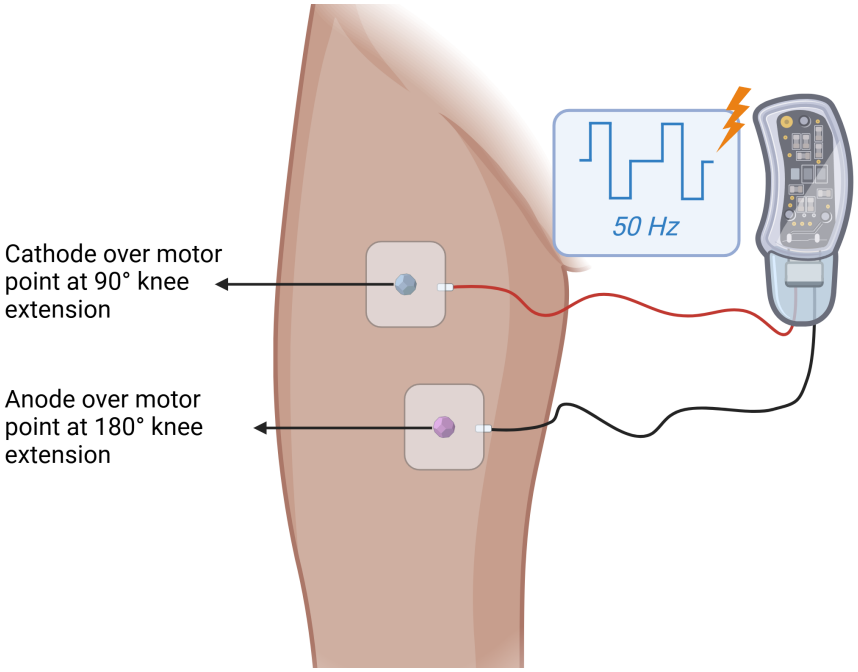

Figure 6.2.6: Electrode placement for the 50 Hz FES experiment setup.

6.2.3.3 Interferential Currents Stimulation and New Electrode Configurations

In this stage, we assessed the motor and sensory responses to six suggested electrode configurations using ICS. Participants were seated comfortably, with their feet resting flat on the floor. A second chair was positioned in front of each subject to accommodate different knee flexion levels and serve as a footrest. The complete test setup is shown in fig. 6.2.7.

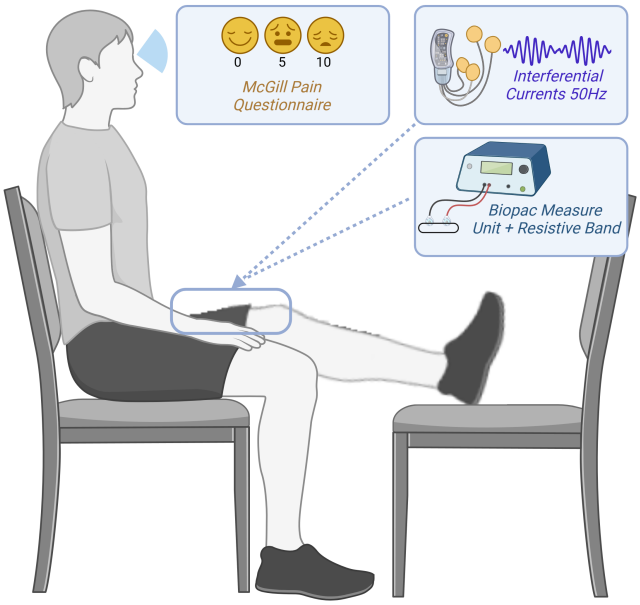

Figure 6.2.7: Diagram of the ICS experiment setup.

A BIOPAC MP35 data acquisition unit was used to detect quadriceps contractions. The Measure unit was connected to a resistive rubber band and placed around the volunteer's thigh belly to transduce the thigh deformation into a measurable electric potential.

The Ultima Neo stimulator operated in IF mode to generate symmetrically balanced sinusoidal waves. The current intensity was increased in increments of 1 mA, reaching a maximum of 30 mA per channel, with both channels rising together.

During this phase, six electrode configurations were evaluated. The first five configurations were positioned over the identified motor points of the rectus femoris, while the sixth configuration targeted the femoral triangle, focusing on the main branch of the femoral nerve:

a) Square electrodes: Channel 1 electrodes were placed over the MP at 90° (cathode) and 180° (anode) knee flexion. Channel 2 electrodes were placed perpendicular to the channel 1.

b) Dual Concentric electrodes: Electrodes for Channel 1 were positioned over the MP at a 90° knee flexion, while Channel 2 electrodes were positioned over the MP at a 180° knee flexion. The centres of the inner cathodes were aligned with the identified MPs.

c) Nested Concentric electrodes: Followed the same placement of b), with the difference of swapping the anodes of each channel. Uses concentric electrodes in a side-by-side pairing.

d) Hybrid configuration: Channel 1 was connected to square electrodes placed over the MP at 90° (cathode) and 180° (anode) knee flexion. A concentric ring electrode was connected to channel 2 and placed mid-distance between the side-to-side electrodes.

e) Multiconcentric over motor points: The centre of the inner electrode was placed over the MP at 90°knee flexion.

f) Multiconcentric over femoral triangle: The centre of the inner electrode will be placed over the femoral triangle.

A scheme of the six proposed configurations is presented in fig. 6.2.8.

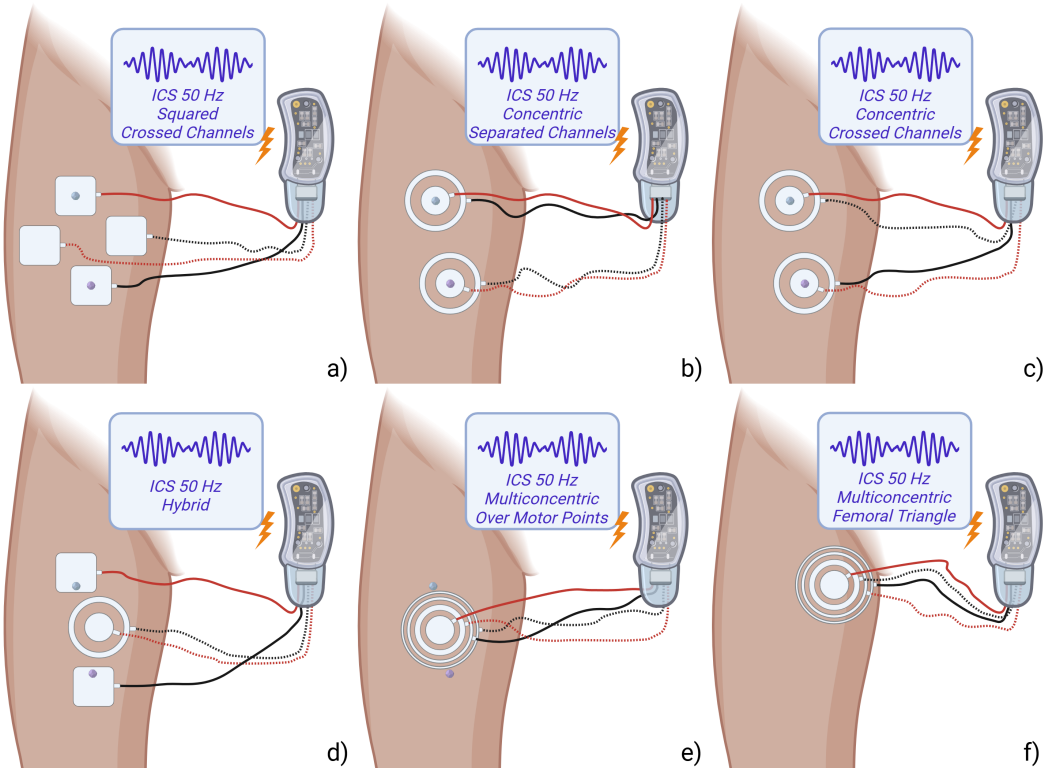

Figure 6.2.8: Electrode placement for the ICS experiments setup. Solid colour wires indicate channel 1, and dotted wires indicate channel 2. a) Square crossed channels, b) Dual concentric, c) Nested Concentric, d) Hybrid, e) Multiconcentric over motor points, f) Multiconcentric over femoral triangle.

6.2.4 Influence of Electrode Shape and Positioning in ICS on Finger Flexors

The forearm testbed offers a practical method for assessing the motor and sensory responses to electrical stimulation. This is primarily due to the superficial depth and proximity of the ulnar, median, and radial nerves. Additionally, when evaluating finger flexion and/or adduction, it is straightforward to identify which nerve is being stimulated and determine the specificity of the stimulation. The oval shape of the wrist and forearm facilitates consistent variation in electrode positioning during various tests, thereby minimizing inter-subject variability.

During these tests, a Visual Analogue Scale (VAS) for pain was applied to assess the intensity of discomfort during the experiments. The VAS is a validated scale used to represent and quantify the subjective sensations of patients. This scale is divided into eleven steps, from 0 (no pain) to 10 (worst pain ever felt). The fig. 6.2.9 illustrates an example of VAS for pain.

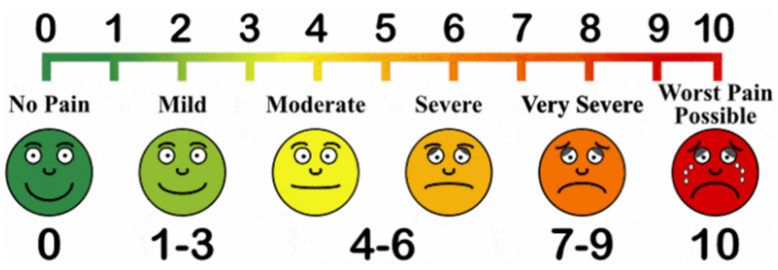

Figure 6.2.9: Visual Analogue Scale for pain.

6.2.4.1 Square Electrodes Around Wrist

Six healthy volunteers (three males and three females, 22-43 years) participated in the study. The subjects were asked to remain seated with their right forearm resting on a table. The subjects' wrist circumferences were measured using a measuring tape (17.35 $cm \pm 1.90$). After an alcohol wipe cleaning, four 4x4 cm squared electrodes were positioned around the wrist as illustrated in fig. 6.2.10. Two different electrode positions were used: lateral and anteroposterior of the wrist (L/AP configuration) and diagonal to the wrist (Diagonal configuration). The stimulation channels were shifted to obtain a crossed or separated pairing, as shown in Figure 6.2.10.

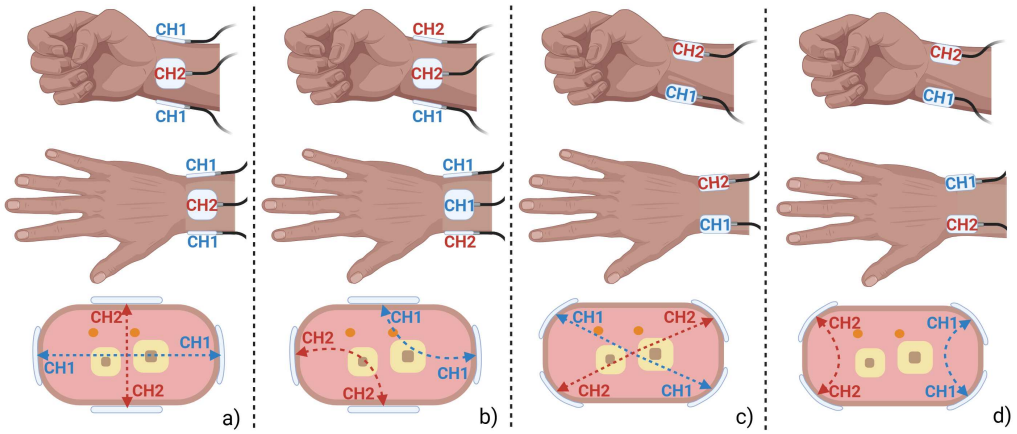

Figure 6.2.10: Representation of the electrode placement around the wrist using 4x4 cm squared electrodes. From top to bottom: Frontal view of the hand, back view of the hand, and transverse section of the wrist viewed from the forearm (The orange dots represent the median and ulnar nerve, the yellow squares represent the ulna and radius). CH1 and CH2 represent the stimulator channels. **a)** Lateral and anteroposterior placement - crossed channels configuration. **b)** Lateral and anteroposterior placement - separated channels configuration. **c)** Diagonal configuration - crossed channels. **d)** Diagonal configuration - separated channels.

The Ultima Neo Pro stimulator generated sinusoidal waves at 4000 Hz and 4020 Hz, obtaining an interferential current with a beat frequency of 20 Hz. Each subject's current intensity was slowly increased by 1 mA until a visual finger motor response was achieved, determining the activation threshold with a maximum of 30 mA per channel. At the threshold current, the stimulation remained active for 4 seconds.

This experiment aimed to determine which configuration performs better for eliciting a flexion and abduction of the thumb by stimulating the median nerve and avoiding motor responses of fingers innervated by the ulnar nerve. Additionally, the plastic probe method allowed us to determine whether the kHz stimulus had

a local effect, as postulated by [46], determining if a conduction block is generated. The participant's sensory appreciation of the level of discomfort at the threshold currents was assessed by applying a Visual Analogue Scale (VAS) for pain [137].

6.2.4.2 Square Electrodes Along Forearm

The study involved five volunteers, three females and two males aged 27 to 32 years. Participants were instructed to sit with their right forearm resting on a table, allowing their hands and fingers to relax. The circumference of their wrists was measured using a measuring tape, averaging 16.3 cm ± 1.79. After cleaning with an alcohol wipe, four electrodes measuring 4x4 cm were placed on the anterior forearm in two different configurations, as illustrated in fig. 6.2.11. The channels were adjusted for each configuration to change the current path interaction and assess its impact on the resulting interferential current.

The Ultima Neo Pro stimulator generated interferential sinusoidal currents at 4000 Hz and 4020 Hz, resulting in an interferential current of 20 Hz. The current intensity for each participant was gradually increased by 1 mA until they could visually perceive finger contractions, which was noted as the current intensity threshold. The participant's sensory appreciation of the level of discomfort at the threshold currents was assessed by applying a Visual Analogue Scale (VAS) for pain. During a 4-second stimulation at this threshold intensity, the activation of skin afferent nerves was assessed using a plastic probe moved across the skin between the electrodes. At the same time, the volunteers were instructed not to observe their forearms.

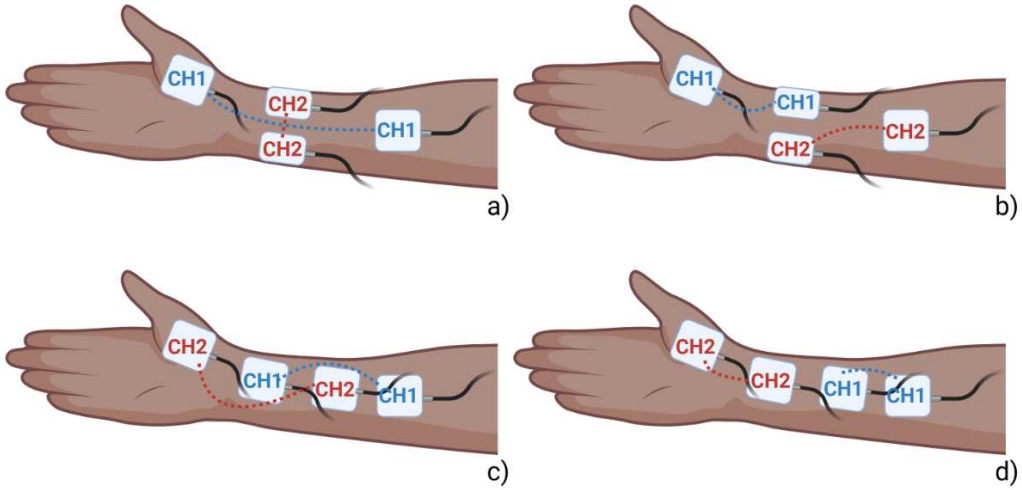

Figure 6.2.11: Representation of the electrode configurations along the forearm using 4x4 cm squared electrodes. The electrodes are placed with the median nerve as a reference. a) Perpendicular placement - crossed channels. b) Perpendicular placement - separated channels. c) In-line placement - crossed channels. d) In-line placement - separated channels. The distal and proximal electrodes are separated by 11 cm. In a) and b), the central electrodes are placed midline between the proximal and distal electrodes, separated by 4 cm. In c) and d), the electrodes are separated by 1 cm.

The configurations of these electrodes aimed to stimulate the median nerve for precise thumb flexion and abduction, assessing how promoting the crossing of current paths influences the management of interference zones. If stimulation activates additional fingers, it is deemed non-specific. Additionally, this setup helps detect any conduction block caused by the input currents at kHz.

CeraVe cream (CeraVe, L'Oréal, USA) was used to evaluate the influence of moisturisation during the use of gel-based surface electrodes. The electrodes were placed as indicated in Figure 6.2.11a. The tests were not replicated for the rest of the configurations shown in Figure 6.2.11, as the moisturising cream reduced the adherence of the electrodes. To ensure the electrode/skin contact, a piece of fabric was used to wrap the forearm and maintain the electrodes in

place. However, current thresholds and sensory assessment were registered for one subject to further compare with ICS stimulation using surface electrodes without the application of cream.

6.2.4.3 Concentric Electrodes Along Forearm

Four volunteers aged 22 to 28 (three males and one female) participated in the study. They were instructed to sit with their right forearm resting on a table. Following cleaning with an alcohol wipe, two concentric ring electrodes were placed in the base of the thumb and the mid-forearm, as indicated fig. 6.2.12. The stimulation channels were adjusted to create either a separated or nested pairing.

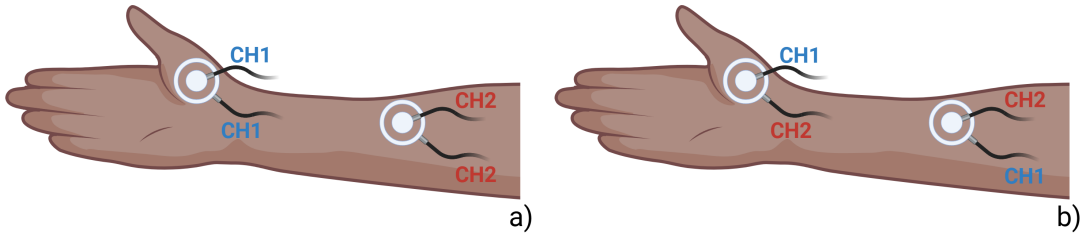

Figure 6.2.12: Representation of the electrode configurations along the forearm using concentric electrodes. The electrodes are placed with the median nerve as a reference. a) Dual concentric, b) Nested concentric.

The Ultima Neo Pro stimulator produced sinusoidal waves at 4000 Hz and 4020 Hz, resulting in an interferential current with a beat frequency of 20 Hz. The current intensity for each participant was gradually increased by 1 mA until a visible thumb motor response occurred, establishing the activation threshold, capped at 30 mA per channel. Once the threshold current was reached, stimulation lasted for 4 seconds.

This experiment aimed to identify which configuration more effectively induces

thumb flexion and abduction by stimulating the median nerve, correlating to the expected interference zones created by distant and nested concentric electrodes. Participants' sensory perception of discomfort during the threshold currents was measured using a Visual Analogue Scale (VAS) for pain.

6.2.5 Unbalanced-Channels Electrical Steering on Finger Flexors

A female subject, aged 27, participated in this exploratory study. She was instructed to sit comfortably, resting her left hand on a desk in front of her. The concentric ring electrodes were positioned at the bases of her thumb and little finger's base, as shown in fig. 6.2.13. The electrodes were arranged in a nested configuration, with one electrode placed over the thumb branch of the median nerve and the other over the ulnar nerve.

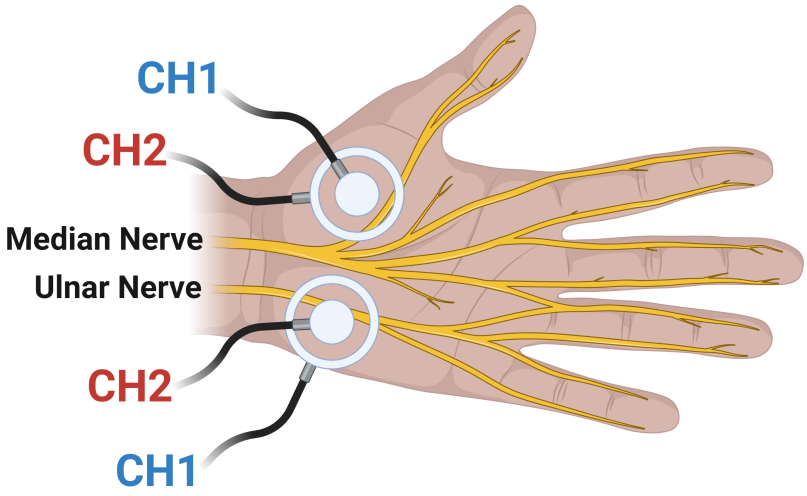

Figure 6.2.13: Electrode configuration for the unbalanced-channels electrical steering experiment. The Ulnar and median nerve are shown to illustrate the relative positioning of each concentric electrode.

Two Ultima Neo Pro stimulators produced sinusoidal waves at 4000 Hz and 4002 Hz each, generating an interferential current with a beat frequency of 2 Hz. The beat frequency was selected to elucidate the pulse contractions of the finger dorsiflexor muscles without aiming for a tetanic contraction.

The activation threshold was determined by simultaneously increasing the current output from the stimulators. Upon achieving a complete pulsatory contraction of the thumb and little finger, the current output of channel 2 was reduced until a distinct pulsatory response from the little finger was observed. Subsequently, the output of channel 1 was raised to the activation threshold, while the output of channel 1 was diminished until a pulsatory response of the thumb was elicited.

This experiment aims to provide evidence regarding the activation zones associated with the steering phenomenon, specifically targeting either the median nerve or the ulnar nerve. These nerves were selected due to their proximity to the relevant anatomical structures.

Chapter 7

Results

7.1 Computational Modelling

The computational models were conducted using COMSOL Multiphysics v6.2 on a machine equipped with an Intel Core i7-10700 CPU @ 3.60 GHz, 32 GB of RAM, a 1 TB SSD, and running Windows 11 Pro 64-bit. The table 7.1.1 show the mean computation times for each type of FEM model evaluated.

Table 7.1.1: Computation times for each type of FEM models simulated.

Model	Mean Computation Time
Thigh ICS + H-H axon	2 h 15 min
Unbalanced-Channels Electrical Steering	3h 50 min
High-Order ICS Modulation + H-H axon	28 min

7.1.1 Thigh Models

7.1.1.1 Activating Function Profiles

In COMSOL v6.2, 1D activation function profiles were determined by solving the built-in Poisson equation to obtain electric potentials for the model. Next, the

second spatial derivative was calculated as outlined in eq. (2.1.1), considering the modulated currents by eq. (3.1.9).

The 1D activation functions were assessed at the nerve, skin, and regions in between. The results are depicted through mesh plots created in MATLAB R2023a, illustrating the unidirectional activation function along the Cut Lines and how it varies over Time. The left vertical axis denotes Time (from 0 to 0.02 s), the right vertical axis indicates Cut Line length (from 0 to 10 cm), and the vertical axis shows the magnitude of the Activation Function.

The fig. 7.1.1 illustrates the 1D distribution of activation functions for each thigh FEM model, with each row displaying from left to right: skin activation function, skin to nerve activation function, and nerve activation function.

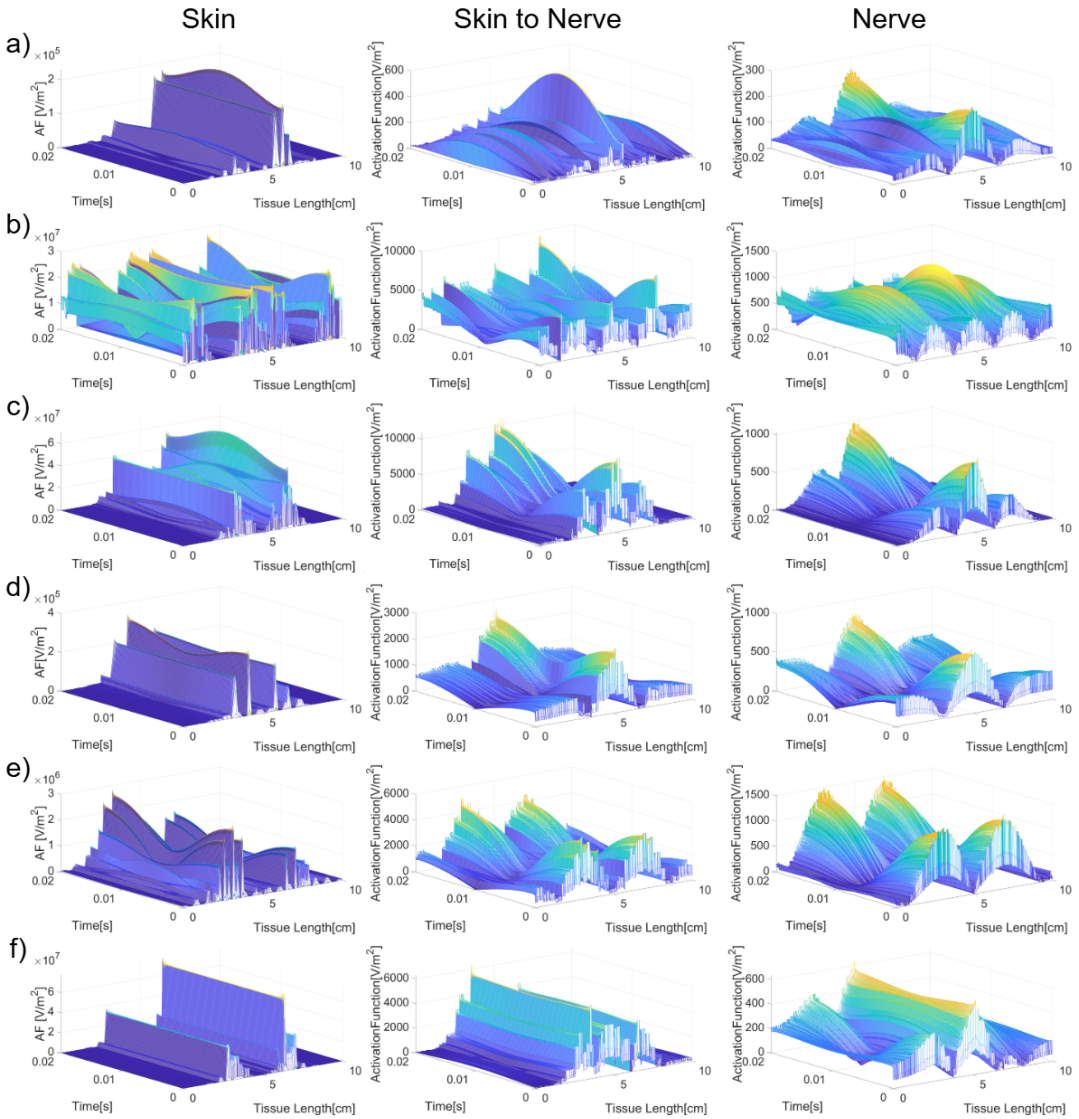

Figure 7.1.1: 1D activation function profiles at the Skin, Skin to Nerve, and Nerve levels. The right axis represents time in seconds, the left axis represents cut line length in centimetres, and the vertical axis represents the activation function in volts per square metre. a) Lateral dual concentric ring, b) Colinear dual concentric ring, c) Multiconcentric ring, d) Front line double pair side by side, e) Front double line double pair side by side, and f) Hybrid configuration

The Activation Function's volumetric distributions were calculated using the three-dimensional expression of eq. (3.1.9) directly in COMSOL version 6.2. The Activation Function was computed for the entire volume and subsequently scaled employing a logarithmic transformation.

Three distinct views of the volumetric Activation Function distribution are provided for each configuration. Values that were less than or equal to zero were excluded, as discussed in chapter 2, due to the fact that AF values equal to or below zero do not indicate regions with a high likelihood of generating action potentials.

The fig. 7.1.2 presents the three-dimensional AF distribution of the thigh models. Each view is organized from left to right, displaying the Top, Front, and Lateral perspectives.

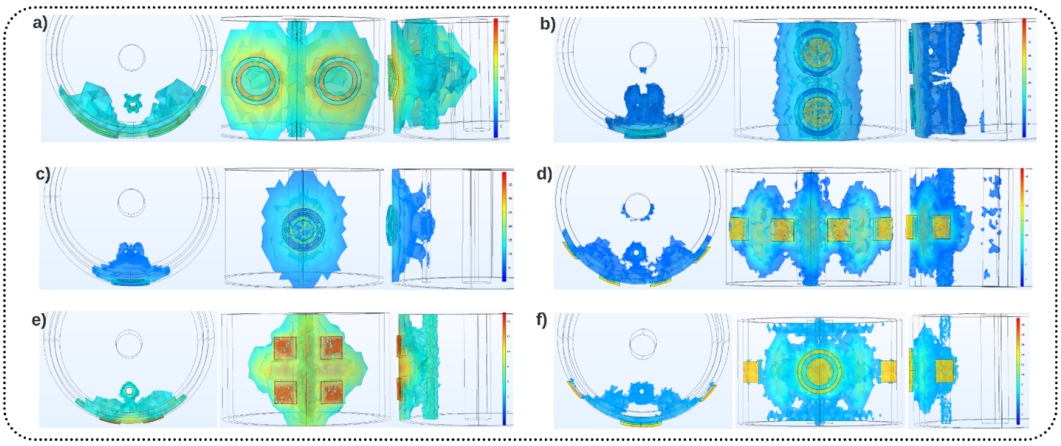

Figure 7.1.2: 3D distributions of activation functions with top, front, and lateral views: a) Lateral dual concentric ring, b) Colinear dual concentric ring, c) Multiconcentric ring, d) Front line double pair side by side, e) Front double line double pair side by side, and f) Hybrid configuration.

7.1.1.2 Hodgkin-Huxley Predicted Action Potentials

The plots presented in fig. 7.1.3 show the calculated membrane potentials with the coupled Hodgkin-Huxley axon model. The marked double spike evidence the generation of action potentials on a simulated unmyelinated axon of 10 μm. It can be seen that the multiconcentric ring electrode (d) and the front line double pair

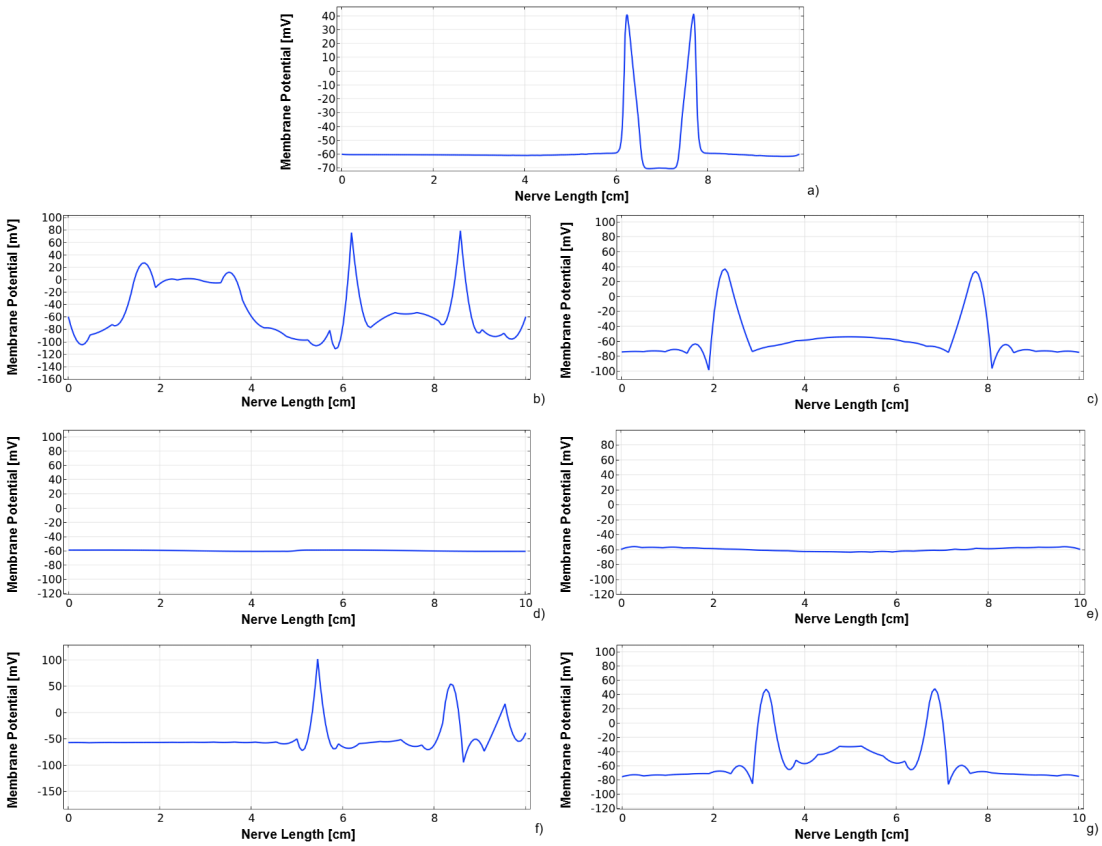

Figure 7.1.3: Action potential evaluation by calculating membrane potentials with an H-H axon model on an unmyelinated axon of 10 μm for the different modelled electrode configurations. a) FES 50 Hz with square electrodes, b) Lateral dual concentric ring, c) Colinear dual concentric ring, d) Multiconcentric ring, e) Front line double pair side by side, f) Front double line double pair side by side, and g) Hybrid configuration.

side by side (e) were the only configurations that did not elicit action potentials.

7.1.2 Unbalanced-Channels Electrical Steering

Volumetric distributions of the activating function were calculated for the models described in section 6.1.6 using the eq. (3.1.9). The fig. 7.1.4 and fig. 7.1.5 show the progression of the movement of the modulated activating function 3D profiles.

The concentrated activating function is steered to the left in both square and concentric electrode setups, where channel 2 electrodes are placed. Channel 2

exhibits a reduced output current amplitude in cases b) to e), suggesting that the activation zones shift toward the lower output channel.

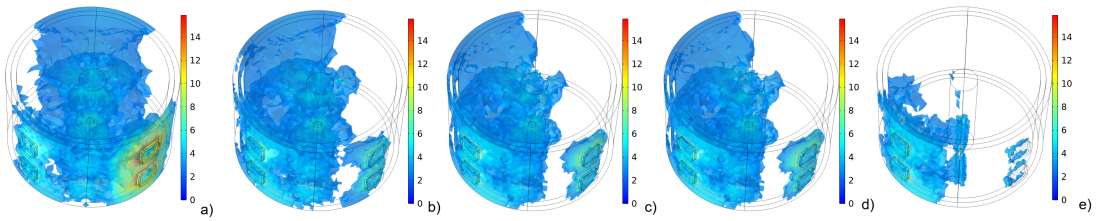

Figure 7.1.4: Activating function profiles using the Unbalanced-Channels Electrical Steering technique with square electrodes paired separately. Each figure represents a different channel output ratio. a)1:1 (25 and 25 mA), b)7:3 (35 and 15 mA), c)4:1 (40 and 10 mA), d)9:1 (45 and 5 mA), b)49:1 (49 and 1 mA).

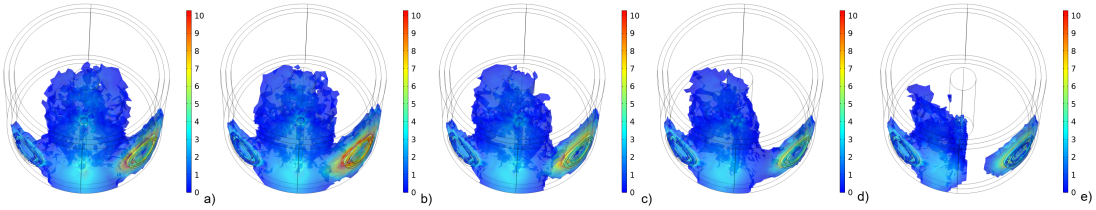

Figure 7.1.5: Activating function profiles using the Unbalanced-Channels Electrical Steering technique with concentric electrodes paired separately. Each figure represents a different channel output ratio. a)1:1 (25 and 25 mA), b)7:3 (35 and 15 mA), c)4:1 (40 and 10 mA), d)9:1 (45 and 5 mA), b)49:1 (49 and 1 mA).

7.1.3 High-Order ICS Modulation

Extracellular electrical potentials in proximity to the nerve and membrane potentials were computed utilizing the cylindrical forearm models presented in section 6.1.7. The extracellular potentials were derived from applying the Poisson equation; the graphical representations provided in this section pertain to a point along the mid-line of an adjacent cut-line near the nerve. The membrane potentials were determined through the resolution of the differential equations of the Hodgkin-Huxley model as delineated by [133] at an edge of the nerve.

Crossed Square electrodes: The extracellular potentials illustrated in fig. 7.1.6 a) exhibit a waveform similar to the modulated current derived from eq. (6.1.3), characterized by a dominant frequency of 50 Hz. The assessed membrane potentials, as displayed in fig. 7.1.6 b), demonstrate the generation of action potentials synchronized with the dominant frequency of the modulated current. In the figure, each pair of action potentials (ascending and descending) occurs with an interval of 0.2 seconds.

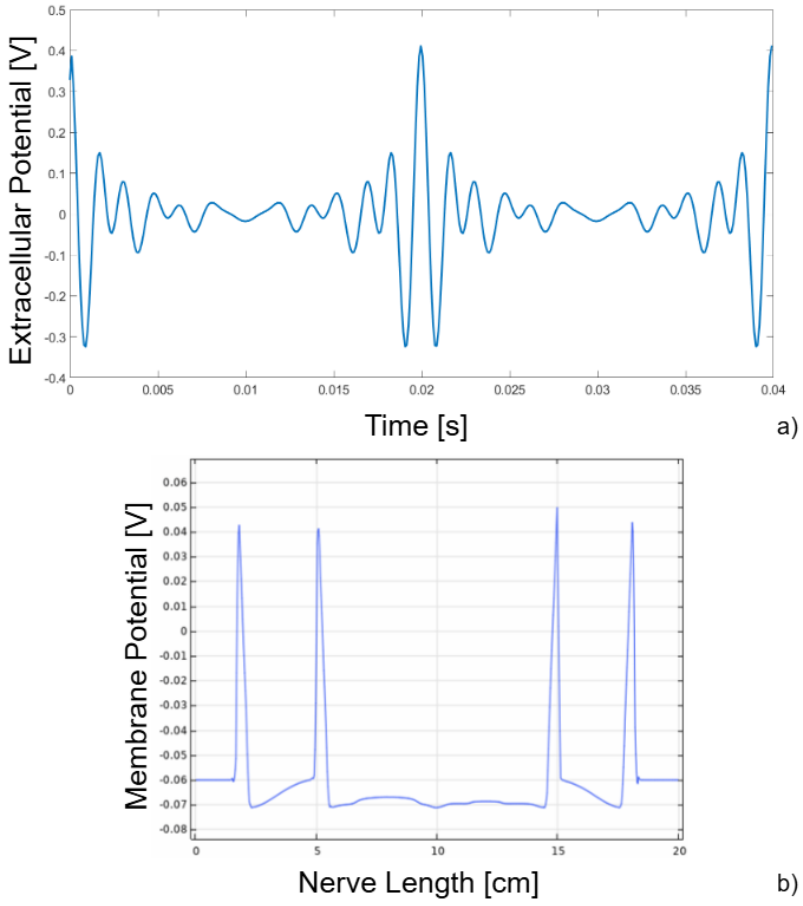

Figure 7.1.6: Calculated extracellular and membrane potentials for the crossed square electrodes configuration. a) Extracellular potentials at mid-line the vicinity of the nerve along time. b) Membrane potentials are calculated using the H-H axon model along the axon membrane.

Collinear Nested Concentric: The behaviour of this technique was analogue to

the crossed square electrodes, with a slightly reduced maximum amplitude of the modulated extracellular potentials. Nevertheless, the waveform of the extracellular potentials shown in fig. 7.1.7 a) follows the same pattern as the expected modulated current. In this case, the action potentials shown in fig. 7.1.7 b) reflect a 50 Hz activation of the nerve, produced over the distal cathode connected to the channel 1.

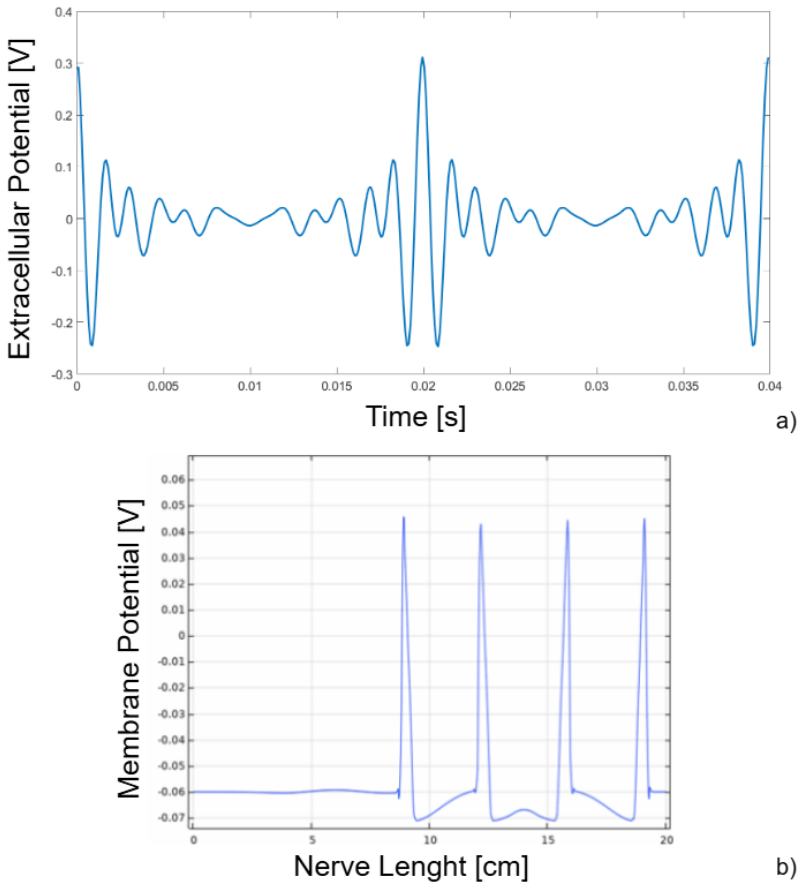

Figure 7.1.7: Calculated extracellular and membrane potentials for the collinear nested concentric electrodes configuration. a) Extracellular potentials at mid-line the vicinity of the nerve along time. b) Membrane potentials are calculated using the H-H axon model along the axon membrane.

Opposite Nested Concentric: The extracellular potentials differed from the expected waveform produced by the current modulation, exhibiting a principal

frequency component at 100 Hz, as shown in fig. 7.1.8 a). This difference impacted on the membrane potentials, where no action potentials were detected, yet generating focalised depolarizations, as illustrates fig. 7.1.8 b).

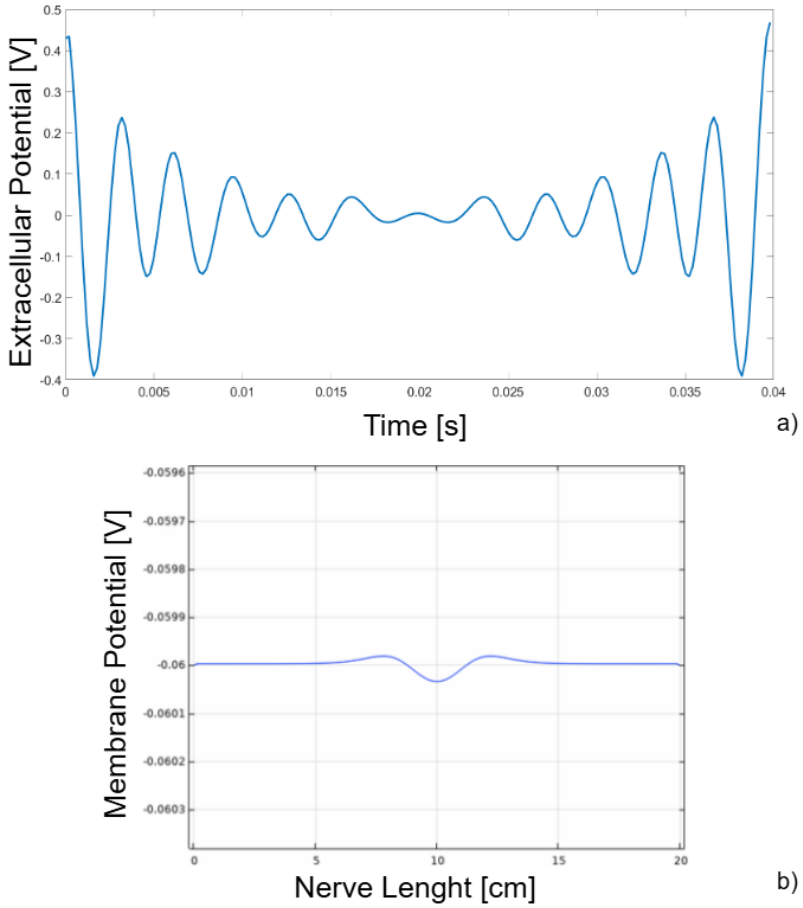

Figure 7.1.8: Calculated extracellular and membrane potentials for the opposite nested concentric electrodes configuration. a) Extracellular potentials at mid-line the vicinity of the nerve along time. b) Membrane potentials are calculated using the H-H axon model along the axon membrane.

7.2 In-Vivo Experiments

7.2.1 Rectus Femoris Stimulation

7.2.1.1 Motor Point Tracking

The motor point positions were registered for the 13 volunteers as described in section 6.2.3.1. The motor point locations were marked using the plastic diamonds over the subject's skin. All the subjects presented their initial motor point location, i.e. at 90° knee flexion, close to the thigh midline.

The normalised trajectories are shown in fig. 7.2.1. 12 subjects presented a similar motor point displacement trajectory towards distal and medial, while one showed a distal and lateral trajectory. In fig. 7.2.2, the average normalised motor point starting point is near the first third of the thigh's length, moving towards the distal direction reaching the middle of the thigh.

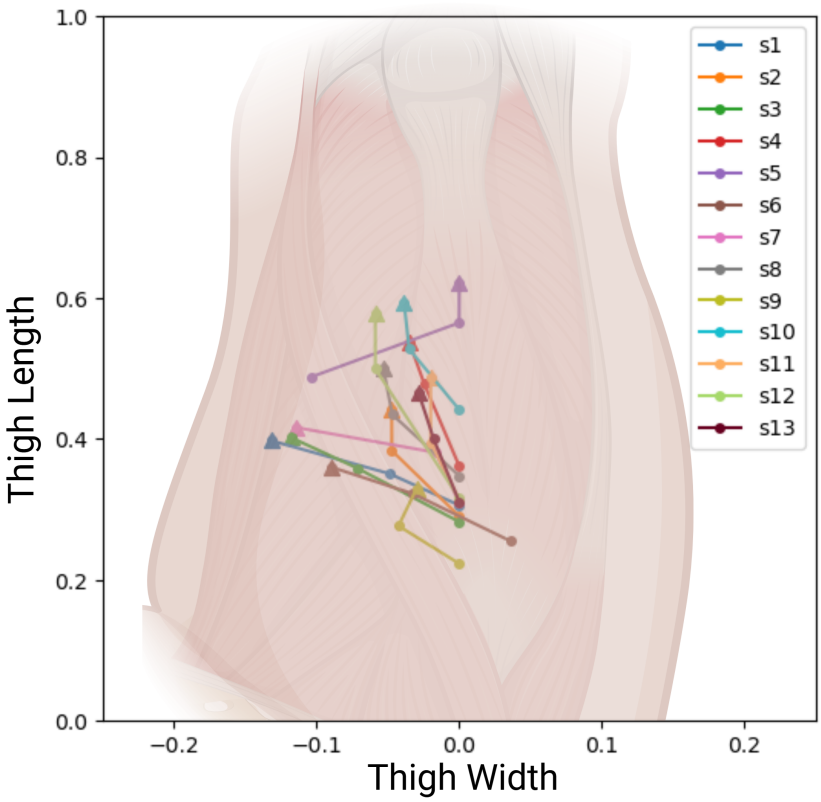

Figure 7.2.1: Normalised motor point trajectory. Each motor point location was normalised considering the respective subject's thigh length and thickness. The initial dot marks the 90° motor point location, the intermediate dot marks the 120° motor point location, and the final arrowhead indicates the 180°.

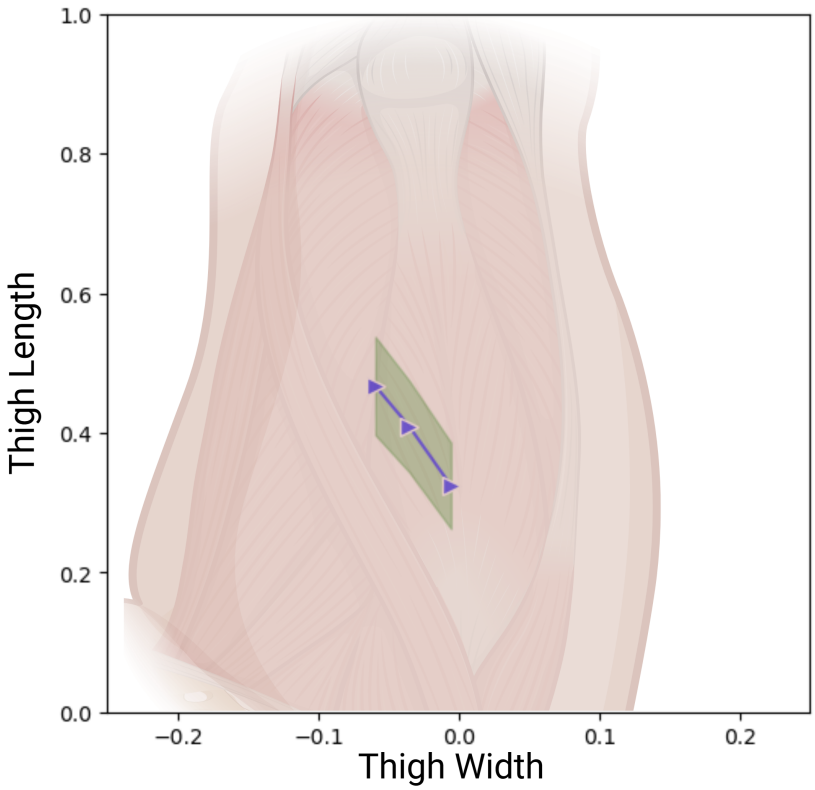

Figure 7.2.2: Average normalised motor point trajectory. In blue is presented the average motor point trajectory, indicating with arrowhead the direction of the displacement. Green indicates the standard deviation of the normalised motor point trajectory.

The Euclidean distance between the 90° and 180° motor point locations was calculated for both normalised and non-normalised trajectories (see fig. 7.2.3). The mean displacement was 6.89 *cm* or 15% of the normalised thigh length.

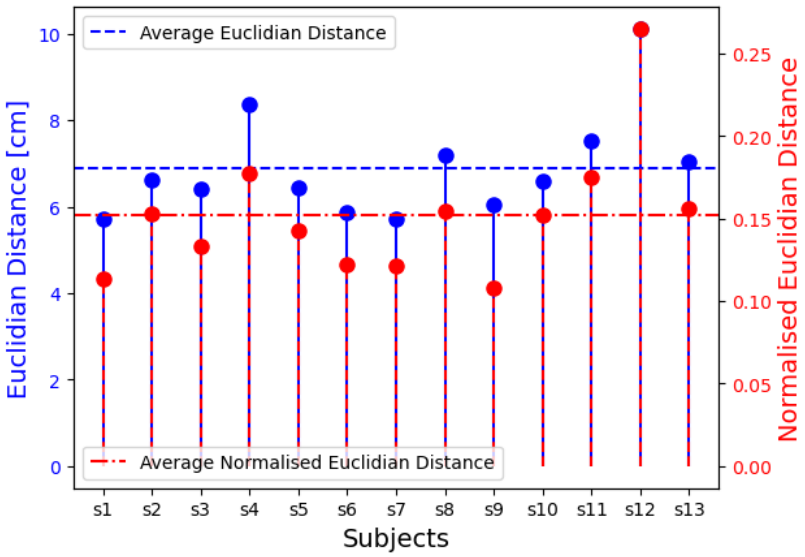

Figure 7.2.3: Normalised and non-normalised Euclidean distance of the motor points displacement. Blue represents the non-normalised Euclidean distance between the initial and final position of the motor point; the dashed blue line marks the mean distance (6.89 cm). In red is presented the normalised Euclidean distance between the initial and final position of the motor point; the dashed red line marks the mean distance (0.15 cm).

The activation thresholds were considered as the minimum current required to generate a palpable and visual full contraction of the rectus femoris when scanning for the motor point at 90° knee flexion. The obtained activation threshold distributions are shown in fig. 7.2.4.

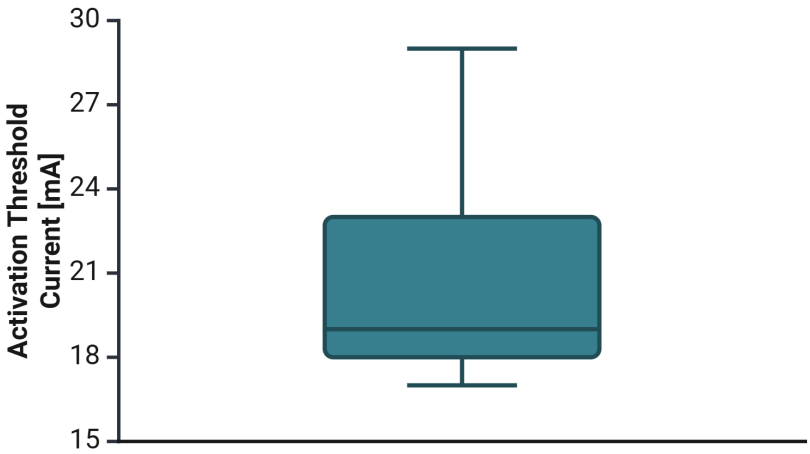

Figure 7.2.4: Current activation thresholds distribution from motor point scanning. The minimum current needed to generate a full rectus femoris contraction.

A demonstrative video of the experiment can be found in gitHub repository - Motor Point Tracking.

7.2.1.2 Evaluating New Electrode Configurations and ICS

A total of 13 subjects took part in the experiments outlined in section 6.2.3.2 and section 6.2.3.3. The results compare a 50 Hz FES technique with various proposed electrode configurations using interferential currents, intending to comfortably stimulate the rectus femoris. Thus, the different stimulation techniques were evaluated using three criteria:

- Capability to generate a motor response: The technique produced a successful response when the resistive rubber band measured deformation in the thigh muscle, resulting in a visible contraction. Conversely, stimulation was deemed a non-responsive technique.

- Current threshold of activation: The current intensity was recorded for all

the techniques, even though it generated activation or reached the maximum output of the stimulator. A threshold of 30 mA, the maximum output for ICS of the Ultima Neo stimulator, was considered as a label for non-responsive techniques.

- Subject impressions on discomfort: The subjects described their experiences using the McGill questionnaire, evaluating the sensations they felt with linguistic and numeric options while applying the electrical stimulations.

The final compared techniques were: Functional stimulation at 50 Hz (FES-50 Hz), Interferential currents with square electrodes (ICS-Square), Interferential currents with dual concentric ring electrodes (ICS-Dual Concentric), Interferential currents with nested concentric ring electrodes (ICS-Nested Concentric), and Interferential currents with hybrid square/concentric electrodes (ICS-Hybrid). The multiconcentric ring electrode over the motor points and the femoral triangle configurations were removed from the scheme due to their ability to induce significant discomfort in the first two subjects without eliciting any motor responses. These techniques were deemed harmful to the subjects and weren't replicated.

In fig. 7.2.5 is presented a comparison of the current thresholds distributions. The plot was generated using bioRender Graph (BioRender, Toronto, Canada). It can be seen that for FES-50 Hz the thresholds are lower than the rest of the methods, with a mean value of 19 mA. ICS-Square obtained a mean of 24 mA, being the group that most compared to the control 50 Hz stimulation. ICS-Nested concentric and ICS-Hybrid showed higher activation thresholds, having mean

values of 29 mA and 28.5 mA, respectively. ICS-Dual Concentric had a mean threshold of 30 mA, being the least effective technique. Note that the thresholds registered for ICS techniques were the output of one channel, so the injected current doubled the shown thresholds.

The boxplot dots represent each subject for each stimulation technique. The dots at 30 mA indicate non-response attempts. FES-50 Hz had no non-responsive subjects, whereas ICS-Square had 2, ICS-Hybrid had 5, ICS-Nested Concentric had 7, and ICS-Dual Concentric recorded 12 non-responsive attempts.

A Kruskal-Wallis test compared the control group's 50 Hz threshold distributions with those of other proposed techniques. This non-parametric method assesses if samples come from the same distribution without normality assumptions [138]. The test, run in bioRender Graph, showed a significant difference between the control group and ICS methods with concentric electrodes (marked with asterisks). However, no statistical difference was found with ICS-Square.

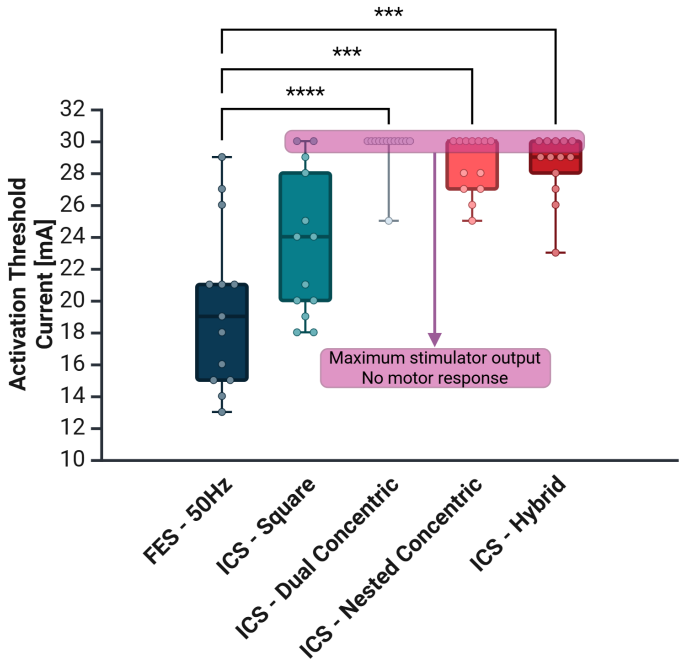

Figure 7.2.5: Current thresholds for the various stimulation techniques applied to the thigh. The asterisks indicate statistical differences between groups, calculated using a Kruskal-Wallis non-parametric test. The dots represent samples for each group; note that a dot at 30 mA signifies no contraction response.

Motor contraction records are presented in fig. 7.2.6 and fig. 7.2.7. These are two selections of recordings of thigh deformations elicited by stimulating the rectus femoris, measured with the resistive rubber band and BIOPAC setup presented in fig. 6.2.2. Each graph shows three plots indicating the subjects' knee extension levels: blue for 90°, orange for 120°, and yellow for 180°. The data was filtered in MATLAB using a low-pass Bartlett window filter with a cutoff frequency of 20 Hz, with an order of 99 samples. The sampling frequency set in the BIOPAC was 1 kHz, so the preprocessed data remains unaffected by the delay caused by the size of the filter. The plots illustrate 6 s of recording, which includes the 5 s of active stimulation during each session.

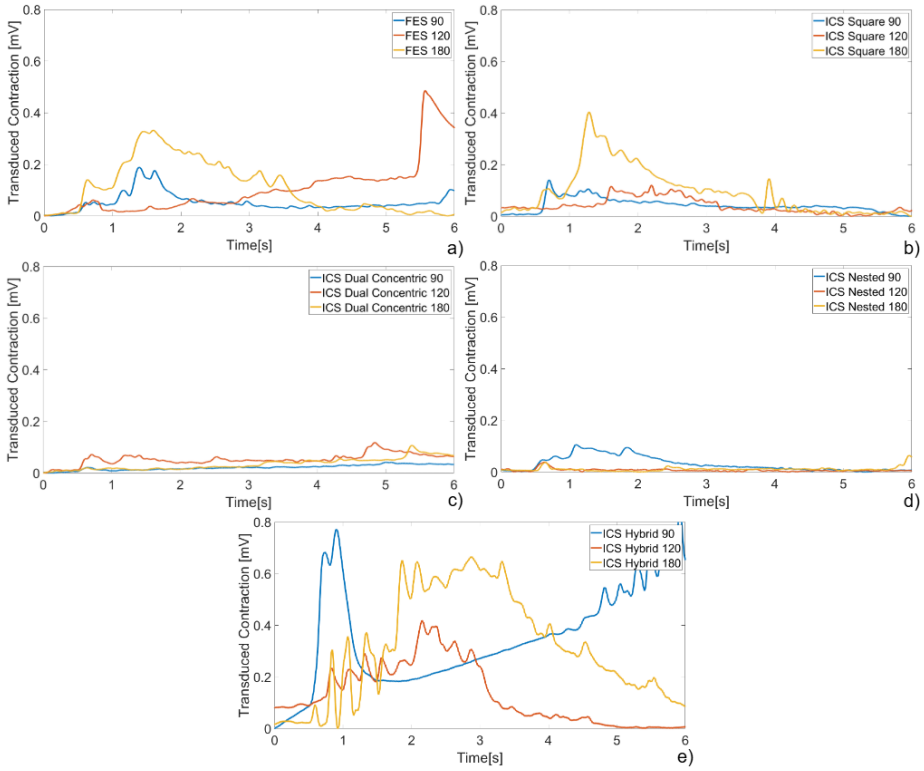

Figure 7.2.6: Sample 1 of rectus femoris contraction responses obtained from the measured thigh deformation using the resistive rubber band. Each plot corresponds to a different electrode configuration at the three levels of knee extension. a) FES-50 Hz, b) ICS-Square, c) ICS-Dual Concentric, d) ICS-Nested Concentric, e) ICS-Hybrid.

In fig. 7.2.6, notable motor responses for the FES-50 Hz, ICS-Square, and ICS-Hybrid can be seen. The latter showed the maximum amplitude of the transduced contraction by the resistive rubber band. Consistently, the contractions were reduced when the knee extension was at 120°. In some cases, at the switching off of the stimulator, a peak of contraction was measured. This was attributed to a voluntary contraction of the subjects by the sensation of turning off the stimulator. The ICS-Nested plots identified minor responses with increased contraction at 90° knee extension. However, it is less powerful than the previously described methods. ICS-Dual Concentric registered lower activity at 120° but no visually

identifiable contractions.

In fig. 7.2.7, similar to the first case, the notorious contractions were generated by the FES-50 Hz, ICS-Square, and ICS-Hybrid methods. The FES-50 Hz technique achieved the highest contractions. In contrast, the ICS-Square stimulation reached its peak contraction at 180° knee extension, half of the maximum contraction recorded with the FES-50 Hz method. ICS-Hybrid showed weaker contractions yet visually identifiable. ICS-Dual concentric and ICS-Nested were non-responsive in this experiment.

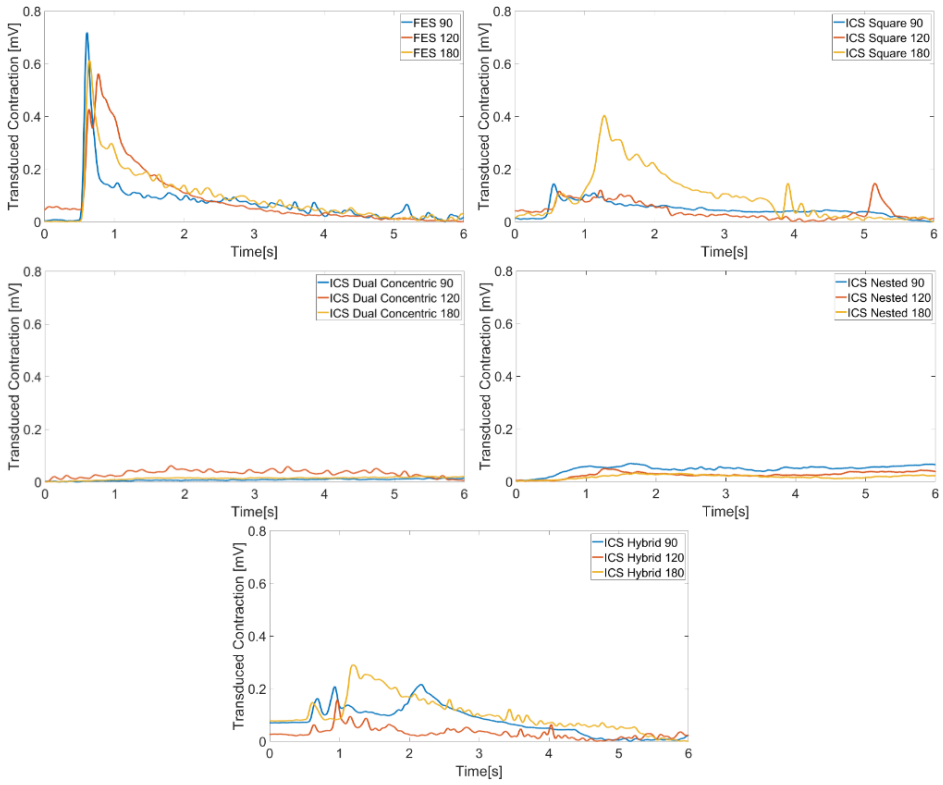

Figure 7.2.7: Sample 2 of rectus femoris contraction responses obtained from the measured thigh deformation using the resistive rubber band. Each plot corresponds to a different electrode configuration at the three levels of knee extension. a) FES 50 Hz, b) ICS Square electrodes, c) ICS Dual Concentric, d) ICS Nested Concentric, e) ICS Hybrid.

Demonstrative videos of the experiment can be found in gitHub repository - Rectus

Femoris Stimulation.

The McGill questionnaire provided insights into the subjects' perceptions of the sensations experienced during the experiments. Through various selections of words grouped by topics, the subjects characterised their experiences. It is worth noting that the subjects were permitted to leave any topic blank if they felt it did not align with their perception. The responses obtained from the topics considered most related to discomfort from electrical stimulation are illustrated from fig. 7.2.8 to fig. 7.2.13, detailing each stimulation technique: Localisation I, Localisation II, Constriction, Puncture, Valorative, and Overall Intensity.

In fig. 7.2.8, it can be observed that for all the stimulation techniques, the predominant expression for Localisation I was *Well Determined*, with *Widespread* following closely. Therefore, the predominant localisation of sensations during the experiments was described as being more precise for the majority of the subjects.

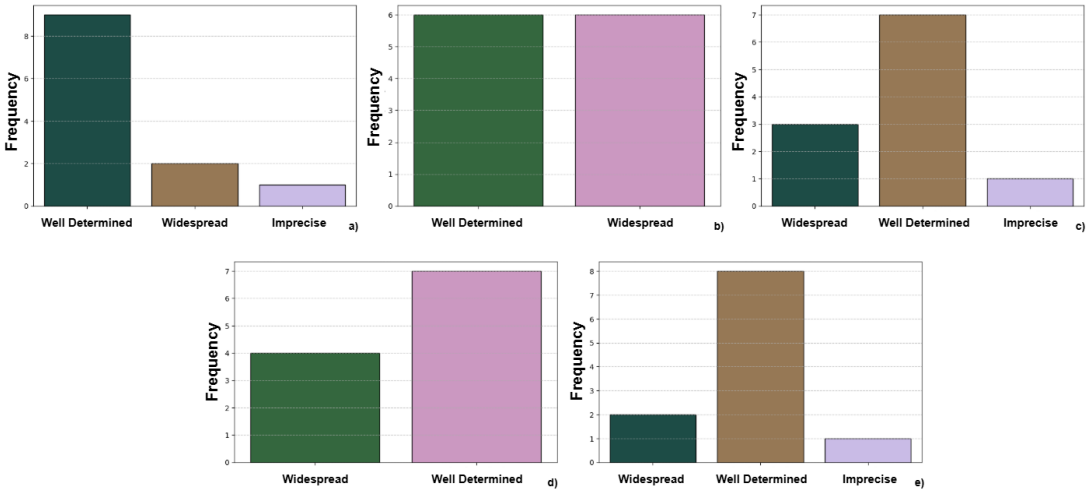

Figure 7.2.8: McGill questionnaire answers for the topic Localisation I. a) FES 50 Hz, b) ICS Square electrodes, c) ICS Dual Concentric, d) ICS Nested Concentric, e) ICS Hybrid.

Localisation II evaluates the dispersion of the sensation, where the subjects assessed it as *propagated* rather than *distributed* in most cases. Note that, in fig. 7.2.9, the graphs c), d) and e) were not answered for several subjects.

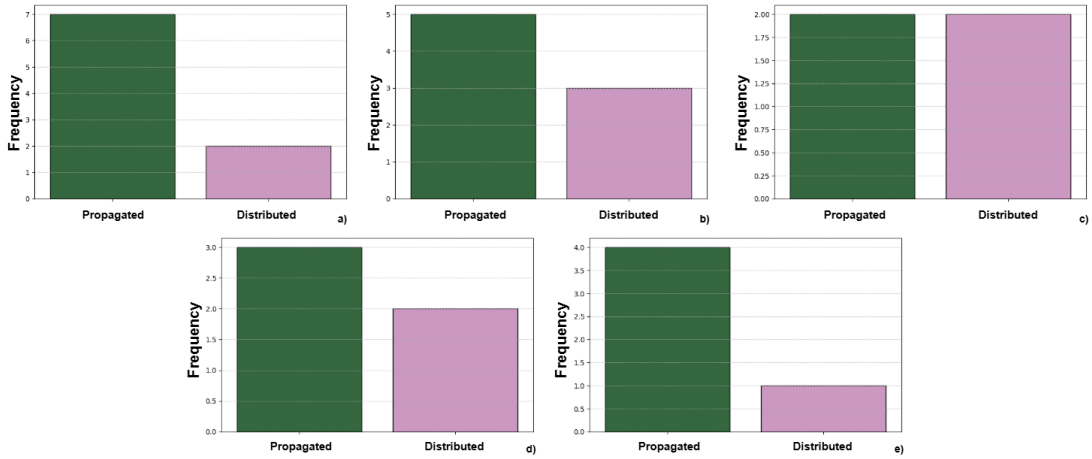

Figure 7.2.9: McGill questionnaire answers for the topic Localisation II. a) FES 50 Hz, b) ICS Square electrodes, c) ICS Dual Concentric, d) ICS Nested Concentric, e) ICS Hybrid.

In fig. 7.2.10, the subjects assessed the constriction sensations experienced during the experiments. It is evident that *constrained* and *pinch* were the most commonly used concepts for this topic. The FES-50 Hz and ICS-Square configurations exhibited the most varied selection of concepts, whereas ICS-Nested displayed only the two weaker concepts from the list.

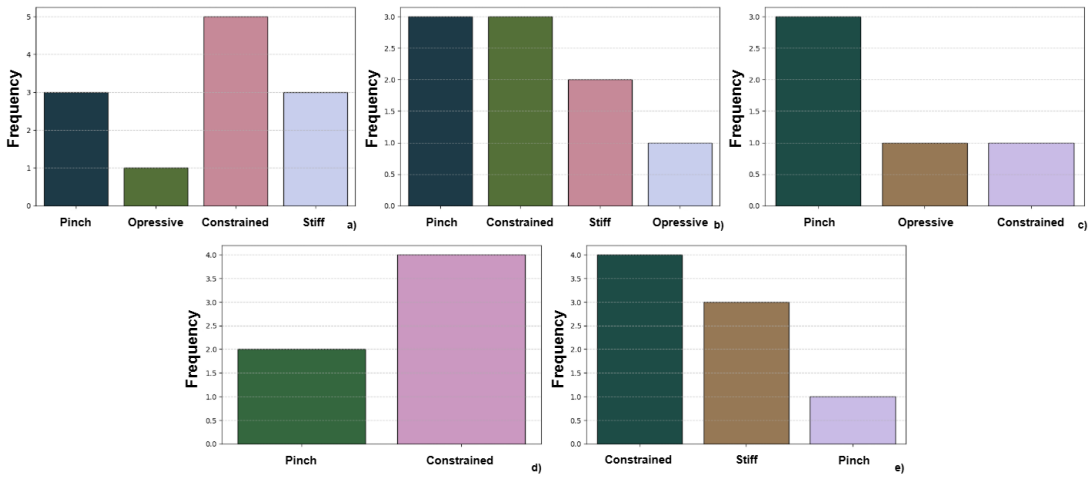

Figure 7.2.10: McGill questionnaire answers for the topic Constriction. a) FES 50 Hz, b) ICS Square electrodes, c) ICS Dual Concentric, d) ICS Nested Concentric, e) ICS Hybrid.

Puncture evaluated the elicited pain sensation, primarily beneath the electrodes, in an area-related perception. A specific pain was recognised as *needles* puncturing the skin, while a strong sensation correlated to a *nail*, and a softer sensation was described as *puncture*. As illustrated in fig. 7.2.11, the predominant concept for the plots related to ICS stimulation with concentric electrodes was *puncture*. However, *needles* were notably present in each stimulation technique. For ICS-Hybrid, two subjects reported the *nail* sensation.

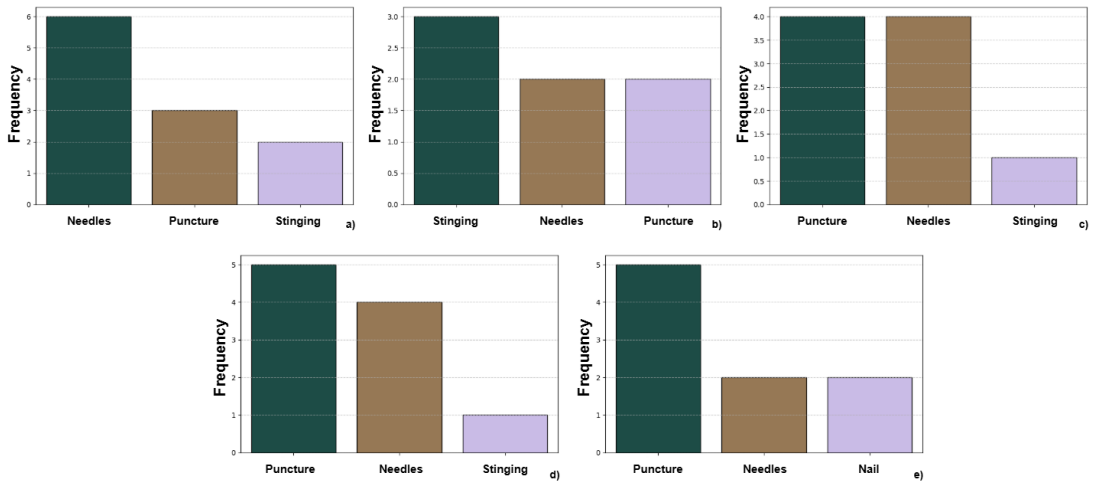

Figure 7.2.11: McGill questionnaire answers for the topic Puncture. a) FES 50 Hz, b) ICS Square electrodes, c) ICS Dual Concentric, d) ICS Nested Concentric, e) ICS Hybrid.

The fig. 7.2.12 displays the questionnaire results for the Valorative topic, which assessed perceptions regarding the bearability of pain and discomfort. A *weak* sensation is more bearable than an *intense* sensation, while a *tolerable* sensation indicates some discomfort but not an instant pain. *Intense* sensations were related to FES-50 Hz and ICS-Hybrid. However, the predominant concept in most experiments was *tolerable*. ICS-Dual Concentric was the only experience which predominated *weak* sensations.

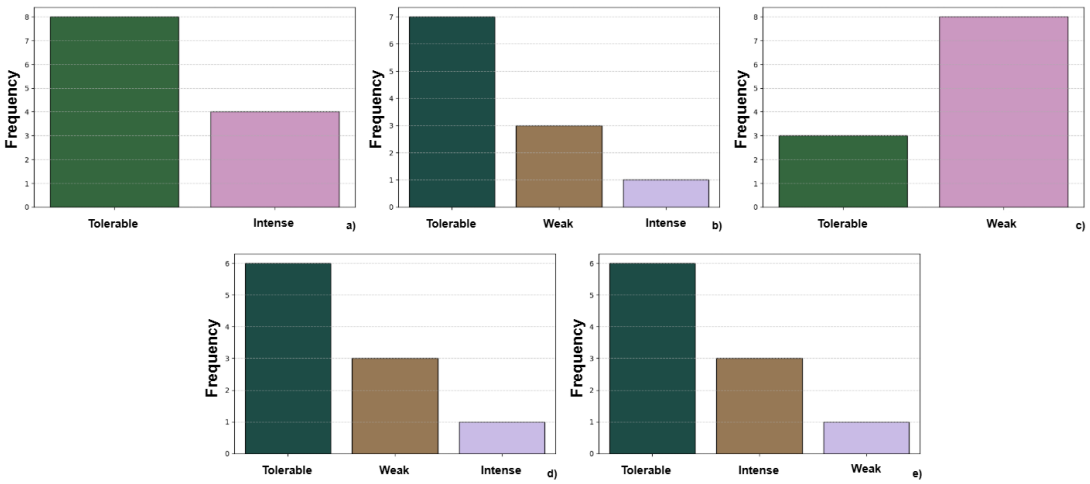

Figure 7.2.12: McGill questionnaire answers for the topic Valorative. a) FES 50 Hz, b) ICS Square electrodes, c) ICS Dual Concentric, d) ICS Nested Concentric, e) ICS Hybrid.

Overall intensity reflects the summarised perception of the subjects for each experience. In this topic, subjects expressed their discomfort/pain sensation in qualitative levels, from *mild* to *insufferable*. None of the subjects surpassed the *strong* concept on this matter. *Annoying* was the predominant concept for FES-50 Hz and ICS-Nested Concentric techniques, while *mild* had more frequency on the rest of the experiences.

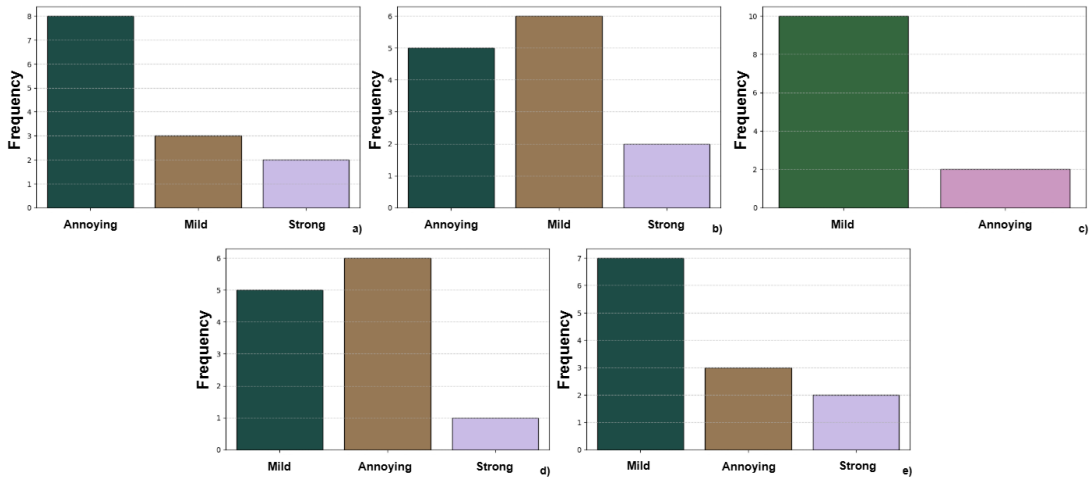

Figure 7.2.13: McGill questionnaire answers for the topic Overall Intensity. a) FES 50 Hz, b) ICS Square electrodes, c) ICS Dual Concentric, d) ICS Nested Concentric, e) ICS Hybrid.

In general, the subjects' discomfort perception was dispersed. However, some characterisations can be made for each stimulation technique:

- FES-50 Hz: Well-determined yet propagated sensations, with a needling effect under the electrodes. Generates a constrain to pinch constriction sensation. It is described as annoying but also tolerable/intense.
- ICS-Square: Well-determined yet propagated sensations, with a stinging/needling effect under the electrodes. Generates a constrain to pinch constriction sensation. Described mostly mild intensity of discomfort, generally tolerable.
- ICS-Dual Concentric: This technique generated the lowest intensity of sensations in the participants. Generated punctures and needle effect under the electrodes. Predominantly weak and mild sensations.
- ICS-Nested Concentric: Well-determined yet propagated sensations with

a puncture effect under the electrodes. Generates constriction sensations. Mild to annoying sensations, mainly described as weak or tolerable.

- ICS-Hybrid: Well-determined yet propagated sensations with a puncture effect under the electrodes. Constrained and stiff sensations. Mainly described as mild and tolerable intense intensity.

Some particularities were noted. A couple of participants noted heat and cold sensations during the experiments. Also, some participants answered the Fear question with *scares*. Even though a few subjects gave these answers, it is worth considering them as warnings for future experiments.

The VAS scores registered in the McGill questionnaire distributions are presented in fig. 7.2.14. The maximum mean score was obtained for the FES-50 Hz technique (5), while the minimum was registered for the ICS-Dual concentric stimulation (1). All the ICS methods have a mean score lower than the control technique. However, as presented in fig. 7.2.5, ICS-Dual Concentric did not elicit a motor response for almost all the subjects. ICS-square presented a similar distribution as FES-50 Hz, with a reduced mean score of 4. On the other side, ICS-Nested concentric and ICS-Hybrid presented the same mean score (2), with similar distributions.

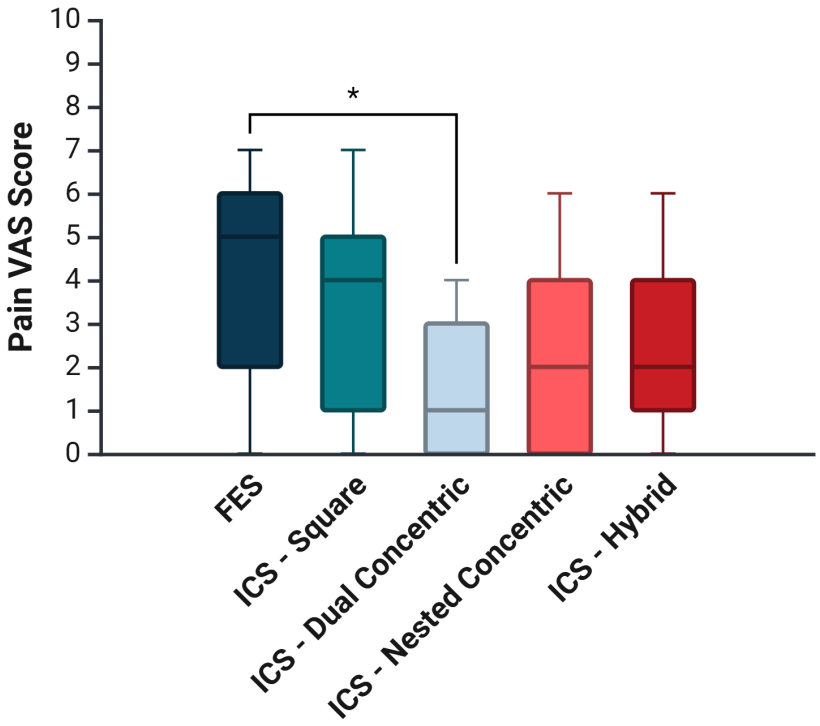

Figure 7.2.14: Distributions of the VAS scores measured during the rectus femoris stimulation tests.

The fig. 7.2.15 compares the distributions of the registered responses to the measured thigh dimensions. The left plot illustrates the relationship between responses and thigh thickness. The Contraction and No Response distributions did not show statistical differences in any of the stimulation techniques. A similar behaviour is illustrated in the right plot, where the effect of the thigh length on eliciting muscle contractions is analysed.

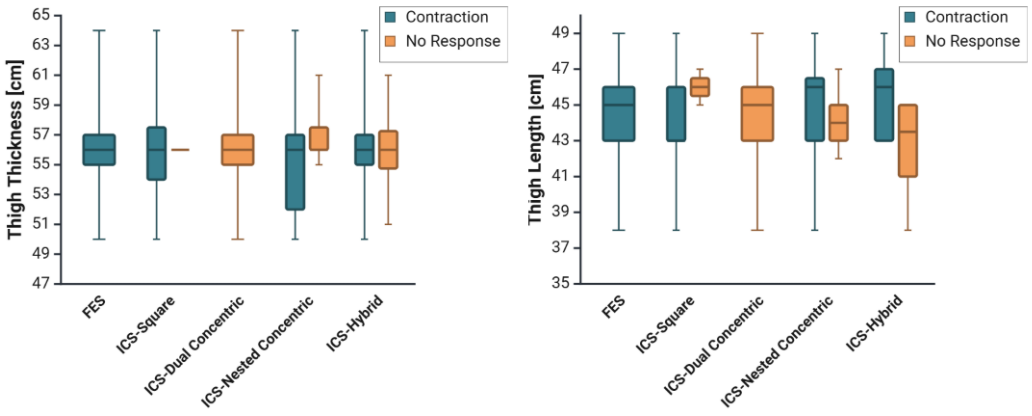

Figure 7.2.15: Distributions of the registered contractions and non-responses analysed by thigh thickness (left) and thigh length (right), separated by stimulation techniques.

A comparison is presented between the participants' sex and their responses during the experiments, as illustrated in fig. 7.2.16. A distinct difference is observable between these groups: males exhibited responses to every stimulation technique except for ICS-Dual Concentric, which was unable to induce contractions in any of the participants. In contrast, females demonstrated varied responses to the remaining ICS-based methods, except for FES-50 Hz.

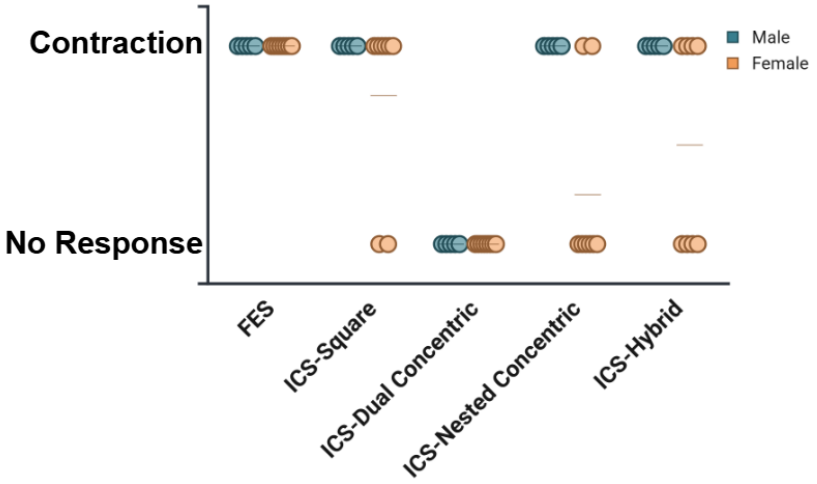

Figure 7.2.16: Distributions of the registered contractions and non-responses analysed by participant's sex, separated by stimulation techniques.

7.2.2 Forearm Stimulation

Demonstrative videos of the experiment can be found in gitHub repository - Forearm Stimulation.

7.2.2.1 Square Electrodes Around Wrist

All participants exhibited motor responses during the experimental protocol. The configuration involving crossed stimulation channels elicited motor responses in the fingers at lower current amplitudes than other configurations with a mean current threshold between 16-17 mA, as shown in 7.2.17. Conversely, the separated channel configurations were observed to be the least effective in producing motor responses. None of the tested configurations resulted in specific thumb adduction without also inducing flexion in other fingers, demonstrating a lack of selectivity.

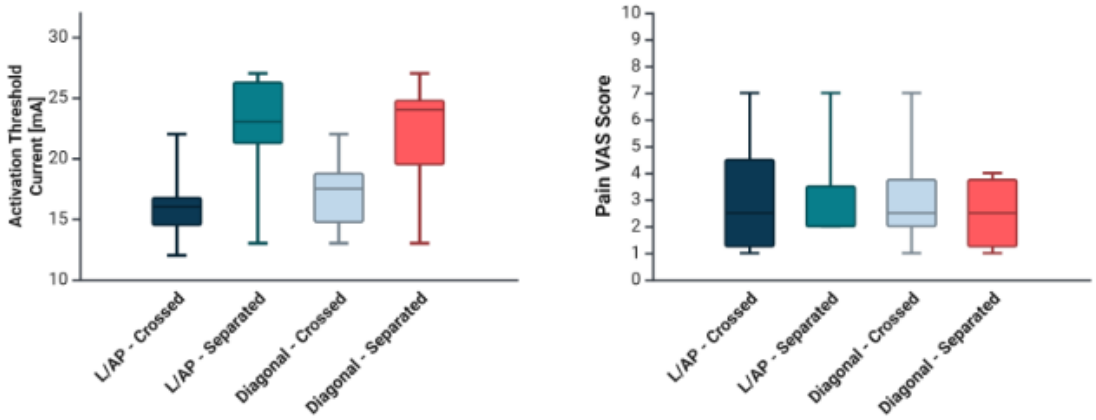

Figure 7.2.17: Comparison of the distribution of current activation threshold (left) and VAS evaluation from the subject perception (right) for the electrodes placed around the wrist experiment.

The sensory evaluation using the Visual Analogue Scale (VAS) revealed a uniform distribution of discomfort perception across participants for all tested configurations, indicating a consistent subjective stimulation experience evaluated in a mean VAS score of 3. Figure 7.2.17 illustrates the distribution of current thresholds obtained alongside the VAS evaluation for each electrode configuration, providing a comparative visual representation of the results.

7.2.2.2 Square Electrodes Along Forearm

All participants displayed motor responses throughout all four stages of the experimental protocol. Among the various configurations assessed, the In-Line configuration induced finger flexion responses at the lowest current thresholds, thereby demonstrating its comparative efficiency. Conversely, no statistically significant differences were noted between the perpendicular crossed and separated configurations, whereas the In-Line separated configuration corresponded with marginally elevated current thresholds, as illustrated in 7.2.18.

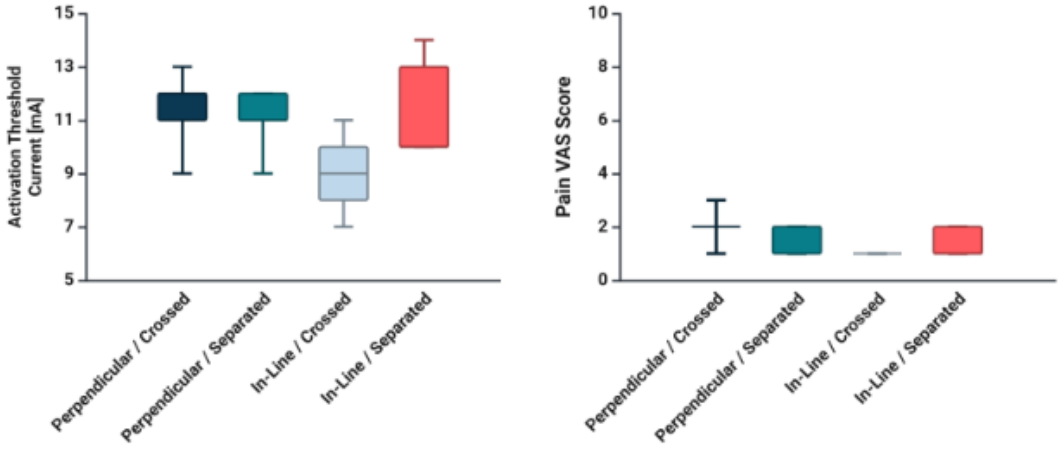

Figure 7.2.18: Comparison of the distribution of current activation threshold (left) and VAS evaluation from the subject perception (right) for the electrodes placed along the forearm experiment.

The In-Line configurations demonstrated significant efficacy in eliciting specific thumb flexion in the majority of instances. This observation contrasts sharply with the perpendicular configurations, which consistently triggered accessory motor responses in the middle and little fingers, thereby elucidating a distinct activation pattern.

The application of the Visual Analogue Scale (VAS) to evaluate discomfort did not uncover significant differences in the participants' perceptions of discomfort across the various configurations. Nonetheless, the In-Line crossed configuration was reported to yield a comparatively more comfortable sensation among the volunteers. Figure 7.2.18 illustrates the distribution of the current thresholds alongside the corresponding VAS evaluations, presenting a comprehensive comparison of the results for each electrode configuration.

All participants indicated a reduction in skin afferent sensation upon activating the ICS and manoeuvring the plastic probe across the skin between the electrodes.

This effect was notably more pronounced in the crossed-channel configurations, where volunteers encountered challenges in accurately discerning whether the probe was in contact with their skin without visual confirmation.

The assessment of moisturized skin employing surface electrodes in a perpendicular or crossed configuration revealed an activation threshold of 20 mA, in comparison to non-moisturized skin, which necessitated only 17 mA to elicit thumb adduction. The activation threshold was lowered to 18 mA when the electrodes were affixed with fabric. Sensory evaluation utilizing the Visual Analogue Scale (VAS) indicated discomfort levels of 5 for non-moisturized skin, 5 for moisturized skin with non-fixed electrodes, and 3 for moisturized skin with fixed electrodes. It is important to note that this test was not replicated in other subjects due to practical challenges and issues related to reproducibility, primarily arising from the loss of electrode adhesion resulting from the application of CeraVe cream.

7.2.2.3 Concentric Electrodes Along Forearm

The four participants demonstrated thumb flexion while interacting with the integrated circuit systems employing the nested concentric electrodes. In contrast, the separated concentric electrodes failed to elicit any thumb movement. The results of this latter condition are illustrated in fig. 7.2.19, wherein the thresholds recorded for the separated concentric electrodes were found to be 30 mA, representing the maximum output of the stimulator. A mean current threshold of approximately 25 mA was observed for the nested concentric electrodes.

The visual analogue scale evaluation revealed no significant differences between

the two stimulation techniques; however, the VAS scores were marginally higher for the nested concentric electrodes.

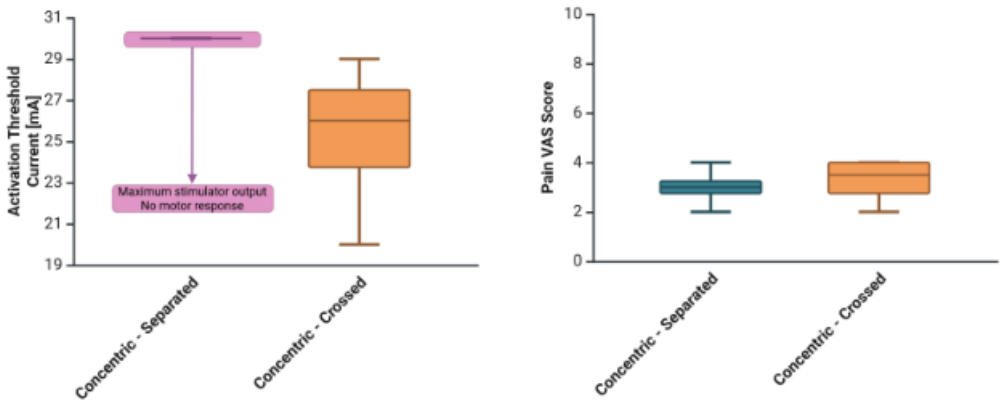

Figure 7.2.19: Comparison of the distribution of current activation threshold (left) and VAS evaluation from the subject perception (right) for the concentric electrodes placed along the forearm experiment.

7.2.3 Unbalanced-Channels Electrical Steering on Finger Flexors

The participant evidenced a selective median and ulnar stimulation by unbalancing each stimulator channel's output currents. The registered threshold for a thumb and little finger pulsatory motor response was 24 mA (fig. 7.2.20 a)). Reducing the current output of channel 2 to 12 mA, isolated little finger dorsiflexion responses were obtained while the thumb remained non-responsive (fig. 7.2.20 b)). Then, with channel 2 at 24 mA and channel 1 at 15 mA, a specific thumb dorsiflexion was obtained, with the little finger remaining non-responsive (fig. 7.2.20 c)).

Figure 7.2.20: Captures of the unbalanced-channels electrical steering experiments. The left pictures show a contraction state and the right pictures show a relaxation between pulsatory contractions. a) Channels balanced, thumb and little finger respond to stimulation. b) Channels unbalanced (channel 1 output reduced), little finger dorsiflexion. c) Channels unbalanced (channel 2 output reduced), thumb dorsiflexion.

A demonstrative video of the experiment can be found in gitHub repository - Steering Stimulation.

Chapter 8

Discussions

This section was organised to discuss the results derived from the fulfilment of the general and specific objectives derived from what was postulated in chapter 5, starting from the computational modelling using FEM anatomical models, the different in vivo testing in lower and upper limbs, and the evaluation of new proposals for optimising the application of electrical stimulation techniques with promising clinical implementation. Then, a perspective on the new research lines that derive from the discussed findings is presented.

8.1 Computational Modelling

8.1.1 Advantages of FEM for Biophysical Modelling

Finite element modelling is an extremely useful tool for simulating the nervous system and calculating electrical variables associated with electrical stimulation. These standardised models allow us to quickly evaluate and compare the influence

of changing electrical variables (e.g., waveforms, frequency, amplitude) or electrode variables (e.g., position and shape). They also help to prepare experimental protocols for in vivo testing, serving as a pre-verification of proposed stimulation techniques.

The visual representation of the activating function, modulated currents, and modulated fields provides insight into the electromagnetic phenomena within biological tissue, thereby facilitating a deeper understanding of otherwise invisible phenomena. These calculations evidence the generation of modulated currents and how they influence neural tissue.

Given the importance of accurate modelling to support applications in functional stimulation of the nervous system, FEM needs to follow reproducible and standardised practices. In [132], we demonstrated that finite element mesh sizes influence the accuracy of the results obtained from FEM simulations. Poor spatial discretisation facilitates the generation of double-derivative noise. Also, implementing multiscale and adaptive meshing supports more accurate modelling of anatomical structures, where the structures have different orders of dimensions and emphasise regions of interest. This combination reduces the computation cost and the double derivative errors in the transition of tissues.

8.1.2 Activating Function and Axon Models

Rattay's activating function and cable equation-based axon models are proficient mathematical tools for evaluating and describing the influence of electric fields

over biological tissue, especially on neural structures.

While their stated equations are similar, they pertain to different phenomena. The activating function describes the extracellular fields and indicates how deep and/or concentrated the influence of a particular stimulation configuration is. Thus, the AF can easily show, for example, the activation zones of the modulated currents when modelling ICS. This became relevant when we planned to evaluate and compare different electrode configurations, waveforms, and frequencies. On the other hand, cable equation-based axon models describe membrane potentials and their variations over time and space simultaneously. These models allow us to predict if specific stimulation configurations can trigger action potentials on a single axon. These models can be adjusted to represent different types of axons, e.g. myelinated or non-myelinated, and various diameters. I advocate using these tools complementarily, taking into account their disparities.

The results presented in fig. 7.1.1 show the 1D profiles of the AF at different depths into the thigh. It can be seen in almost all the cases, at the nerve level, the 50 Hz modulation produced by the interferential currents. The profiles along the nerve depend on the specific electrode configurations, generating 1 or 2 spots of high amplitude-modulated fields. Some models at intermediate and surface levels do not exhibit the 50 Hz slopes presented at the nerve level. This can indicate a non-interference zone where the kilohertz stimuli are predominant.

The fig. 7.1.2 plots show the 3D profiles of the AF on the whole thigh volume. These distributions evidence the influence of the electrode shapes and positioning

on the generated interference zones. It can be seen that a separated electrode configuration generates two lobes that wrap the nerve. The hybrid configuration generated an interesting distribution, with a space of non-interference between the skin and the nerve. Even though every configuration successfully reached the femoral nerve, it is necessary to evaluate the ability to trigger action potentials with an axon model.

The action potentials predicted by the Hodgkin-Huxley axon model are illustrated in fig. 7.1.3. The plots represent the membrane potential along the modelled axon at a specific time instant. An action potential can be recognised as a narrow high-amplitude peak, reaching values $\approx 60\ mV$. The action potentials are generated in pairs, having a common starting point under one of the cathodes, and progressively move in opposite directions. Note that one of these action potentials has real physiological relevance, depending on the direction of the neural connections (i.e. afferent or efferent). The configurations that did not exhibit action potentials were the Multiconcentric ring and Front line double pair side by side.

In this work, an unmyelinated axon model was used to evaluate the generation of action potentials. The Hodgkin-Huxley axon model is among the most accepted and widely used in computational neuroscience. However, it differs from the myelinated axons of mammals. This model was chosen for its simplicity, but other complex axon models (e.g., the MRG axon model) may yield more physiologically accurate results.

8.1.3 High-Order ICS modulation

The models with the crossed squared and collinear nested concentric electrode configurations exhibited an interferential effect almost identical to the mathematical summation of harmonics. Both can generate activation by the principal component of the interferential current (50 Hz) with an approximated 25 mA per channel. Both present oscillations on the calculated membrane potentials associated with other carrier frequencies, but those oscillations don't interfere with the propagation of the action potentials.

When using the opposite nested concentric electrode positioning, the resultant interference current differs from the mathematical summation of harmonics, having as a principal frequency 1/2 times the targeted beat frequency. This configuration does not activate the nerve, even when applying high current amplitudes ($>100mA$).

The behaviour presented in the first two experiments supports the theory of a "demodulator" in the axon membrane. This mechanism differentiates the low-frequency beat from the high-frequency carriers, activating the nerve if the beat is predominant over the carriers. The opposite placement of the Dual Concentric Ring electrodes suggests that the interferential effect is not adequately produced due to their location. Further studies will be conducted to determine if a perpendicular current path to the nerve generates activation and collinear arrangements.

8.2 In-vivo Experiments

8.2.1 Custom Made Electrodes

Commercially available electrodes are predominantly square, rectangular or circular shaped. In this work, a non-conventional arrangement of concentric electrodes was the core of the proposed electrode configurations: It was necessary to manufacture these shapes. The first attempts included a non-standardised scissor-cutting process using commercially available electrodes, presenting adequate results. Nevertheless, the time/effort cost was high thinking on producing the necessary numbers for the in-vivo tests.

The laser-cutting machine allowed for the standardisation of the manufacturing process, reducing inter-subject variance due to electrode malfunctioning or dimension differences and improving the experiments' reproducibility. For the scissor-cutting process, including measurement, marking and cutting, one electrode took about 20 minutes to be redimensioned. The laser-cutting process can generate a batch of 100 electrodes in about 45 minutes.

This process allows us to swiftly obtain resized electrodes with tailored shapes, which is advantageous for rapid prototyping electrodes for experimental tests. However, there are limitations worth noting: the new size is capped by the original electrode size, the design must include protection for the connector, and the laser power must be adjusted so as not to burn the conductive layer or the hydrogel. The latter is extremely important, as carbonisated edges may induce high peaks

of current densities, potentially dangerous for the subjects. In this work, the laser power was adjusted in an iterative process.

8.2.2 Motor Point Displacement

The experiments described in section 6.2.3.1 and their results presented in section 7.2.1.1 demonstrated that the proximal rectus femoris motor point shifted in non-isokinetic positions across three levels of knee extension.

In the study involving thirteen subjects, a significant displacement of the motor point was observed, moving from 90° knee flexion to a fully extended position at 180°. On average, the shift was nearly 7 cm, corresponding to 15% of their thigh length. A mean current of 19 mA was necessary to elicit contraction in the rectus femoris. Most subjects exhibited a similar displacement pattern, moving medially along the x-axis and distally on the y-axis.

These shifts in motor points during limb movement are noteworthy, as they may weaken contraction force due to the misalignment between the electric fields generated by the electrodes and the new motor point position. This misalignment poses a potential risk for rehabilitation programs utilising FES or similar techniques, as it may hinder complete movement or produce sufficient force for exercises. These findings align with those in related studies [108; 117; 118] that tracked motor points in upper limb muscles, which also identified a correlation between elbow flexion and motor point displacement.

A point to consider is that the return electrode, identified as the anode, is positioned

near the neural target tissue rather than at a distance. While it is correct to note that the electrode was placed distally, it remains over the distal portions of the vastus medialis and vastus lateralis. The stimulation procedure demonstrated a degree of non-selectivity, as the return electrode may have contributed, at least in part, to some of the elicited responses. Future work will focus on tracking the MPs of other limb muscles and optimising electrode positioning.

8.2.3 Advantages and Disadvantages of ICS

The presented experiments show the potential use of interferential currents (ICS) for motor control neuromuscular stimulation. In both the thigh and forearm stimulation tests, ICS generated motor responses. Compared to conventional FES, the gold-standard motor control technique, ICS tends to generate waker contractions.

ICS requires more current rather than FES. For example, FES has a lower mean threshold when analysing the activation thresholds in fig. 7.2.5. Noting that ICS required at least one additional channel, the required current for ICS was more than double the needed for FES. Thus, ICS is a less efficient technique than FES. The presence of shuttered currents leaked on the skin may explain this efficiency reduction. As the skin impedance is reduced at high frequencies, the input currents confront a superficial path of low impedance [139].

Results showed sex-dependent motor responses during the rectus femoris stimulation tests, where some female subjects displayed a non-motor response. At

the same time, males exhibited muscle activation in every technique except for the ICS-Dual Concentric electrodes. According to [140], even with similar BMI, the females in the study had 107% more subcutaneous fat in their thighs compared to the males. This discrepancy in adipose tissue may result in increased impedance in female thighs relative to males, making it more challenging to access the motor points behind the thigh fat.

However, the latter can also explain the main advantage of using ICS. During the experiments, a simple test of a plastic probe rubbing the skin's surface between the electrodes showed an anaesthetic effect. The subjects claimed that even though they saw the plastic probe touching their skin, they couldn't sense it, or the sensation was highly reduced. This seems to be produced by a localised conduction block on the skin afferent axons produced by these high-frequency shunted currents.

The VAS evaluation of the rectus femoris tests showed a notable reduction in discomfort when ICS was applied compared to FES. This effect is mostly attributable to the reduction of the skin sensation. A particular result was obtained for the ICS-Dual Concentric, where the reduced sensation is also associated with its inability to generate motor contractions. The McGill questionnaire results showed that the subjects chose "stronger" adjectives and expressions for the FES-50 Hz technique while using "softer" expressions to define the ICS techniques. This is well correlated to the VAS score's mean values.

The applied ICS currents are considered to be purely sinusoidal near the electrodes,

alleviating discomfort caused by skin afferent activation. In the tissue, amplitude modulation takes place as the carrier currents combine, creating areas ranging from slight modulation to complete (equal amplitudes) modulation of the carrier. At these ICS kilohertz frequencies, there may also be regions of nerve blockade [141].

The forearm is an excellent site for testing hand flexor and extensor contractions using the nearby median and ulnar nerves, which allows for the assessment of stimulation specificity. In tests conducted on the forearm, at least two sets of electrodes are utilised to target the nerve activation area. Configurations arranged along the nerve, instead of in a circular manner, lower the intensity threshold and reduce discomfort from the stimulation. These findings are significant for NMES, especially in cases where sensation remains intact or where stimulation might trigger unwanted reflex responses [139].

These findings helped validate the specific hypothesis presented in the introduction section: The combination of superficial high-frequency stimulation and deep low-frequency modulation generates a comfortable skin sensation, along with muscle contractions.

8.2.4 Influence of Electrodes Shape and Positioning

The experiments conducted in this study examined a variety of electrode shapes and their respective positions. The results indicated differing responses based on the configurations of the electrodes. Generally, square electrodes elicited greater

discomfort than concentric electrodes; however, the latter necessitated a higher current to achieve the activation thresholds.

In the comparative analysis of square electrodes and concentric rings utilizing the ICS on rectus femoris assessments, the concentric rings demonstrated a significantly reduced level of perceived discomfort, as indicated by the scores derived from the Visual Analog Scale (VAS) and the McGill Pain Questionnaire. The separate channels were found to lack the ability to elicit motor responses, as evidenced in experiments conducted on both the thigh and forearm. This phenomenon may be attributed to the fact that the intersection of the stimulation currents fails to produce modulated activation zones. Additionally, computational models and in-vivo testing of the forearm revealed an absence of axonal activation when the channels were strategically positioned opposite one another.

The multiconcentric ring electrode design demonstrated no axon activation in both computational and experimental tests. The H-H axon model indicated that no action potentials were generated, while the experiments on the rectus femoris MP were similarly unsatisfactory. Multiconcentric electrodes placed over the femoral triangle did not produce motor contractions; rather, this configuration stimulated skin nociceptor afferents, resulting in notable discomfort for two subjects. The initial hypothesis posited that this configuration would perform better than the traditional FES or ICS techniques over the MPs. Consequently, the hypothesis is rejected. However, alternative techniques emerged as comparable options to single-channel FES: nested concentric electrodes during the forearm experiments

and hybrid configurations at the thigh exhibited good performance, balancing motor control and minimising pain sensations.

Thus, the following specific hypotheses presented in the introduction section are valid:

1. The electrode geometry influences the areas where electrical stimulation can generate a nerve activation.

2. The electrode positioning affects the effects of the modulation of ICS techniques.

8.2.5 Electrical Steering of Activation Zones

The unbalanced-channel electrical steering technique yielded encouraging results. Modifying the relative amplitudes of the current output from each channel produced a distinctive response in two adjacent nerves. This technique effectively redirected the activation to either the median or ulnar nerve, eliciting dorsiflexion responses in the thumb or little finger, respectively. This experiment correlates to the simulation results, where the activating function 3D distributions can be steered next to the lower amplitude channel electrodes.

This experiment specifically necessitated the use of two Ultima Neo Pro stimulators. This requirement primarily stems from the configuration of the stimulator, which automatically escalates the output of both channels when functioning in interferential mode. One channel from each stimulator was used to acquire the unbalanced channel output.

This novel technique is captivating because it can alter the influence of a specific electrode configuration without replacing the electrodes or utilising an electrode matrix. However, extensive studies should be conducted to characterise and further develop this method.

8.3 Associated investigations and New Research Lines

8.3.1 Electrical Steering for MP track and Activation Fine Tuning

The motor point tracking experiments evidenced the considerable shift of the rectus femoris motor points. This MP movement may affect the effectiveness of motor control stimulations during movements on rehabilitation therapies or sports training. The MP shift is related to joint movements. The relative movement of the muscle below the skin generates instants where the electrodes are not positioned over the MP, reducing or not producing the muscle contraction.

Once the MP shift track was identified, positioning electrodes at the starting and ending points did not show losses in generating muscle contractions when evaluating motor responses at different knee extension levels. Thus, this may be a feasible solution to the MP shift loose contractions.

It may be possible to complement and optimise the location of MP and its shifts

in conjunction with electrical steering. By employing the unbalanced-channel electrical steering method, one can standardise the position of the electrodes with anatomical references (as is typically done in clinical practice) and refine inter-subject differences by unbalancing the output currents to steer the activation zones.

An application that can benefit from this is a non-invasive stimulation for bladder control. The current non-invasive electrical stimulation for overactive bladder works via a vaginal or anal probe or through a fine needle inserted into the tibial nerve around the ankle [142]. With the proposed techniques, combining ICS and electrical steering, electrodes can be placed superficially on the lower back and fine-tune the activation zones to the sacral root nerves that control the bladder muscles.

8.3.2 Development of Programmable Interferential Currents Stimulator

Commercially available interferential stimulators are pre-configured for analgesic treatments, limiting the maximum current outputs. During the presented experiments, some subjects who hadn't experienced motor responses claimed that they felt the muscle almost reacting to the stimulation at the maximum 30 mA per channel that the Ultima Neo could produce.

Further experiments would need higher current amplitudes to exceed the activation thresholds and achieve stronger muscle contractions. A custom-made

programmable interference stimulator could overcome these limitations. Also, it would allow the testing of different waveforms, such as the High-Order ICS modulation.

8.3.3 Evaluating the Influence of Skin Impedance and Hydration on ICS

The effectiveness of stimulation is determined by the electrical parameters used in the stimulator and the electrical properties of the skin itself, which serves as a contact interface with the electrodes when the treatment is applied. One such skin parameter is conductivity, defined as the skin's ability to allow the flow of electrical current. Various factors, including skin hydration, can affect this capacity [143].

A Corneometer is a device that measures skin hydration by assessing the amount of water and oil composition in the stratum corneum (the most superficial layer of the skin). The hydration state of the stratum corneum is a significant parameter in various dermatocosmetic applications, with its determination generally based on electrical measurements of the skin surface [144; 145].

Different topical preparations can alter the skin's hydration and, consequently, its conductivity. Furthermore, measuring skin impedance will reveal changes in the tissue's dielectric properties. This study will enable us to evaluate and quantify the impact of these hydration changes on skin impedance and conductivity, as well as their influence on the current intensities required to generate a motor effect

through electrical stimulation.

8.3.4 Perspectives on ICS Therapies for Sports Rehabilitation and Training

ICS demonstrated promising results as an alternative to neuromuscular stimulation therapies for motor control. ICS provides proportional control of muscle force and greater comfort than traditional rectangular pulse stimulation. Reducing discomfort may enhance the patient's adherence to treatment, creating a more pleasant experience. This becomes increasingly important when considering prolonged treatment or training sessions, during which the stimulus is present for the majority of the time.

Future work aims to support rowing therapy treatments for patients with partial and complete spinal cord injuries. The knowledge and experience acquired during this study will serve as the foundation for developing FESRowing therapies in conjunction with interferential currents, which aim to achieve comparable motor responses to FES while preserving the discomfort-reduction effects of ICS.

8.3.5 Publications

Two papers were submitted to journals showing different results obtained during the investigation:

- "Finite element modelling for biophysical models of nervous system stimulation: Best practices for multiscale adaptive meshing". Published

in IEEE Transactions on Neural Systems and Rehabilitation Engineering, January 2025 [132].

The study focuses on the use of Finite Element Method (FEM) models to calculate electric fields and related variables, such as the Activating Function proposed by Rattay in 1986 and membrane potentials. These calculations rely on double derivatives of electric potentials, which can be prone to errors, mainly when dealing with noisy data. These models were primarily implemented to evaluate various electrode designs and electrical parameter configurations of neurostimulation techniques, highlighting the need to assess the reliability of these models.

Two case studies were conducted to assess the impact of double derivative errors on neural simulations. The first focused on a thigh model utilising a Hodgkin-Huxley axon framework with 4x4 cm bipolar square electrodes, delivering monophasic pulses of 10 ms at currents between 55 and 57.5 mA. Various mesh sizes—coarse and extremely fine, as well as triangular and quadrangular shapes were tested. Results indicated that coarser meshes produced significant errors, which were mitigated in finer meshes but not entirely eliminated. Triangular meshes were preferred for defining tissue volumes. The activation thresholds were 57.5 mA for coarse and 55 mA for fine meshes, indicating that while errors did not obstruct action potential predictions, they could influence the interpretation of the activating function. The second case involved a cortical model examining errors during transitions

across tissues with varying magnitudes. This model employed 1.77 cm^2 bipolar circular electrodes delivering 1 mA monophasic pulses. Three custom mesh sizes—ultra-fine uniform, highly refined, and finest refined—were implemented using a multiscale approach for enhanced accuracy. This method reduced errors during tissue transitions, although some smoothing of the activating function was still apparent.

The study concluded that poor spatial discretisation leads to double derivative errors in FEM models. However, these errors did not result in premature action potentials. The study strongly recommends using finer mesh sizes, multiscale techniques, or adaptive filtering methodologies to reduce these errors and improve the reliability of FEM models.

- "Characterization and Evaluation of Interferential Current Stimulation for Functional Electrical Stimulation". Published in Artificial Organs, May 2025 [139].

  The study focuses on the evaluation of interferential current stimulation technique as an alternative for motor control strategies. Experiments were conducted on human participants, focusing on the activation of the ulnar and median nerves using stainless steel and commercial conductive hydrogel electrodes. Key parameters, including electrode configuration, frequency, current amplitude, and skin preparation, were examined to assess their impact on activation thresholds, force generation, and user comfort.

  Our results revealed that ICS can achieve proportional muscle force control,

although its efficiency was lower than rectangular biphasic pulse stimulation. The application of moisturising cream and gel significantly improved comfort and reduced activation thresholds, underscoring their importance in optimising ICS protocols. However, ICS required higher electrical power and caused discomfort during burst initiation with all electrodes, presenting challenges for its practical use in FES. Furthermore, our findings indicated that ICS did not exclusively activate neural regions at the difference or "beat" frequency but also by the carrier frequency, challenging some prior assumptions in the literature.

These results highlight the need for further research and practical measurements of neural recruitment and muscle fatigue, as well as an understanding of the mechanisms of nerve activation and neuromuscular junction transmission with stimulation via the skin surface. Innovations in electrode design, stimulation waveforms, and protocols are also needed to enhance the efficacy and comfort of ICS.

Chapter 9

Conclusions

This study offers significant insights into the mechanisms and effects of interferential current stimulation on muscle activation across various cases of functional electrical stimulation, with a focus on different electrode geometries and positioning techniques. The findings emphasise the critical importance of electrode placement and configuration in optimising the effect of electrical stimulation.

The proposed investigation methodology was useful to complete the general and specific objectives presented in chapter 5. Moreover, the findings from both in silico and in vivo experiments were sufficient to answer the research questions posed in section 1.4.

The computational models and in vivo experiments have elucidated that ICS, utilising diverse electrode configurations, can effectively stimulate the quadriceps muscle, yet this effect is dependent on the specific positioning of the electrodes. However, the amplitude of the muscle response exhibits variability. Notably, the ICS square electrodes demonstrated performance that is comparable to that

of the conventional 50 Hz FES technique, with a marginally elevated current threshold required for activation. In contrast, the nested concentric and hybrid electrode configurations, while indicating potential for efficacy, also exhibited limitations, particularly regarding stimulation intensity and the consistency of muscle contractions.

The study also emphasised the challenges associated with ICS. One key issue is that this method requires higher current amplitudes compared to traditional FES. Additionally, there is considerable variability in the responses observed among different subjects. Furthermore, the analysis of pain and discomfort perceptions offers valuable insights for the practical application of these techniques in clinical settings. The findings suggest that ICS generally produces tolerable levels of discomfort; however, certain configurations, such as the Dual Concentric approach, may not generate sufficient motor responses.

The principal hypothesis, "Interferential Current Stimulation (ICS) over the femoral nerve, using multipolar concentric ring electrodes, produces stronger muscle activation and less sensory discomfort than standard single-channel Functional Electrical Stimulation (FES) using side-to-side electrodes," is rejected, as the multiconcentric ring electrode configuration did not yield desirable outcomes. This approach elicited pure pain receptor activation, without any motor responses.

Answering the research questions previously introduced in the Introduction section (see section 1.4):

1. How do different electrode geometries impact the intensity of induced muscle

contractions and the sensation of discomfort during Functional Electrical Stimulation and Interferential Current Stimulation?

Concentric ring electrodes tend to generate concentrated electric fields, yet no experimental test has evaluated this electrode geometry for ICS before. Concentric ring electrodes showed a concentrated effect compared to square electrodes, reflected on the FEM analysis. The nested concentric ring electrode and hybrid configurations with ICS demonstrated an improvement in motor responses elicited registered with the elastic rubber setup, compared to separated concentric ring configurations (see fig. 7.2.6 and fig. 7.2.7), without compromising comfort sensation (see fig. 7.2.14) when evaluating the McGill questionnaire and VAS.

2. How does the electrode positioning influence the elicited muscle contractions while applying FES and ICS?

   ICS is a technique that critically depends on the spatial distribution of electric fields. Concentric ring electrodes present a novel positioning opportunity to be nested (i.e., crossing the cathode-anode of two channels). The electrode positioning, based on tracking the movement of the motor point, can optimise and maintain muscle contraction during limb movements. Electrodes positioned perpendicular to the nerve, specifically in front of each, did not elicit motor responses. Electrodes positioned parallel to the nerve are more likely to generate muscle contractions. The motor point displacement tracking technique was effective in maintaining muscle contractions, despite

the motor point movement in a knee angular displacement between 90 and 180 degrees of flexion, as seen in fig. 7.2.6 and fig. 7.2.7, where the contractions were not loose when changing the knee extension angle.

3. Can comparable muscle contraction intensities be achieved with ICS compared to FES, while simultaneously reducing pain sensation?

   Earlier studies demonstrated the anaesthetic effect of kilohertz stimulation by producing conduction blocking. ICS and the novel electrode geometries, considering the positioning of the electrodes, can concentrate the kilohertz stimuli influence at the skin while producing the modulation next to the target nerve or motor unit. The presence of conduction-blocking effects on skin afferents enhances the comfort of the experience for the subject and may even produce a localised anaesthetic sensation in the skin between the electrodes. While ICS generates less intense muscle contractions compared to FES techniques, most electrode configurations can still maintain muscle contractions without causing the same level of discomfort associated with FES. These subjective assessments of discomfort were evaluated using pain questionnaires, including the McGill and VAS scales.

4. Can the region of ICS nerve activation be extended to accommodate the displacement of motor points?

   The findings on the analysis of the 3D Activating Function (see fig. 7.1.2) of ICS showed that the distributions of the activation zones are highly dependent on the shape, size and positioning of the electrodes. Thus, we can

accommodate these regions next to our nerve target by choosing the optimum electrode configuration. Addressed the motor point displacement issue, the proposed technique was to combine the novel electrode configurations with a strategic placement of the electrodes: at least one electrode placed over the motor point tracked positions at the beginning of the angular knee range (90 degrees flexion) and the end (180 degrees flexion). This technique demonstrated that, despite the motor point's movement, the contractions remained tight when adjusting the angle of knee extension as shown in fig. 7.2.6 and fig. 7.2.7 for certain configurations.

5. Can the region of ICS nerve activation be electronically "steered" to enable automatic adjustment without requiring the electrodes to be removed and reapplied manually?

   This research question presented significant challenges, primarily attributable to the limited evidence available from in vivo human experiments. The FEM modelling showed that unbalancing the relative current amplitudes of the channels, yet maintaining the total current injected to the model, steered the activation zones towards the electrodes connected to the lower amplitude stimuli, represented by the Activating Function in fig. 7.1.4 and fig. 7.1.5. The results of the experiment conducted on a human forearm demonstrated the feasibility of selectively stimulating either the median or ulnar nerve. This intriguing finding arises from the anatomical proximity of these two nerves, which are typically activated simultaneously when

employing conventional stimulation techniques. Then, we proposed the Unbalanced-Channels Electrical Steering technique as a promising method to selectively activate different adjacent structures, without removing and reapplied surface electrodes.

Future research should concentrate on enhancing electrode designs, optimising current modulation techniques, and investigating the long-term effects of ICS for rehabilitation purposes. Furthermore, additional studies on motor point tracking and the impact of skin impedance may contribute to improving the precision and efficiency of integrated electrical stimulation systems.

In conclusion, the novel ICS techniques with optimised electrode placements present a promising alternative for muscle activation, with significant potential for improving rehabilitation therapies and muscle training in individuals with neuromuscular disorders, making it a potentially more comfortable technique than traditional FES therapies.

Bibliography

[1] R. S. Gibbons, R. E. Shave, A. Gall, and B. J. Andrews, "Fes-rowing in tetraplegia: a preliminary report," *Spinal Cord*, vol. 52, no. 12, pp. 880–886, Sep. 2014.

[2] D. M. Hettinga and B. J. Andrews, "The feasibility of functional electrical stimulation indoor rowing for high-energy training and sport," *Neuromodulation: Technology at the Neural Interface*, vol. 10, no. 3, pp. 291–297, Jul. 2007.

[3] (2024, Apr.) C.r.a.s.h.-b international world indoor rowing championship history. [Online]. Available: http://www.crash-b.org/about/c-r-a-s-h-b-history/

[4] P. J. Grahn, G. W. Mallory, B. M. Berry, J. T. Hachmann, D. A. Lobel, and J. L. Lujan, "Restoration of motor function following spinal cord injury via optimal control of intraspinal microstimulation: toward a next generation closed-loop neural prosthesis," *Frontiers in Neuroscience*, vol. 8, Sep. 2014.

[5] S. Parittotokkaporn, C. Varghese, G. O'Grady, D. Svirskis, S. Subramanian, and S. J. O'Carroll, "Non-invasive neuromodulation for bowel, bladder and sexual restoration following spinal cord injury: A systematic review," *Clinical Neurology and Neurosurgery*, vol. 194, p. 105822, Jul. 2020.

[6] M. I. B. Debenham, C. K. Franz, and M. J. Berger, "Neuromuscular consequences of spinal cord injury: New mechanistic insights and clinical considerations," *Muscle amp; Nerve*, vol. 70, no. 1, pp. 12–27, Mar. 2024.

[7] M. Safdarian, E. Trinka, V. Rahimi-Movaghar, A. Thomschewski, A. Aali, G. G. Abady, S. M. Abate, F. Abd-Allah, A. Abedi, D. E. Adane, S. Afzal, B. O. Ahinkorah, S. Ahmad, H. Ahmed, N. Amanat, D. Angappan, J. Arabloo, A. Aryannejad, S. S. Athari, A. Atreya, S. Azadnajafabad, A. Y. Azzam, H. Babamohamadi, P. C. Banik, M. Bardhan, A. Bashiri, A. Y. Berhie, A. N. Bhat, J. Brown, A. P. Champs, P. Charalampous, I. S. Chukwu, K. Coberly, O. Dadras, D. Y. Yada, X. Dai, L. Dandona, R. Dandona, F. N. Dessalegn, A. A. Desta, S. Dhingra, N. Diao, D. Diaz, M. Dibas, D. Dongarwar, H. L. Dsouza, M. Ekholuenetale, N. El Nahas, M. Elhadi, S. Eskandarieh, A. F. Fagbamigbe, J. Fares, A. Fatehizadeh, S.-M. Fereshtehnejad, F. Fischer, R. C. Franklin, T. Garg, M. Getachew,

F. Ghaffarpasand, A. Gholamrezanezhad, M. Gholizadeh Mesgarha, S. Ghozy, M. Golechha, P. Goleij, S. M. Graham, V. K. Gupta, J. A. Haagsma, S. Hamidi, N. I. Harlianto, M. Harorani, M. Hasanian, A. Hassan, M. B. Hassen, A. H. Hoveidaei, F. Iravanpour, R. Irilouzadian, C. C. D. Iwu, L. Jacob, C. J. Jaja, N. Joseph, C. E. Joshua, J. J. Jozwiak, V. Kadashetti, A. Kandel, R. S. Kantar, I. M. Karaye, S. Karkhah, Y. S. Khader, E. A. Khan, M. J. Khan, H. R. Khayat Kashani, M. S. Khonji, M. Khormali, G. Kim, V. Krishnamoorthy, S. D. Kumaran, M.-R. Malekpour, T. J. Meretoja, M. K. Mesregah, T. Mestrovic, A. C. Micheletti Gomide Nogueira de Sá, T. R. Miller, A. Mirahmadi, S. P. Mirghaderi, M. Mirza, A. Misganaw, S. Misra, Y. Mohammad, E. Mohammadi, A. H. Mokdad, H. Möller, S. Momtazmanesh, M. A. Moni, E. Mostafavi, F. Mulita, M. Naghavi, H. Nassereldine, Z. S. Natto, K. Nejati, H. L. T. Nguyen, V. T. Nguyen, A. T. Nogueira de Sá, A. T. Olagunju, I. I. Olufadewa, A. O. Omotayo, M. O. Owolabi, S. Patil, S. Pawar, P. Pedersini, I.-R. Petcu, S. Polinder, A. M. Pourbagher-Shahri, M. F. Qureshi, P. R. Raghav, M. Rahman, N. Rahnavard, A. Rajabpour-Sanati, M.-M. Rashidi, S. Rawaf, N. L. S. Roberts, B. Saddik, U. Saeed, S. Samadzadeh, A. M. Samy, A. Sarveazad, A. Seylani, M. Shafie, A. Shahbandi, M. M. S. Sharew, R. A. Sheikhi, P. H. Shetty, A. Yigit, P. Shobeiri, S. Shool, S. A. Shorofi, M. M. Sibhat, E. Sinaei, P. Singh, S. Singh, Y. Solomon, H. Sotoudeh, B. A. Tadesse, M. Umair, S. Valadan Tahbaz, P. R. Valdez, N. Venketasubramanian, L. G. Vu, N. D. Wickramasinghe, I. Zare, F. Yazdanpanah, A.-M. Wu, and Z.-J. Zhang, "Global, regional, and national burden of spinal cord injury, 1990–2019: a systematic analysis for the global burden of disease study 2019," *The Lancet Neurology*, vol. 22, no. 11, pp. 1026–1047, Nov. 2023.

[8] W. H. Organization, "Spinal cord injury," 2024, accessed: 2025-04-16. [Online]. Available: https://www.who.int/news-room/fact-sheets/detail/spinal-cord-injury

[9] N. S. C. I. S. Center, "Spinal cord injury facts and figures at a glance," *The Journal of Spinal Cord Medicine*, vol. 36, no. 1, pp. 1–2, Jan. 2013.

[10] M. J. DeVivo, "Epidemiology of traumatic spinal cord injury: trends and future implications," *Spinal Cord*, vol. 50, no. 5, pp. 365–372, Jan. 2012.

[11] R. M. Dorrian, C. F. Berryman, A. Lauto, and A. V. Leonard, "Electrical stimulation for the treatment of spinal cord injuries: A review of the cellular and molecular mechanisms that drive functional improvements," *Frontiers in Cellular Neuroscience*, vol. 17, Feb. 2023.

[12] R. Martin, C. Sadowsky, K. Obst, B. Meyer, and J. McDonald, "Functional electrical stimulation in spinal cord injury: From theory to practice," *Topics in Spinal Cord Injury Rehabilitation*, vol. 18, no. 1, pp. 28–33, Jan. 2012.

[13] R. C. Chou, J. A. Taylor, and R. Solinsky, "Effects of hybrid-functional electrical stimulation (fes) rowing whole-body exercise on neurologic

improvement in subacute spinal cord injury: secondary outcomes analysis of a randomized controlled trial," *Spinal Cord*, vol. 58, no. 8, pp. 914–920, Feb. 2020.

[14] A. Bass, M. Aubertin-Leheudre, C. Vincent, C. Duclos, and D. H. Gagnon, "Upper limb muscle strength and wheelchair-related abilities following an exoskeleton-assisted walking programme in individuals with chronic spinal cord injury: An exploratory study," *Journal of Rehabilitation Medicine*, vol. 56, p. jrm19461, Nov. 2024.

[15] T. R. Deer, R. Naidu, N. Strand, D. Sparks, A. Abd-Elsayed, H. Kalia, J. M. Hah, P. Mehta, D. Sayed, and A. Gulati, "A review of the bioelectronic implications of stimulation of the peripheral nervous system for chronic pain conditions," *Bioelectronic Medicine*, vol. 6, no. 1, Apr. 2020.

[16] H.-L. Su, C.-Y. Chiang, Z.-H. Lu, F.-C. Cheng, C.-J. Chen, M.-L. Sheu, J. Sheehan, and H.-C. Pan, "Late administration of high-frequency electrical stimulation increases nerve regeneration without aggravating neuropathic pain in a nerve crush injury," *BMC Neuroscience*, vol. 19, no. 1, Jun. 2018.

[17] H. R. Martins, R. Zanetti, C. C. d. Santos, G. M. Manzano, and C. J. Tierra-Criollo, "Current perception threshold and reaction time in the assessment of sensory peripheral nerve fibers through sinusoidal electrical stimulation at different frequencies," *Revista Brasileira de Engenharia Biomédica*, vol. 29, no. 3, pp. 278–285, 2013.

[18] C. Lynch and M. Popovic, "Functional electrical stimulation," *IEEE Control Systems Magazine*, vol. 28, pp. 40–50, 2008.

[19] M. Johnson, "Transcutaneous electrical nerve stimulation: Mechanisms, clinical application and evidence," *Reviews in Pain*, vol. 1, no. 1, pp. 7–11, Aug. 2007.

[20] S. Bounyong, S. Adachi, T. Yoshimoto, T. Ota, and J. Ozawa, "Controlling interfered area in interferential current stimulation by electrode-area patterning," in *2016 38th Annual International Conference of the IEEE Engineering in Medicine and Biology Society (EMBC)*. IEEE, Aug. 2016, pp. 1721–1724.

[21] A. d. O. Gomes, A. C. Silvestre, C. F. d. Silva, M. R. Gomes, M. L. Bonfleur, and G. R. F. Bertolini, "Influence of different frequencies of transcutaneous electrical nerve stimulation on the threshold and pain intensity in young subjects," *Einstein (São Paulo)*, vol. 12, no. 3, pp. 318–322, Sep. 2014.

[22] K. Takeda, G. Tanino, and H. Miyasaka, "Review of devices used in neuromuscular electrical stimulation for stroke rehabilitation," *Medical Devices: Evidence and Research*, vol. Volume 10, pp. 207–213, Aug. 2017.

[23] C. Neudorfer, C. T. Chow, A. Boutet, A. Loh, J. Germann, G. J. Elias, W. D. Hutchison, and A. M. Lozano, "Kilohertz-frequency stimulation of the

nervous system: A review of underlying mechanisms," *Brain Stimulation*, vol. 14, no. 3, pp. 513–530, May 2021.

[24] J. L. Vargas Luna, M. Krenn, J. A. Cortés Ramírez, and W. Mayr, "Dynamic impedance model of the skin-electrode interface for transcutaneous electrical stimulation," *PLOS ONE*, vol. 10, no. 5, p. e0125609, May 2015.

[25] C. Alon, G. Kantor, and H. S. Ho, "Effects of electrode size on basic excitatory responses and on selected stimulus parameters," *Journal of Orthopaedic amp; Sports Physical Therapy*, vol. 20, no. 1, pp. 29–35, Jul. 1994.

[26] B. Forrester and J. Petrofsky, "Effect of electrode size, shape, and placement during electrical stimulation," *The Journal of Applied Research*, vol. 4, no. 2, pp. 346–354, 2004.

[27] A. van Oosterom and J. Strackee, "Computing the lead field of electrodes with axial symmetry," *Medical and Biological Engineering and Computing*, vol. 21, no. 4, pp. 473–481, Jul. 1983.

[28] W. Besio, V. Sharma, and J. Spaulding, "The effects of concentric ring electrode electrical stimulation on rat skin," *Annals of Biomedical Engineering*, vol. 38, no. 3, pp. 1111–1118, Jan. 2010.

[29] G. Prats-Boluda, J. Garcia-Casado, J. L. Martinez-de Juan, and Y. Ye-Lin, "Active concentric ring electrode for non-invasive detection of intestinal myoelectric signals," *Medical Engineering amp; Physics*, vol. 33, no. 4, pp. 446–455, May 2011.

[30] F. Rattay, "Analysis of models for external stimulation of axons," *IEEE transactions on biomedical engineering*, no. 10, pp. 974–977, 1986.

[31] E. N. Warman, W. M. Grill, and D. Durand, "Modeling the effects of electric fields on nerve fibers: determination of excitation thresholds," *IEEE Transactions on Biomedical Engineering*, vol. 39, no. 12, pp. 1244–1254, 1992.

[32] C. C. McIntyre and W. M. Grill, "Selective microstimulation of central nervous system neurons," *Annals of biomedical engineering*, vol. 28, pp. 219–233, 2000.

[33] A. S. Aberra, A. V. Peterchev, and W. M. Grill, "Biophysically realistic neuron models for simulation of cortical stimulation," *Journal of neural engineering*, vol. 15, no. 6, p. 066023, 2018.

[34] F. Rattay, L. Paredes, and R. Leao, "Strength–duration relationship for intra-versus extracellular stimulation with microelectrodes," *Neuroscience*, vol. 214, pp. 1–13, 2012.

[35] F. Rattay, "Simulation of artificial neural reactions produced with electric fields," *Simulation Practice and Theory*, vol. 1, no. 3, pp. 137–152, 1993.

[36] P. J. Basser and B. J. Roth, "New currents in electrical stimulation of excitable tissues," *Annual Review of Biomedical Engineering*, vol. 2, no. 1, pp. 377–397, Aug. 2000.

[37] A. L. Hodgkin and A. F. Huxley, "A quantitative description of membrane current and its application to conduction and excitation in nerve," *The Journal of Physiology*, vol. 117, no. 4, pp. 500–544, Aug. 1952.

[38] C. C. McIntyre, A. G. Richardson, and W. M. Grill, "Modeling the excitability of mammalian nerve fibers: Influence of afterpotentials on the recovery cycle," *Journal of Neurophysiology*, vol. 87, no. 2, pp. 995–1006, Feb. 2002.

[39] J. Bell, *Encyclopedia of Neuroscience.* Springer Berlin Heidelberg.

[40] H. Monai, T. Omori, M. Okada, M. Inoue, H. Miyakawa, and T. Aonishi, "An analytic solution of the cable equation predicts frequency preference of a passive shunt-end cylindrical cable in response to extracellular oscillating electric fields," *Biophysical Journal*, vol. 98, no. 4, pp. 524–533, feb 2010.

[41] W. Gerstner, W. M. Kistler, R. Naud, and L. Paninski, *Neuronal Dynamics: From Single Neurons to Networks and Models of Cognition.* USA: Cambridge University Press, 2014.

[42] G. C. Goats, "Interferential current therapy." *British Journal of Sports Medicine*, vol. 24, no. 2, pp. 87–92, Jun. 1990.

[43] M. Agharezaee and A. Mahnam, "A computational study to evaluate the activation pattern of nerve fibers in response to interferential currents stimulation," *Medical amp; Biological Engineering amp; Computing*, vol. 53, no. 8, pp. 713–720, Apr. 2015.

[44] R. A. Adedoyin, M. O. Olaogun, and O. O. Fagbeja, "Effect of interferential current stimulation in management of osteo-arthritic knee pain," *Physiotherapy*, vol. 88, no. 8, pp. 493–499, Aug. 2002.

[45] G. De Domenico, *Basic guidelines for interferential therapy.* Theramed Books, 1981.

[46] E. Mirzakhalili, B. Barra, M. Capogrosso, and S. F. Lempka, "Biophysics of temporal interference stimulation," *Cell Systems*, vol. 11, no. 6, pp. 557–572.e5, Dec. 2020.

[47] N. Grossman, D. Bono, N. Dedic, S. B. Kodandaramaiah, A. Rudenko, H.-J. Suk, A. M. Cassara, E. Neufeld, N. Kuster, L.-H. Tsai, A. Pascual-Leone, and E. S. Boyden, "Noninvasive deep brain stimulation via temporally interfering electric fields," *Cell*, vol. 169, no. 6, pp. 1029–1041.e16, Jun. 2017.

[48] L. Jabban, D. Zhang, and B. W. Metcalfe, "Interferential current stimulation for non-invasive somatotopic sensory feedback for upper-limb prosthesis: Simulation results using a computable human phantom," in *2021 10th*

International IEEE/EMBS Conference on Neural Engineering (NER). IEEE, May 2021, pp. 765–768.

[49] Y. A. Patel and R. J. Butera, "Challenges associated with nerve conduction block using kilohertz electrical stimulation," *Journal of Neural Engineering*, vol. 15, no. 3, p. 031002, Mar. 2018.

[50] S. Zhao, G. Yang, J. Wang, J. R. Roppolo, W. C. de Groat, and C. Tai, "Conduction block in myelinated axons induced by high-frequency (khz) non-symmetric biphasic stimulation," *Frontiers in Computational Neuroscience*, vol. 9, Jul. 2015.

[51] Y. A. Patel, B. S. Kim, and R. J. Butera, "Kilohertz electrical stimulation nerve conduction block: Effects of electrode material," *IEEE Transactions on Neural Systems and Rehabilitation Engineering*, vol. 26, no. 1, pp. 11–17, Jan. 2018.

[52] A. R. Ward and V. J. Robertson, "Sensory, motor, and pain thresholds for stimulation with medium frequency alternating current," *Archives of Physical Medicine and Rehabilitation*, vol. 79, no. 3, pp. 273–278, Mar. 1998.

[53] P. Finch, L. Price, and P. Drummond, "High-frequency (10 khz) electrical stimulation of peripheral nerves for treating chronic pain: A double-blind trial of presence vs absence of stimulation," *Neuromodulation: Technology at the Neural Interface*, vol. 22, no. 5, pp. 529–536, Jul. 2019.

[54] E. Barkanov, "Introduction to the finite element method," *Institute of Materials and Structures Faculty of Civil Engineering Riga Technical University*, pp. 1–70, 2001.

[55] H. Watanabe, S. Sugiura, H. Kafuku, and T. Hisada, "Multiphysics simulation of left ventricular filling dynamics using fluid-structure interaction finite element method," *Biophysical Journal*, vol. 87, no. 3, pp. 2074–2085, Sep. 2004.

[56] T. Tian, H.-y. Huang, W. Wang, B. Shi, Q. Zheng, and C.-h. Li, "Three-dimensional finite element analysis of the effect of alveolar cleft bone graft on the maxillofacial biomechanical stabilities of unilateral complete cleft lip and palate," Oct. 2021.

[57] U. Andreaus and M. Colloca, "Prediction of micromotion initiation of an implanted femur under physiological loads and constraints using the finite element method," *Proceedings of the Institution of Mechanical Engineers, Part H: Journal of Engineering in Medicine*, vol. 223, no. 5, pp. 589–605, Apr. 2009.

[58] Y. Mohandes, M. Tahani, G. Rouhi, and M. Tahami, "A mechanobiological approach to find the optimal thickness for the locking compression plate: Finite element investigations," *Proceedings of the Institution of Mechanical*

Engineers, Part H: Journal of Engineering in Medicine, vol. 235, no. 4, pp. 408–418, Jan. 2021.

[59] F. Tarlochan, H. Mehboob, A. Mehboob, and S.-H. Chang, "Influence of functionally graded pores on bone ingrowth in cementless hip prosthesis: a finite element study using mechano-regulatory algorithm," *Biomechanics and Modeling in Mechanobiology*, vol. 17, no. 3, pp. 701–716, Nov. 2017.

[60] E. P. Doheny, B. M. Caulfield, C. M. Minogue, and M. M. Lowery, "Effect of subcutaneous fat thickness and surface electrode configuration during neuromuscular electrical stimulation," *Medical Engineering amp; Physics*, vol. 32, no. 5, pp. 468–474, Jun. 2010.

[61] N. RaviChandran, K. Aw, and A. McDaid, "Influence of electrode geometry on selectivity and comfort for functional electrical stimulation," 2019.

[62] F. Saavedra, R. Osorio, P. Aqueveque, and B. Andrews, "Effect of the current intensity and inter-electrode distance in surface electrical stimulation: A fem simulation study," in *2022 44th Annual International Conference of the IEEE Engineering in Medicine amp; Biology Society (EMBC)*. IEEE, Jul. 2022, pp. 752–755.

[63] N. A. Pelot, B. J. Thio, and W. M. Grill, "Modeling current sources for neural stimulation in comsol," *Frontiers in Computational Neuroscience*, vol. 12, Jun. 2018.

[64] J. FitzGerald, S. Lacour, S. McMahon, and J. Fawcett, "Microchannels as axonal amplifiers," *IEEE Transactions on Biomedical Engineering*, vol. 55, no. 3, pp. 1136–1146, Mar. 2008.

[65] E. Kreisberg, Z. Esmaeilpour, D. Adair, N. Khadka, A. Datta, B. W. Badran, J. D. Bremner, and M. Bikson, "High-resolution computational modeling of the current flow in the outer ear during transcutaneous auricular vagus nerve stimulation (tavns)," *Brain Stimulation*, vol. 14, no. 6, pp. 1419–1430, Nov. 2021.

[66] X. Chu, X. Song, R. Li, Q. Li, Q. Li, X. Gu, and D. Ming, "Multielectrode array-based percutaneous nerve stimulation strategy with ultrasound guidance for ulnar nerve injury," *IEEE Transactions on Neural Systems and Rehabilitation Engineering*, vol. 31, pp. 1502–1510, 2023.

[67] X.-S. Gu, D. Ming, X.-L. Chu, X.-Z. Song, Y.-R. Li, Z.-R. Wu, Q. Li, and Q.-W. Li, "An ultrasound-guided percutaneous electrical nerve stimulation regimen devised using finite element modeling promotes functional recovery after median nerve transection," *Neural Regeneration Research*, vol. 18, no. 3, p. 683, 2023.

[68] C. C. McIntyre and W. M. Grill, "Finite element analysis of the current-density and electric field generated by metal microelectrodes," *Annals of Biomedical Engineering*, vol. 29, no. 3, pp. 227–235, Mar. 2001.

[69] A. M. Kuncel and W. M. Grill, "Selection of stimulus parameters for deep brain stimulation," *Clinical Neurophysiology*, vol. 115, no. 11, pp. 2431–2441, Nov. 2004.

[70] A. G. Richardson, C. C. McIntyre, and W. M. Grill, "Modelling the effects of electric fields on nerve fibres: Influence of the myelin sheath," *Medical amp; Biological Engineering amp; Computing*, vol. 38, no. 4, pp. 438–446, Jul. 2000.

[71] J. Cao and P. Grover, "Do single neuron models exhibit temporal interference stimulation?" in *2018 IEEE Biomedical Circuits and Systems Conference (BioCAS)*. IEEE, Oct. 2018, pp. 1–4.

[72] F. Manzouri, A. Mahnam, and M. E. Andani, "A computational study to evaluate the mechanism of selectivity in interferential current therapy," in *2011 18th Iranian Conference of Biomedical Engineering (ICBME)*. IEEE, Dec. 2011, pp. 171–174.

[73] P. Rampazo and R. E. Liebano, "Analgesic effects of interferential current therapy: A narrative review," *Medicina*, vol. 58, no. 1, p. 141, Jan. 2022.

[74] B. Botzanowski, M. J. Donahue, M. S. Ejneby, A. L. Gallina, I. Ngom, F. Missey, E. Acerbo, D. Byun, R. Carron, A. M. Cassarà, E. Neufeld, V. Jirsa, P. S. Olofsson, E. D. Głowacki, and A. Williamson, "Noninvasive stimulation of peripheral nerves using temporally-interfering electrical fields," *Advanced Healthcare Materials*, vol. 11, no. 17, Jul. 2022.

[75] I. Koca, A. Boyaci, A. Tutoglu, M. Ucar, and O. Kocaturk, "Assessment of the effectiveness of interferential current therapy and tens in the management of carpal tunnel syndrome: a randomized controlled study," *Rheumatology International*, vol. 34, no. 12, pp. 1639–1645, Apr. 2014.

[76] K. Kozasa, R. Fujihara, H. Hirai, and H. I. Krebs, "Interferential electrical stimulation applied to the soleus muscle in humans: Preliminary study on the relationship among stimulation parameters, force output, and pain sensation," in *2018 7th IEEE International Conference on Biomedical Robotics and Biomechatronics (Biorob)*. IEEE, Aug. 2018, pp. 1038–1043.

[77] S. Rogan, Y. Brulhart, T. Ledermann, N. Schmutz, and E. Lujickx, "Effectiveness analysis of muscle stretching during interferential current in soccer players – an explorative study," *Journal of Physical Education and Sport*, vol. 2016, no. 02, Jun. 2016.

[78] J. W. Bellew, Z. Beiswanger, E. Freeman, C. Gaerte, and J. Trafton, "Interferential and burst-modulated biphasic pulsed currents yield greater muscular force than russian current," *Physiotherapy Theory and Practice*, vol. 28, no. 5, pp. 384–390, Dec. 2011.

[79] V. D. Zivkovic, I. Stankovic, L. Dimitrijevic, M. Kocic, H. Colovic, M. Vlajkovic, A. Slavkovic, and M. Lazovic, "Are interferential electrical

stimulation and diaphragmatic breathing exercises beneficial in children with bladder and bowel dysfunction?" *Urology*, vol. 102, pp. 207–212, Apr. 2017.

[80] J. S. Moore, P. R. Gibson, and R. E. Burgell, "Neuromodulation via interferential electrical stimulation as a novel therapy in gastrointestinal motility disorders," *Journal of Neurogastroenterology and Motility*, vol. 24, no. 1, pp. 19–29, Jan. 2018.

[81] Y. Iizumi, Y. Ihara, J. Koike, and K. Takahashi, "Effects of interferential current electrical stimulation (ifcs) on mastication and swallowing function in healthy young adults: A preliminary study," *Clinical and Experimental Dental Research*, vol. 9, no. 3, pp. 491–499, May 2023.

[82] Y. Hasegawa, K. Sugahara, S. Sano, A. Sakuramoto, H. Kishimoto, and Y. Oku, "Enhanced salivary secretion by interferential current stimulation in patients with dry mouth: a pilot study," *Oral Surgery, Oral Medicine, Oral Pathology and Oral Radiology*, vol. 121, no. 5, pp. 481–489, May 2016.

[83] J.-M. GANNE, "Stimulation of bone healing with interferential therapy," *Australian Journal of Physiotherapy*, vol. 34, no. 1, pp. 9–20, 1988.

[84] F. V. Santos, G. R. Chiappa, P. J. C. Vieira, D. Umpierre, J. P. Ribeiro, and G. Cipriano Jr, "Interferential electrical stimulation improves peripheral vasodilatation in healthy individuals," *Brazilian Journal of Physical Therapy*, vol. 17, no. 3, pp. 281–288, Jun. 2013.

[85] A. Botter, G. Oprandi, F. Lanfranco, S. Allasia, N. A. Maffiuletti, and M. A. Minetto, "Atlas of the muscle motor points for the lower limb: implications for electrical stimulation procedures and electrode positioning," *European Journal of Applied Physiology*, vol. 111, no. 10, pp. 2461–2471, Jul. 2011.

[86] A. Kuhn, T. Keller, M. Lawrence, and M. Morari, "The influence of electrode size on selectivity and comfort in transcutaneous electrical stimulation of the forearm," *IEEE Transactions on Neural Systems and Rehabilitation Engineering*, vol. 18, no. 3, pp. 255–262, Jun. 2010.

[87] W. Besio and A. Prasad, "Analysis of skin-electrode impedance using concentric ring electrode," in *2006 International Conference of the IEEE Engineering in Medicine and Biology Society.* IEEE, Aug. 2006, pp. 6414–6417.

[88] S. I. Alzahrani and C. W. Anderson, "A comparison of conventional and tri-polar eeg electrodes for decoding real and imaginary finger movements from one hand," *International Journal of Neural Systems*, vol. 31, no. 09, p. 2150036, Jul. 2021.

[89] M. G. Cassar, C. Sebu, M. Pidcock, B. Andrews, and S. Chandak, "Optimal design of concentric electrodes for functional electrical stimulation in multilayered isotropic tissues," in *2023 3rd International Conference*

on Electrical, Computer, Communications and Mechatronics Engineering (ICECCME). IEEE, Jul. 2023, pp. 1–11.

[90] S. Kumar and P. Gurudut, "Comparative effectiveness of neuromuscular electrical stimulation and russian current stimulation of tibialis posterior in individuals with flexible flat foot: A prospective randomized controlled trial," *Journal of Datta Meghe Institute of Medical Sciences University*, vol. 19, no. 4, pp. 714–721, Oct. 2024.

[91] R. G. Dawson, R. J. Lockwood, J. D. Wilson, and G. Freeman, "The rowing cycle: Sources of variance and invariance in ergometer and on-the-water performance," *Journal of Motor Behavior*, vol. 30, no. 1, pp. 33–43, Mar. 1998.

[92] V. Kleshnev, *Biomechanics of Rowing*. Crowood, 2016. [Online]. Available: https://books.google.cl/books?id=bfXADAAAQBAJ

[93] S. Volianitis, C. C. Yoshiga, and N. H. Secher, "The physiology of rowing with perspective on training and health," *European Journal of Applied Physiology*, vol. 120, no. 9, pp. 1943–1963, Jul. 2020.

[94] S. Held, T. Siebert, and L. Donath, "10

[95] T. M. Vieira, G. L. Cerone, C. Stocchi, M. Lalli, B. Andrews, and M. Gazzoni, "Timing and modulation of activity in the lower limb muscles during indoor rowing: What are the key muscles to target in fes-rowing protocols?" *Sensors*, vol. 20, no. 6, p. 1666, Mar. 2020.

[96] V. D. Chandran, R. L. Lambach, R. S. Gibbons, B. J. Andrews, G. S. Beaupre, and S. Pal, "Tibiofemoral forces during fes rowing in individuals with spinal cord injury," *Computer Methods in Biomechanics and Biomedical Engineering*, vol. 24, no. 3, pp. 231–244, Sep. 2020.

[97] G. Ye, E. P. Grabke, M. Pakosh, J. C. Furlan, and K. Masani, "Clinical benefits and system design of fes-rowing exercise for rehabilitation of individuals with spinal cord injury: A systematic review," *Archives of Physical Medicine and Rehabilitation*, vol. 102, no. 8, pp. 1595–1605, Aug. 2021.

[98] M. Gobbo, N. A. Maffiuletti, C. Orizio, and M. A. Minetto, "Muscle motor point identification is essential for optimizing neuromuscular electrical stimulation use," *Journal of NeuroEngineering and Rehabilitation*, vol. 11, no. 1, Feb. 2014.

[99] N. Kaneko, K. L. Fok, K. Nakazawa, and K. Masani, "Motor point stimulation induces more robust f-waves than peripheral nerve stimulation," *European Journal of Neuroscience*, vol. 55, no. 6, pp. 1614–1628, Mar. 2022.

[100] K. Nakagawa, K. L. Fok, and K. Masani, "Neuromuscular recruitment pattern in motor point stimulation," *Artificial Organs*, vol. 47, no. 3, pp. 537–546, Nov. 2022.

[101] M. Behringer, A. Franz, M. McCourt, and J. Mester, "Motor point map of upper body muscles," *European Journal of Applied Physiology*, vol. 114, no. 8, pp. 1605–1617, Apr. 2014.

[102] Ventura, L. Gomes, J. Cavalcante, D. Vieira, C. V. Sousa, R. d. C. Marqueti, N. Babault, and J. L. Durigan, "Does electrode sensor positioning over motor points affect different portions of quadriceps muscle architecture during submaximal evoked torque?" *Journal of Sensors*, vol. 2023, no. 1, Jan. 2023.

[103] J.-Y. Moon, T.-S. Hwang, S.-J. Sim, S.-i. Chun, and M. Kim, "Surface mapping of motor points in biceps brachii muscle," *Annals of Rehabilitation Medicine*, vol. 36, no. 2, p. 187, 2012.

[104] R. A. Guzmán-Venegas, O. F. Araneda, and R. A. Silvestre, "Differences between motor point and innervation zone locations in the biceps brachii. an exploratory consideration for the treatment of spasticity with botulinum toxin," *Journal of Electromyography and Kinesiology*, vol. 24, no. 6, pp. 923–927, Dec. 2014.

[105] N. RaviChandran, K. C. Aw, and A. McDaid, "Characterizing the motor points of forearm muscles for dexterous neuroprostheses," *IEEE Transactions on Biomedical Engineering*, vol. 67, no. 1, pp. 50–59, Jan. 2020.

[106] N. Dunkelberger, S. A. Carlson, J. Berning, K. C. Stovicek, E. M. Schearer, and M. K. O'Malley, "Shared control of elbow movements with functional electrical stimulation and exoskeleton assistance," in *2022 International Conference on Rehabilitation Robotics (ICORR)*. IEEE, Jul. 2022.

[107] J. Flodin, R. Juthberg, and P. Ackermann, "Motor point heatmap guide for neuromuscular electrical stimulation of the quadriceps muscle," *Journal of Electromyography and Kinesiology*, vol. 70, p. 102771, Jun. 2023.

[108] K. Ichikawa, Y. Jiang, M. Sugi, S. Togo, and H. Yokoi, "Joint angle based motor point tracking stimulation for surface fes: A study on biceps brachii," *Medical Engineering amp; Physics*, vol. 88, pp. 9–18, Feb. 2021.

[109] T. Fukui, Y. Otake, and T. Kondo, "Skin movement rules relative to joint motions," *Clinical Research on Foot amp; Ankle*, vol. 05, no. 02, 2017.

[110] J. Wilke and S. Tenberg, "Semimembranosus muscle displacement is associated with movement of the superficial fascia: An in vivo ultrasound investigation," *Journal of Anatomy*, vol. 237, no. 6, pp. 1026–1031, Aug. 2020.

[111] W. M. Elsais, S. J. Preece, R. K. Jones, and L. Herrington, "Could relative movement between the adductor muscles and the skin invalidate surface electromyography measurement?" *Journal of Applied Biomechanics*, vol. 36, no. 5, pp. 319–325, Oct. 2020.

[112] S. H. Choi, B. J. Lee, and S. Y. Lee, "A study on skin mobility according to joint movement: Variations in mobility according to joint motion range

and correlation and influence with hydrica composition," *Skin Research and Technology*, vol. 29, no. 2, Feb. 2023.

[113] Y. Sednieva, K. Bruyère-Garnier, A. Naaim, A. Viste, and L. Gras, "Assessment of the thigh skin and fascia strains during knee flexion-extension: an ex-vivo study," *Computer Methods in Biomechanics and Biomedical Engineering*, vol. 22, no. sup1, pp. S172–S174, May 2019.

[114] B. J. Page, O. D. Mrowczynski, R. A. Payne, S. E. Tilden, H. Lopez, E. Rizk, and K. Harbaugh, "The relative location of the major femoral nerve motor branches in the thigh," *Cureus*, Jan. 2019.

[115] H. Narita, H. Yoshida, S. Chiba, A. Oda, T. Ishikawa, N. Takahashi, T. Tani, S. Watanabe, and Y. Tonosaki, "Does the location of the motor point identified with electrical stimulation correspond to that identified with the gross anatomical method?" *Journal of Physical Therapy Science*, vol. 23, no. 5, pp. 737–739, 2011.

[116] E. J. Gonzalez, R. J. Downey, C. A. Rouse, and W. E. Dixon, "Influence of elbow flexion and stimulation site on neuromuscular electrical stimulation of the biceps brachii," *IEEE Transactions on Neural Systems and Rehabilitation Engineering*, vol. 26, no. 4, pp. 904–910, Apr. 2018.

[117] K. Ichikawa, Y. Jiang, M. Sugi, S. Togo, and H. Yokoi, "Motor point tracking stimulation of biceps brachii using multi electrodes based on functional electrical stimulation," in *2019 IEEE International Conference on Cyborg and Bionic Systems (CBS)*. IEEE, Sep. 2019, pp. 1–4.

[118] T. Hirai, Y. Jiang, M. Sugi, S. Togo, and H. Yokoi, "Investigation of motor point shift and contraction force of triceps brachii for functional electrical stimulation," in *2021 43rd Annual International Conference of the IEEE Engineering in Medicine amp; Biology Society (EMBC)*, vol. 111. IEEE, Nov. 2021, pp. 6330–6333.

[119] S. Matsubara, T. Watanabe, T. Suzuki, S. Wakisaka, K. Aoyama, and M. Inami, "Optimal motor point search using mm-order electrode arrays," *IEEE Access*, vol. 11, pp. 58 970–58 981, 2023.

[120] H. J. Basinger H, "Anatomy, Abdomen and Pelvis: Femoral Triangle - ncbi.nlm.nih.gov," https://www.ncbi.nlm.nih.gov/books/NBK541140/, Mar. 2023, [Accessed 21-01-2025].

[121] J.-M. J. Wilson, D. G. E. Robertson, and J. P. Stothart, "Analysis of lower limb muscle function in ergometer rowing," *International Journal of Sport Biomechanics*, vol. 4, no. 4, pp. 315–325, Nov. 1988.

[122] Z. Hussain and M. Tokhi, "Modelling of muscle extension and flexion for fes-assisted indoor rowing exercise," in *2008 Second Asia International Conference on Modelling amp; Simulation (AMS)*. IEEE, May 2008, pp. 963–967.

[123] A. E. Draghici, G. Picard, J. A. Taylor, and S. J. Shefelbine, "Assessing kinematics and kinetics of functional electrical stimulation rowing," *Journal of Biomechanics*, vol. 53, pp. 120–126, Feb. 2017.

[124] E. Imatz-Ojanguren, U. Hoffmann, J. Veneman, N. Malešević, and T. Keller, "Stimulation discomfort comparison of asynchronous and synchronous methods with multi-field surface electrodes," in *18th Annual Conference of the International Functional Electrical Stimulation Society (IFESS)*, Jun. 2013.

[125] M. G. Garcia-Garcia, L. I. Jovanovic, and M. R. Popovic, "Comparing preference related to comfort in torque-matched muscle contractions between two different types of functional electrical stimulation pulses in able-bodied participants," *The Journal of Spinal Cord Medicine*, vol. 44, no. sup1, pp. S215–S224, Sep. 2021.

[126] S. C. Naaman, R. B. Stein, and C. Thomas, "Minimizing discomfort with surface neuromuscular stimulation," *Neurorehabilitation and Neural Repair*, vol. 14, no. 3, pp. 223–228, Sep. 2000.

[127] R. L. Sakugawa, L. B. R. Orssatto, L. T. Sampaio, H. de Brito Fontana, and F. Diefenthaeler, "Pressure on the electrode to reduce discomfort during neuromuscular electrical stimulation in individuals with different subcutaneous-fat thickness: Is the procedure effective and reliable?" *IEEE Transactions on Neural Systems and Rehabilitation Engineering*, vol. 30, pp. 1–7, 2022.

[128] J. Chae and R. Hart, "Comparisson of discomfort associated with surface and percutaneous intramuscular electrical stimulation for persons with chronic hemipleghia," *American Journal of Physical Medicine amp; Rehabilitation*, vol. 77, no. 6, pp. 516–522, Nov. 1998.

[129] S. Chaudhury, A. Ghosh, and A. Datta, "A cadaveric anthropometric study of femoral nerve. anatomical guide to successful femoral nerve block," *Revista Argentina de Anatomía Online*, vol. 10, no. 3, pp. 112–117, 2019.

[130] J. Gómez-Tames, J. González, and W. Yu, "Influence of different geometric representations of the volume conductor on nerve activation during electrical stimulation," *Computational and Mathematical Methods in Medicine*, 2014.

[131] (2024, Oct.) Tissue properties - dielectric properties. [Online]. Available: https://itis.swiss/virtual-population/tissue-properties/database/dielectric-properties/

[132] R. Osorio L., S. M. Hall, F. Saavedra, P. Aqueveque, J. J. FitzGerald, and B. J. Andrews, "Finite element modelling for biophysical models of nervous system stimulation: Best practices for multiscale adaptive meshing," *IEEE Transactions on Neural Systems and Rehabilitation Engineering*, 2025.

[133] S. Dokos, "Modelling organs, tissues, cells and devices," Berlin, Heidelberg, 2017.

[134] S. Herasymov, V. Soroka, S. Milevskyi, N. Voropay, H. Zviertsev, and Y. Motalyhin, "Development of a method for digital synthesis of electrical signals with a normalized harmonic coefficient," in *2023 5th International Congress on Human-Computer Interaction, Optimization and Robotic Applications (HORA)*. IEEE, Jun. 2023, pp. 1–5.

[135] J. Ruiz and M. A. Colominas, "Wave-shape function model order estimation by trigonometric regression," *Signal Processing*, vol. 197, p. 108543, Aug. 2022.

[136] R. Melzack, "The mcgill pain questionnaire: Major properties and scoring methods," *Pain*, vol. 1, no. 3, pp. 277–299, Sep. 1975.

[137] M. Makatsori, O. Pfaar, and M. A. Calderon, "Allergen immunotherapy: Clinical outcomes assessment," *The Journal of Allergy and Clinical Immunology: In Practice*, vol. 2, no. 2, pp. 123–129, Mar. 2014.

[138] Y. Xia, *Correlation and association analyses in microbiome study integrating multiomics in health and disease*. Elsevier, 2020, pp. 309–491.

[139] R. Osorio, J. Edmondson, S. M. Hall, F. Saavedra, J. Sáez, A. Poulton, J. FitzGerald, P. Aqueveque, B. Andrews, and J. Jarvis, "Characterization and evaluation of interferential current stimulation for functional electrical stimulation," *Artificial Organs*, May 2025.

[140] R. E. van Pelt, C. M. Jankowski, W. S. Gozansky, P. Wolfe, R. S. Schwartz, and W. M. Kohrt, "Sex differences in the association of thigh fat and metabolic risk in older adults," *Obesity*, vol. 19, no. 2, pp. 422–428, Feb. 2011.

[141] L. E. Medina and W. M. Grill, "Volume conductor model of transcutaneous electrical stimulation with kilohertz signals," *Journal of Neural Engineering*, vol. 11, no. 6, p. 066012, Nov. 2014.

[142] F. Stewart, L. F. Gameiro, R. El Dib, M. O. Gameiro, A. Kapoor, and J. L. Amaro, "Electrical stimulation with non-implanted electrodes for overactive bladder in adults," *Cochrane Database of Systematic Reviews*, vol. 2017, no. 2, Dec. 2016.

[143] A. Lebiedowska, M. Hartman-Petrycka, A. Stolecka-Warzecha, W. Odrzywołek, M. Bożek, and S. Wilczyński, "The influence of skin parameters and body composition on the tolerance of pain stimulus generated during electrical muscle stimulation (ems) in women - pilot study," *Clinical, Cosmetic and Investigational Dermatology*, vol. Volume 17, pp. 1227–1243, May 2024.

[144] C. W. Blichmann and J. Serup, "Assessment of skin moisture. measurement

of electrical conductance, capacitance and transepidermal water loss," *Acta dermato-venereologica*, vol. 68, no. 4, pp. 284–290, 1988.

[145] P. Clarys, R. Clijsen, J. Taeymans, and A. O. Barel, "Hydration measurements of the stratum corneum: comparison between the capacitance method (digital version of the corneometer cm 825®) and the impedance method (skicon-200ex®)," *Skin Research and Technology*, vol. 18, no. 3, pp. 316–323, Aug. 2011.